THE UNIVERSITY OF MANITOBA

UTILIZATION OF POLARIZATION-DEPOLARIZATION CHARACTERISTICS IN ELECTROMAGNETIC INVERSE SCATTERING

by

SUJEET KUMAR CHAUDHURI

A THESIS

SUBMITTED TO THE FACULTY OF GRADUATE STUDIES

IN PARTIAL FULFILLMENT OF THE REQUIREMENTS FOR THE DEGREE

OF DOCTOR OF PHILOSOPHY

DEPARTMENT OF ELECTRICAL ENGINEERING

WINNIPEG, MANITOBA R3T 2N2

November 1976

"UTILIZATION OF POLARIZATION-DEPOLARIZATION CHARACTERISTICS IN ELECTROMAGNETIC INVERSE SCATTERING"

by

SUJEET KUMAR CHAUDHURI

A dissertation submitted to the Faculty of Graduate Studies of the University of Manitoba in partial fulfillment of the requirements of the degree of

DOCTOR OF PHILOSOPHY

ABSTRACT

A new model for the solution of the inverse problem of electromagnetic scattering by smooth, convex-shaped, perfectly conducting, three-dimensional scatterers has been developed. Certain geometrical as well as physical optics approximations were used to incorporate the concepts of the Minkowski problem of differential geometry into the space-time integral solution of electromagnetic scattering to yield the formal solution for the recovery of the surface profile of the scatterer from the backscattered far-field data. Although various efficient solutions for target identification are available, still information contained in polarization-depolarization characteristics of the scatterer is not yet exploited to its full extent. Therefore, the underlying assumption in this investigation was based on the fact that the depolarization characteristics of the scattered field do necessarily contain information regarding the surface profile of the scatterer.

Application of this new inverse scattering model to the test case of a perfectly conducting prolate spheroid has been undertaken. Various results, along with error bounds and limitations are discussed.

ZUSAMMENFASSUNG

Ein neues Model der Lösung für das inverse Problem der elektromagnetischen Streuung an konvexen, unendlich leitenden drei-dimensionalen Streuern wurde entwickelt. Gewisse geometrische wie auch physikalisch-optische Approximationen wurden benutzt um das Minkowski'sche Problem der differentiellen Geometrie in die Raum-Zeit-Integral-Lösung der elektromagnetischen Streuung einzuführen so, daß die formale Lösung der Zurückgewinnung der Streuungsoberflächengestalt von dem rückgestreuten Fernfeld gewährleistet wird. Obwohl etliche wirkungsvolle Lösungen der Zielerkennung bekannt sind, so wurde Information die in den Polarisations/Depolarisations-Eigenschaften des Streuers enthalten ist nicht völlig ausgenutzt. Deshalb wurde die dieser Arbeit unterliegenden Annahme auf die Depolarisationseigenschaften des Streufelds gestützt, das notwendigerweise Eigenschaften über die Oberflächengestalt des Streuers enthalten muß. Die Anwendung dieses neu eingeführten inversen Streuungsmodels für den Fall eines ideal leitenden Prolaten Sphäroids wurde ausgeführt. Verschiedene Ergebnisse zusammen mit Fehlergrenzen und Anwendungsbeschränkungen werden untersucht.

RÉSUMÉ

On a developpé un nouveau modèle pour la solution du problème inverse de la diffraction d'ondes électromagnétiques; les objects diffusants à trois dimensions que l'on considère sont perfaitement conducteurs et ils ont une surface lisse de forme convexe ne présentant aucunes discontinuités. Certaines approximations d'optique géométrique et d'optique physique ont été utilisées pour introduire les concepts du probléme de Minkowski relatif à la géomêtrie differentielle dans la soulution intégrale (reliant l'espace et le temps) de la diffusion électromagnétique. Ainsi, le profil de la surface de l'object diffusant a été déterminé à partir des données sur le le champs lointain de retour. Différentes solutions efficaces permettent de reconnaître la cible, cependant l'information contenue dans les caractéristiques de polarisation - dépolarixation du diffuseur n'a pas encore été entièrement exploitée. Par consequent, l'hypothèse fondamentale de cette investigation était basée sur le fait que les caractéristiques de dépolarisation du champs diffusé contiennent nécessairement des renseignements sur le profil de la surface du diffuseur.

On a considéré les applications de ce nouveau modèle dans le cas d'essai d'une sphère allongée, parfaitement conductrice. Des résultats différents, ainsi que les erreurs de troncatures et les limitations sont discutés.

ACKNOWLEDGEMENTS

I am indebted to the members of my advisory committee, which consisted of Professors W. M. Boerner, E. Bridges, L. Shafai and R. Venkataraman, for their guidance and direction in my post-graduate study program.

In particular, innumerable hours of consultation and discussion with Dr. W. M. Boerner, who supervised the dissertation and suggested the topic, have provided inspiration for this project. His frank and constructive criticism of the research, which proved to be invaluable, is gratefully acknowledged.

I also wish to adknowledge my gratitude to Dr. C. L. Bennett of Sperry Research Center, Sudbury, Ma. for helpful suggestions and for providing many research reports, data and other related information.

I wish to express my deep appreciation to my parents for their blessings and moral support, without which none of this would have been possible. I must make use of this opportunity to express my gratitude to Janet Mckone, who through her virtues of patience, tolerance and deep understanding has provided constant encouragement to continue and complete this work.

I wish to express my appreciation for the financial support of the National Research Council of Canada, Defence Research Board of Canada, and the Shriner's Research Foundation, without which it would have been impossible to complete this work. The computation work was performed with the facilities of the University of Manitoba Computer Center.

I would like to thank Mrs. Shirley Clubine for her patient and skillful typing of the final version of the thesis.

Finally, I wish to thank all my friends, particularly Mr. Y. Das, who have encouraged me directly and indirectly during the entire period of my post-graduate studies at the University of Manitoba.

Sujeet K. Chaudhuri

TABLE OF CONTENTS

LIST OF FIGURES

List of Figures cont.

List of Figures cont.

LIST OF TABLES

LIST OF SYMBOLS

Greek Alphabet:

α	Polarization angle
α'	Decay constant explained in (5.3c)
β	Constant explained in (5.3c)
γ	Characteristic function of the target
δ	Impulse function
∇^2	Laplacian operator
(θ,ϕ)	Spherical coordinates
$\overline{\kappa}$	Three-dimensional space of vectors
λ	Wavelength
μ	Permiability
(ξ,η,ζ)	Direction cosines of a vector in three-dimensional space
π	Pi (3.14159265)
ρ	Function dependent on backscattered far-field
ρ^*	Complex conjugate of ρ
ρ_0	Radius of a circular shaped patch about the specular point
ρ_1,ρ_2	Principal radii of curvature at any point of an object
σ	Backscattered radar cross-section
σ_+,σ_-	Backscattered radar cross-section corresponding to two different incident waves coming from opposite directions
ϕ_1,ϕ_2	Constants explained in (5.4)
$\phi_{1p}-\phi_{2p}$	Phase difference between $\vec{H}_{1p}$ and $\vec{H}_{2p}$
ψ	Phase function
τ	Shifted time

Γ	Constant explained in (II-5)
ω	Normalized phasor frequency
ω_0	Fundamental frequency
ω_L	Lowest frequency under consideration
ω_c	Cut off frequency

Latin Alphabet:

a	Characteristic dimension of a scatterer (e.g., semi axis of a prolate spheroid or ellipsoid)
a_0, a_1, a_2	First three expansion coefficients as explained in (3.7)
$\hat{a}_1, \hat{a}_2$	Unit tangent vectors to the principal lines of curvature at the specular point
$\hat{a}_{H_i}$	Unit vector in the direction of the incident magnetic field
$\hat{a}_{c_r}$	Unit vector perpendicular to $\hat{a}_{H_i}$
$\hat{a}_R$	Unit vector at the integration point, pointing to observation point
$\hat{a}_r$	Unit vector in the direction of $\vec{r}$
$\hat{a}_x, \hat{a}_y, \hat{a}_z$	Unit vectors in x,y,z direction respectively
A	Projected area function along the monostatic direction
A_1, A_2, A_3, A_4	Constants in the expression for impulse response model as explained in (5.2)
$\vec{A}_p$	Vector potential due to a surface current distribution
b	Characteristic dimension of a scatterer (e.g., semi axis of a prolate spheroid or ellipsoid)
$\hat{b}$	Unit vector tangent to a surface
B_1	Constant as explained in (5.8)
c_0	Free space propagation velocity

c	Characteristic dimension of a scatterer (e.g., semi axis of a prolate spheroid or ellipsoid)
C_1	Constant as explained in (5.8)
dh	Incremental distance along the ray path
$d\Omega$	Differential surface of the unit sphere
$d\Sigma_0, d\Sigma$	Cross-sections of tube of rays shown in Fig.4.2
D	Radius of curvature
D_1, D_2	Principal radii of curvature at the specular point
D_e	Depolarization factor
E	Input to a passive linear two-port
E_x	x component of the electric field
$\vec{E}_i$	Incident electric field
$\vec{E}_r$	Reflected electric field
E_s^x	x component of the scattered electric field
E_s	Scattered electric field
E_1	Constant as explained in (5.8)
EX1,EX2,EX3	Exit criteria for the iteration scheme of Fig. 6.1
EI2,EI3	Exit criteria for the modified iteration scheme of Fig. 6.5
f	Profile function of a body of revolution
f'	Inverse Fourier transform of F
f_0	Function of a, b, c defined in (6.6)
f_1, f_2	Constants explained in (II-2) and (II-3)
F	$N(\overline{\kappa})\Gamma(\overline{\kappa})$
F_I	Impulse response waveform
F_U	Step response waveform
F_R	Ramp response waveform

F_{I_1}	Portion of impulse response waveform responsible for high frequency portion of the phasor response
F_{I_2}	Portion of impulse response waveform responsible for low frequency portion of the phasor response
g	Function of a, b, c defined in (6.2)
g_1, g_2	Constants defined in (II-2) and (II-3)
G	Constant explained in (II-6)
G'	Constant explained in (5.9)
h	Function of a, b, c defined in (6.3)
$\hat{h}_a$	Augmented impulse response
h_1, h_2	Constants defined in (II-2) and (II-3)
$\vec{H}$	Total magnetic field
H_a'	Augmented frequency response
$\hat{H}_a$	Estimate of the high frequency behaviour of augmented frequency response
$\vec{H}_{co}$	Co-polarized component of the scattered magnetic field
$\vec{H}_{cr}$	Cross-polarized component of the scattered magnetic field
$\vec{H}_i$	Incident magnetic field
H_{i_1}	Component of $\vec{H}_i$ in $\hat{a}_1$ direction
H_{i_2}	Component of $\vec{H}_i$ in $\hat{a}_2$ direction
$\vec{H}_{po}$	Physical optics approximation to the magnetic field
$\vec{H}_{po1}$	First order correction to $\vec{H}_{po}$
$\bar{H}_S$	Scattered magnetic field
$\vec{H}_{1c}$	Cross-polarized component of the scattered field under situation 1
$\vec{H}_{2c}$	Cross-polarized component of the scattered field under situation 2

$\vec{H}_{1p}$	Co-polarized component of the scattered field under situation 1
$\vec{H}_{2p}$	Co-polarized component of the scattered field under situation 2
$\hat{i}_1$	Direction of the incident field
$\hat{i}_2$	Direction of the response field
I^2, I_0^2	Intensity of the field
I_1, I_2, I_3	First three moments of $F_{I_1}(t')$
j	$\sqrt{-1}$
$\vec{J}_{po}$	Physical optics approximation to the surface current
$\vec{J}_{po1}$	First order correction to $\vec{J}_{po}$
$\vec{J}_S$	Surface current
J_{1po}	Component of $\vec{J}_{po}$ in $\hat{a}_1$ direction
J_{2po}	Component of $\vec{J}_{po}$ in $\hat{a}_2$ direction
k	Wave number
k'	Inverse Fourier transform of N
K	Gaussian curvature
K_r	Rayleigh coefficient
K_1, K_2	Principal curvatures at the specular point
K_{12}	Constant as explained in (6.1)
ℓ	Location of the shadow boundary
L	Number of cycles in iteration loop
m	Integer
M	Minkowski's support function
M_i	$\partial M/\partial i$; $i = \xi, \eta, \zeta$
M_{ik}	$\partial^2 M/\partial i \partial k$; $i,k = \xi, \eta, \zeta$
n	Real number

$\hat{n}$	Unit normal vector
n'	Refractive index
N	Function which is zero outside Q and non-zero inside Q
N_0	Noise
p	Constant as explained in (I-4)
p'	Distance from the origin to the plane tangent to a surface
p_2	Constant as explained in (II-3)
P_1	Peak creeping wave contribution
Q	The region in which the backscattered far-field is known
Q'	Reflection of Q through the origin
$\vec{r}$	Position vector
$\vec{r}'$	Position vector to integration point
r_a	Augmented smoothed impulse response
R	Distance of the observation point from the origin
R_e	Reflection coefficient
R_a	Fourier transform of r_a
s	$j\omega$
$S[M]$	Sum of the diagonal minors of the matrix $[M]$
$S^{i\ell\ell}$	Illuminated portion of the scattering surface
S'	Surface of the scatterer
S_ε	Surface of the scatterer excluding the integration point
t	Time
t'	Retarded time $t - R/c_0$
t'_1	Initial time at which the incident plane wave reaches the specular point

t_1, t_2	Constants as explained in (II-2) and (II-3)
t_0	Reference time
T	Total path length
T_c	Creeping wave path length
TE	Transverse electric
TM	Transverse magnetic
u	Unit step function
(x,y,z)	Cartesian coordinate system
(x',y',z')	Cartesian coordinate system after rotation about one axis
(x'',y'',z'')	Cartesian coordinate system after rotation about two axes
$\overline{x}$	Configuration space
$\hat{X}$	Vector space spanning a closed convex surface

chapter one

REVIEW OF THE LITERATURE

1.1 INTRODUCTION

The phenomena of scattering and diffraction have been known to and studied by mankind for about three hundred years, however the research in this field has found particular interest and application mostly in the last quarter century. The advent of microwave technology, in particular of the radar system during the second world war, has led to a renewed interest in scattering and inverse scattering theories. The identification of remote objects has been the goal of radar operators, designers and researchers since the first radar set was built. While this problem has not been solved for the general case, various approximations, e.g., high frequency limits, and restricting the class of scattering bodies, have resulted in formal solutions for the unknown shape [2,30]. In derivations of inverse scattering techniques, stringent requirements were generally placed on the nature of the scatterer; this resulted in methods which can determine only a very narrow class of unknown shapes. Furthermore, these existing techniques, owing to the exhaustive amount of input information requirements, seem increasingly unfeasible. Thus, although the inverse scattering field has generated a great deal of interest in the past decade, the demand for new basic model theories is as strong as ever, as those model theories are fundamental to remote sensing problems such as air traffic control, oceanography, telemetry, satellite tracking, etc.

When radiation of any type is incident upon an object, some of the radiation is scattered in all directions by the object. The direct problem of the theory of scattering or diffraction is that of determining the radiation scattered in each direction when the properties of the incident radiation as well as those of the object are known. The inverse scattering problem requires the determination of the size and shape of a scattering target from some given scattered radiation data, such as the far-field backscattered at certain aspects and frequencies for a given incident field. It is evident that any approach to this problem must be based on either the exact or some approximate theory of direct scattering. Thus in order to establish new inverse scattering model theories which can be applied more effectively and reliably to the recovery of targets,a simultaneous mathematical analysis of direct and inverse scattering theories needs to be undertaken.

In general, two fundamental approaches for obtaining approximate solutions to electromagnetic scattering problems [1] are known, i.e. estimates of either the frequency-dependent phasor response, or, the time-dependent impulse response can be attempted. Extensive amount of work in the frequency as well as the time domain have been done in the past [3,9,12,27, 45,61,67]. The inverse solution of Bojarski [21,25,51,66,81] in the frequency domain and Cosgriff-Kennaugh-Moffatt's [44,45,61] "time domain approach" fail to be the practical solutions because of a very large input information requirement; however, they provide an excellent mathematical treatment of the problem. In contrast, the polarization-depolarization characteristics of the electromagnetic waves which appear to have the potential to add new dimensions to inverse scattering techniques [7,8,32,33] have had very little importance in the direct and the inverse scattering investigations so far. Depolarization as understood in this investigation, refers to the change of the polarization of an electromagnetic wave from one state to another, brought about by the interaction of the wave with the scatterer. An electromagnetic wave has four basic characteristics: amplitude, frequency, phase and polarization; however, the research devoted to polarization problems, whether in optics or radio physics, has in the past represented only a small fraction of the research in electromagnetic wave propagation. This situation is gradually changing. Problems of polarization and depolarization have appeared with increasing frequency in recent years: In optics, due to the advent of the laser and coherent light; in radio physics, due to space communications, and the more exacting requirements on theoretical predictions for scattering by various classes of radar targets. In many cases observation of change in polarization permits greater insight into physical phenomena and this should be sufficient justification for studying the problem of polarization and depolarization in intimate detail. Thus, the purpose of this study is to use polarization-depolarization characteristics of electromagnetic wave scattering as a basic tool in developing improved techniques which can be applied successfully to the recovery of radar targets under various difficult situations. Based on the fact [7,19] that the "depolarization characteristics" of the scattered field do necessarily depend on the surface profile of the scatterer, the solution of the inverse problem of electromagnetic scattering by smooth, convex shaped, perfectly conducting, three-dimensional scatterers is analysed. To the best of the author's knowledge, this is the first attempt to solve the inverse problem of electromagnetic scattering along these lines. Therefore the main objective of this work is to show that the polarization-depolarization characteristics can indeed be used to recover the shape of the surface from observation of the monostatic backscattered field data.

At present, two inverse scattering model theories have found particular application in target recovery schemes. These are the Bojarski-Lewis inverse scattering theory [21,51] and the Kennaugh-Moffat time domain transient response method [45,61], both of which are based on the physical optics approximation [51,61]. Therefore, these methods can only be applied to identification of perfectly conducting shapes and furthermore, radar frequencies must be chosen such that the high-frequency approximation is satisfied. The objective thus is to investigate the possibility of extending the findings of the polarization-depolarization studies and thus to add a new dimension to the Bojarski-Lewis, the Kennaugh-Moffat and other inverse scattering theories. At this point it is appropriate to give a brief presentation of the various existing techniques mentioned above.

1.2 THE BOJARSKI-LEWIS INVERSE SCATTERING THEORY

The theory developed here was based on the physical optics or Kirchhoff approximation [51,61] for direct scattering. The starting point for this inverse scattering model is a remarkable identity obtained by Bojarski [21,22,25] and rederived by Lewis [50,51]. There,a three-dimensional space of vectors $\overline{\kappa}$ was introduced whose direction coincides with the aspect direction and whose magnitude is $\kappa = |\overline{\kappa}| = 2\omega/c_0$,where ω is the frequency. They also defined the characteristic function $\gamma(\overline{x})$ of the target and a function $\rho(\overline{\kappa})$ which can be obtained by measuring the far-field backscattered in the direction of $\overline{\kappa}$ at the frequency $\omega = |\overline{\kappa}|c_0/2$ See Fig.1.1 . The function $\gamma(\overline{x})$ is 1 inside the target and 0 outside

$\gamma(\overline{r})$ = 1 for $\overline{r}$ inside the (surface of the) scatterer
= 0 for $\overline{r}$ outside the (surface of the) scatterer

c_0 = Free space propagation velocity

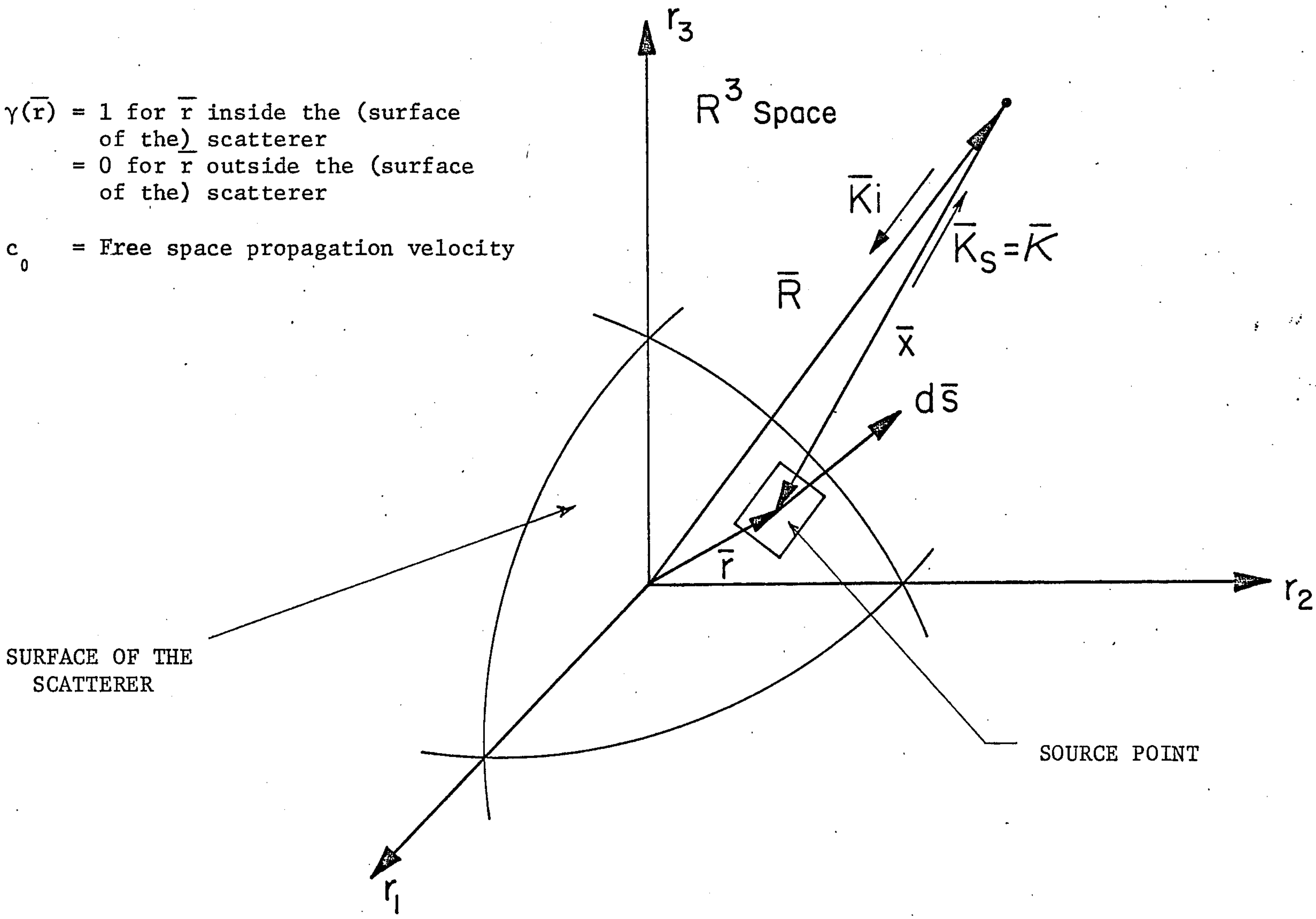

Fig. 1.1 Target Coordinates For Bojarski-Lewis Inverse Problem

of it. Then Bojarski's identity states that the functions $\gamma(\bar{x})$ and

$$\Gamma(\bar{\kappa}) = 2\sqrt{\pi}\ \frac{\rho(\bar{\kappa})+\rho^{*}(-\kappa)}{|\bar{\kappa}|^{2}} \tag{1.1}$$

are a Fourier-transform pair. Thus if $\rho(\bar{\kappa})$ could be measured in all of $\bar{\kappa}$ space one could immediately obtain $\gamma(\bar{x})$ and hence determine the target.

In practice, $\rho(\bar{\kappa})$, and hence $\Gamma(\bar{\kappa})$, can be measured only in a restricted range of aspects and frequencies, i.e., in a certain subset of $\bar{\kappa}$ space and thus, the inverse Fourier transform can no longer be used to directly obtain $\gamma(\bar{x})$. At this point Lewis [51] showed that if Q is the region in which Γ is known, one can choose a function $N(\bar{\kappa})$ which is zero outside Q and nonzero inside Q, so that $N(\bar{\kappa})\Gamma(\bar{\kappa}) = F(\bar{\kappa})$ can be measured in Q. Furthermore, it is possible to choose N such that $N(\bar{\kappa})\Gamma(\bar{\kappa})$ has an inverse Fourier transform and the convolution theorem holds. In this way one obtains the convolution integral equation of the first kind

$$f'(\bar{x}) = \int_{R^3} k'(\bar{x}-\bar{s})\gamma(\bar{s})d\bar{s} \quad , \quad \bar{x}\varepsilon R^3 \tag{1.2}$$

where f' and k' are the inverse Fourier transforms of F and N respectively. If this equation can be solved, then the size and the shape of a perfectly conducting target can be determined.

The expression for $\Gamma(\bar{\kappa})$ given by (1.1) indicates that the measurement of $\Gamma(\bar{\kappa})$ in a domain Q requires measurement of ρ in Q and in Q', which is the reflection of Q through the origin. Thus if Q corresponds to an aspect near the "front" of the target, ρ must unfortunately be measured also near the "back". Since this would, in many applications, be a severe limitation, Lewis [51] attempted to eliminate the domain Q'. There, a modification to the general theory is presented which, under suitable conditions, yields the "front half" of the target using measurements of ρ in Q. Lewis [50,51], Tabbara [81] and Bojarski, in a multitude of reports [21,22,24,25], have obtained solutions of (1.2) for specific apertures. However, a study of these reports reveals that a staggering amount of data is required, and that the Bojarski-Lewis inverse scattering technique, at the present time, cannot be applied in practice.

The fundamental difficulty in obtaining a solution to the Bojarski-Lewis inverse problem is that the available method used in solving the Bojarski identity, that is the solution of (1.2), is an ill-posed problem [48,51, 66]. A detailed study of the shortcomings of the Bojarski-Lewis inverse scattering solution was presented by Perry [66] who not only showed that (1.2) is illposed, but that for stable inversion the lowest eigenfrequency of the kernel in (1.2) corresponds to the value of $|\overline{\kappa}|$ far below the high-frequency region. This fact, however, rules out the judicious application of the Bojarski-Lewis inverse scattering technique as it is based on the physical optics approximation which holds only for high-frequency scattering.

From the large body of literature dealing with the Bojarski-Lewis problem it is apparent that the Bojarski-Lewis inverse theory requires fundamental improvement. For example, it does not incorporate complete polarization information which can be made available with modern polarization doppler radar systems. Utilization of polarization as related to inverse scattering is discussed later in this chapter.

1.3 TIME DOMAIN APPROACH

Compared to the frequency domain and the classical approach to electromagnetic scattering problems, there has been relatively little work done on scattering problems with general time variation. Yet the most distinctive radar signature of an object surely lies in the time variation of the scattered signal. Probably the most fundamental and useful result would be the computation of the field scattered by an arbitrary shape when the incident wave is an impulse. This scattered field is called the electromagnetic impulse response.

For a number of reasons the electromagnetic impulse response of a scatterer is one of the most interesting results to be obtained from the time domain analysis. First, the transient scattering produced by an arbitrary time-varying excitation field can be obtained from the impulse response by use of the convolution integral. Second, the Fourier transform of the impulse response leads to the spectral or frequency domain characteristic. One practical use of the transient behaviour is the analysis of radar returns wherein the impulse response can serve as a "signature" for target identification. Thus in an inverse scattering problem, the impulse response itself may be used as a characteristic function of the scattering object.

Various approaches have been used to obtain the response of different scatterers to impulse excitation. The physical optics approximation was evidently first employed by Kennaugh and Cosgriff [44] to calculate the monostatic far-field impulse response of a rectangular plate, a spheroid, and a sphere. Further extensions of the physical optics approach were carried out in a series of publications by Kennaugh and Moffatt [45,59-61]. They defined an impulse response transform pair $[F_I(t), G(j\omega)]$ for the scattering system, i.e.

$$G(j\omega) = \int_0^\infty F_I(t)e^{-j\omega t}dt \tag{1.3}$$

Furthermore by using the power series expansion of $G(j\omega)$ they obtained a restriction on $F_I(t)$ in the form of moment conditions [61]. With Rayleigh's law of scattering postulations, and utilizing the moment conditions along with the assumption that the currents set up on the scatterer surface are approximated by the physical optics approximation, Kennaugh-Cosgriff [44] obtained the approximate result that the "projected area function", $A(t)$, of a target is proportional to its ramp response (Fig.1.2). This implies that the impulse response predicted by physical optics is a waveform equal to a multiple of the second derivative of $A(t)$. The exact expression given by Kennaugh and Moffatt [45] is:

$$F_I(t) = -\frac{1}{2\pi c_0}\frac{d^2A(t)}{dt^2} \quad ; \quad c_0 \text{ , velocity of light in free space} \tag{1.4}$$

Time domain scattering analysis has also been done in the area of acoustics. Sound pulse diffraction by infinite length, arbitrary cross-section cylinders has been considered by Friedman and Shaw [35], while transient scattering by rigid spheres has been studied by Soules and Mitzner [76].

The available published work in time domain scattering can be separated into different classes. In one approach the calculated frequency response

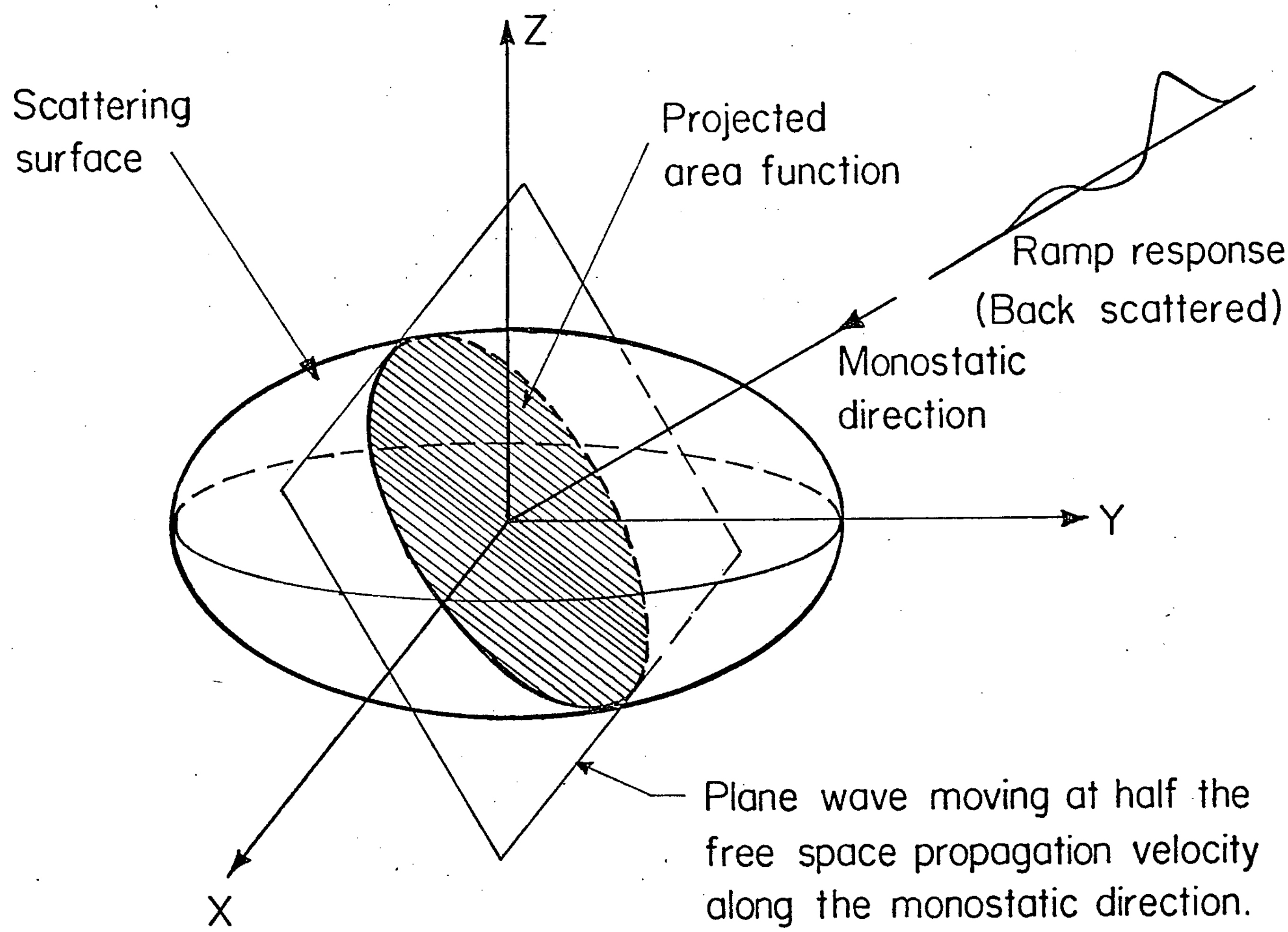

Fig. 1.2 Projected Area Function Along The Direction of Incidence

of the scatterer is used to synthesize the time domain response for a specified excitation. Two separate catagories are contained within this approach, one of which uses the analytical frequency domain solution which has a very limited scope, while the other makes use of numerically evaluated frequency domain solutions. A second approach includes those analyses which employ approximations to the frequency domain response such as physical and gemoetrical optics. Obviously this particular approach has its limitations; however, it does indeed show merits at high frequencies. A third method for obtaining the impulse response of scatterers is one which originated from a strictly time domain view point. This method has been applied to acoustics by Soules and Mitzner [76] and to electromagnetic problems by Bennett and Weeks [10] and also by Sayer and Harrington [71]. It is this particular approach, using the time domain integral equation, which has been followed in this investigation and used to develop an inverse scattering model in later chapters.

A solution for the inverse scattering problem using a space-time integral equation was reported by Bennett and co-workers [11,13]. In this study the inverse scattering problem is formulated as an inversion of the space-time integral equation. An iterative technique was developed for the solution of the inversion equation and applied to some simple symmetrical cases with success. The results of this work provide a sound foundation on which a viable time domain approach to the inverse scattering problem can be built. This technique also pointed out the fact (as expected from the asymptotic nature of the physical optics solution) that the relation between the impulse response and two derivatives of the projected area function is exact only at the leading edge of the scattered field response, a single point in time. After the leading edge, the response is altered by currents arriving from other space points. Therefore, the physical optics solution must be "corrected" to account for these currents flowing on the body. For a given object, if the incident pulse width is small compared to body size (the high frequency limit), then the correction currents will have a small effect and optical rays can be placed in one-to-one correspondence with points on the body. Contrary to this, if the body is comparable in size to the pulse width, then the "correction" terms have a strong effect on the solution and the physical optics solution is degraded. In the case of small bodies, the correction terms dominate the result and the physical optics solution is meaningless.

A second approach to time domain inverse scattering was based on the observation that the low frequency approximation of the impulse response of the scatterer determines the waveform,shape and size, whereas the high-frequency information relates to the fine structure and detail in the waveform [61]. This fact has been used in obtaining a technique for radar target classification by using multi-frequency radar returns [57, 63,69,83]. The time domain signature used in such a technique is the ramp response waveform, which was first suggested for implementation in radar identification by Kennaugh and Moffatt [45]. As described earlier, the ramp response is the second integral of the impulse response of a target, and hence shares several of its useful properties. The ramp response is unique with respect to target shape, orientation, and material composition. It is the inverse Fourier transform of a target's complex backscattered frequency spectrum multiplied by the factor $(1/(j\omega))^2$[61]. Because of this factor, Kennaugh and Moffatt predicted that a satisfactory approximate ramp response could be obtained with a comparatively narrower bandwidth interrogating signal than for the impulse response. Thus, the complex harmonic samples of the backscattered response for three orthogonal look angles [95,96] at ten harmonic frequencies (with ω_0 as the fundamental frequency the tenth harmonic would be $10\omega_0$) lying in the low resonance range of the target response spectrum,are used as input data for this approach. A periodic ramp response waveform synthesized from these data is used to construct the surface of the scatterer. Two general relationships which are important for target imaging have been utilized in this method for generating the target surface. First, the amplitude of the waveform versus time is approximately proportional to the "target profile function" [61]. The profile function is defined as an artificial time domain waveform equal to the target cross-sectional area intersected by an imaginary transverse plane moving along the line of sight at one half the velocity of the transient incident signal as shown in Fig. 1.2. The second relationship utilized is that the integral of the ramp response waveform is proportional to the Rayleigh coefficient. This has also been predicted from analysis of the lower order moments [61]. Thus an approximate volume estimate was obtained from the ramp response waveform.

The above relationships and their applications in this technique indicate that the ramp response is a promising signature for target identification purposes. However, because of the nature of the data, i.e. three orthogonal look angles, a three-dimensional image cannot be uniquely specified. It can be proven that more than one shape satisfies any three look angle profile function set. Thus, this method generates a "likely" image using simplified, rather than generalized surfaces with a few adjustable parameters. There are obviously many questions unanswered concerning this technique. For example, the possibility of estimation of target orientation using the polarization properties of the Rayleigh coefficient could be investigated. Also, in all the above mentioned techniques only the first three terms of the power series expansion of $G(j\omega)$ were considered, however it might be possible to study higher order terms which might yield an important relationship between target wave-form response and target polarization-depolarization characteristics.

1.4 CLASSICAL ANALYSIS

The classical approach to electromagnetic scattering problems is an analysis based on the differential equations for the fields, together with the boundary conditions at the scatterer. A classical inverse method of portraying rotationally symmetric scatterers was based on the inversion of the scattered field matrix associated with the representation of the far scatterered field in terms of a series expansion in appropriate vector wave functions. As an application of the above mentioned method, the circular cylinder [16], the sphere [17], the elliptic cylinder [86], and the prolate spheroid [87] have been specified uniquely in terms of associated expansion coefficients. In this series of publications it has been demonstrated that for the cases of the above mentioned rotationally symmetric scatterers the electrical radii of curvature can be recovered directly from a limited set of contiguous expansion coefficients, which are obtained to an accuracy dictated only by the measurement techniques if a certain specific optimization procedure [89] is employed.

However, if the electrical radius is much larger than unity, which increases the order of the scattered field matrix, or if the domain of observation is limited to a small solid angle, the inversion of the matrix remains highly unstable and leads to partially erroneous results. Further investigation has revealed that although this classical approach to the recovery of the curvature results in a great saving of time in computation and rather simplified calculations, it suffers several limitations in practice which require further analysis. First of all this classical approach [16,17,86,87] is strictly concerned with the identification of the shape of rotationally symmetric objects, for which separation of the wave equation into orthonormal vector wave functions is possible. Secondly, in order to recover the electrical radius with a high degree of confidence, the field coefficients [79] must be specified up to the first four significant digits [18]. In practice, the accuracy and the resolution of any measurement technique is not likely to be up to this standard, especially if both amplitude and phase of the far-scattered field must be measured as is required here. Thus it can be summed up by saying that this classical inversion method is presently not applicable in practice where other techniques demanding less accuracy are desirable. This classical approach, however, continues to be of much importance in present theoretical and possible future practical problems.

Another classical approach to inverse scattering which makes use of the so called concept of electromagnetic inverse boundary conditions was introduced by Weston and Boerner and others [92-94]. Methods using these inverse boundary conditions to recover both the shape and the averaged material surface properties η of a closed scatterer, if the near field can be recovered accurately, were shown by Boerner and others [18,20]. In direct problems of scattering and diffraction the shape and the material constituents of the scatterer, which are known a priori together with the prespecified incident field, may be incorporated into the boundary conditions. In an inverse problem, in general, no information about the scatterer may be assumed. Therefore, in this case such boundary conditions must be sought which do not depend on the shape or the material properties of the scattering body, but allow to specify those characteristic parameters uniquely from the near field which needs to be recovered from far-field measurements.

In principle, the inverse boundary conditions derived by Weston, Boerner and others [92-94] result from the inversion of the Leontovich or scalar impedance boundary condition [49] which is an approximation and thus its application is restricted. To point out the major restrictions imposed on the nature of the scatterer which can be treated with the Leontovich boundary condition, it is noted that this boundary condition is a valid approximation to the true condition if the radii of curvature are large everywhere compared with the wavelength [72]. It can also be justified [73] even when η varies from point to point, provided the variation is sufficiently slow. For an open surface the aforementioned conditions are sufficient, whereas for a closed surface it is required in addition [18] that the penetration depth is small compared with the smallest radius of curvature in question, so that inward-traveling fields do not reach the surface again. Consequently, loss-less objects such as dielectric slabs, cylinders, spheres etc. are untreatable by the surface impedance conditions regardless of their dimensions. The question of uniqueness of the inverse boundary conditions derived from the Leontovich boundary condition was studied in detail recently [20] and it was shown that for both the perfectly as well as the imperfectly conducting cases, the uniqueness of the inverse boundary conditions depend on polarization and target symmetry. For example, incidence of a circularly polarized plane wave along the invariant axis of a rotationally symmetric scatterer will result in the fact that the inverse boundary conditions are satisfied everywhere, thus they cannot be applied in this particular degenerate case. Otherwise, it was shown that it is possible that the shape, the phase and the modulus of the averaged surface impedance of the scatterer can be recovered uniquely. Finally, it is pointed out that although in practice the measurements required for the aforementioned exact inverse problem are not possible, the understanding of the exact problem gives a better insight into the limitations and errors when approximate or asymptotic techniques are employed, and can lead to further development of these methods.

1.5 SIGNATURE COMPARISON TECHNIQUES

Two representative signature comparison techniques are discussed in this section.

(i) Iterative averaging method [88]:

Based on the fact that smooth and convex-shaped scatterers of identical curvature about the monostatic direction give rise to identical far-scattered field magnitude in the high frequency case, an inverse scattering technique for the recovery of the local radii of curvature of remote scatterers about the specular point was developed [88]. It was assumed that measured data are available for various directions of illumination covering all sets of overlapping finite domains of the scattering surface.

From the theory of geometrical optics, as applied to the problem of high-frequency diffraction by scatterers of slowly varying convex shape [41,43], it is known that the leading term in the asymptotic expansion of the scattered field depends primarily on the local radius of curvature of the illuminated area. This behaviour, in the backscattering direction, is the foundation of the system synthesis approach introduced in this recovery technique referred to as the iterative-averaging method. This method uses the fact that a knowledge of the field's magnitude necessarily reflects some information on the curvature of the scatterer. By comparing the scattering pattern of various objects it was found that the larger the radius of curvature, the larger is the magnitude of the backscattered field. Notwithstanding this general overall behaviour, small superimposed amplitude oscillations about a mean value of the field magnitude often arise. These second order effects are dependent on the second term in the asymptotic expansion [41] which includes both the local radius of curvature of a smooth, convex shaped scatterer and its space rate of change with respect to the surface coordinate. The iterative averaging method however neglects these superimposed, small-field oscillations. Applying techniques well-known in system systhesis, this iterative averaging method compares the averaged magnitude of the backscattered field, given off by the unknown, with that resulting from a known rotationally symmetric scatterer, which can be most easily calculated. Thus, from the mean value of the field, calculated at various backscattered directions, the local radius of curvature of the scatterer is obtained via an iterative comparison process, employing well established methods of system synthesis. The recovery of the local radius is, hence, viewed as the synthesis of the system described by the relationship between the geometry of the remote scatterer and the measured backscattered field's magnitude for given wave incidence. It should be observed that the suggested iterative-averaging method is applicable only in high frequency cases i.e., when the local radii of curvature are large enough so that creeping wave effects are negligible in determining the field distribution near the backscattering angle.

(ii) Pattern recognition technique [37]:

This technique investigates the radar target identification problem through an approach that does not depend on obtaining radar imagery of optical quality and high resolution in range and azimuth. Instead, pattern recognition techniques are applied to radar magnitude and phase-versus-frequency data which are obtained at resonance region frequencies. Furthermore it is also understood in this problem that no aspect angle information is either known *a priori* or measured.

In this work, it was concluded that the solution to the problem lies in the resonance region. If the frequency is too low (Rayleigh region) there is no shape-dependent information in the scattering. If it is too high, the scattering becomes highly aspect-angle dependent. If the exact aspect angle of the target is not known, application of the pattern recognition technique to magnitude-versus-frequency data obtained at high frequency may become an enormous task because of the huge amount of data that have to be catalogued. At resonance region frequencies, small changes in aspect angle do not cause rapid fluctuations in the data, yet there is shape-dependence of the data. For the objects studied in this investigation, there appears to be enough information in one or two octaves (if the lowest frequency used is ω_L, one octave would be $2\omega_L$) of radar bandwidth to allow separation and classification of radar targets. Thus the design logic here is based on two constituents: the use of lower radar frequencies as discriminants [45], and data processing by pattern recognition technique to achieve target identification. Based on digital spatial frequency filtering of curves of the radar return versus the radar frequency, algorithms which optimize separation between pairs of input data were developed.

From the results obtained by the above technique it is evident that there is enough information in the data contained in one or two octaves of resonance region frequencies for a radar to discriminate between targets that are the same in size but different in shape. To achieve identification, the wavelength need be just short enough for the differentiating features to be at least a quarter-wavelength apart. Within the limits of this restriction, however, the wavelength should be as long as possible to minimize aspect angle-dependence. It is also concluded that a practical multifrequency radar system that can measure phase and cancel out polarization effects by means of the method developed in this technique is feasible. Such a system can provide data suitable for pattern recognition algorithms. For the phase measurement to be absolute rather than relative, the phase of the backscattered field must be known at one frequency. This can be ensured by choosing a frequency low enough for the targets of interest to be in the upper Rayleigh region; it has been shown that in this region the phase shift is zero.

From the review of various available signature comparison techniques it is realized that these methods are applicable only to a restricted class of objects whose characteristic scattering behaviour is known *a priori*. Thus such an approach to inverse scattering problems can at best provide a partial solution. Furthermore very little insight to the physical phenomena is provided by such approaches.

1.6 SINGULARITY EXPANSION METHOD (SEM)

SEM provides a new approach [6] to the problem of the interaction of electromagnetic fields with bodies located in free space or in other simple media. The basic idea involved in this technique is to expand the solution to an electromagnetic interaction problem [scattering problem, propagation problem, or any linear problem (not necessarily electromagnetic)] in terms of the singularities of the response in the complex frequency plane. Such singularities can take various forms such as poles, branch points (and associated branch cuts), essential singularities, and singularities at infinity. For restricted classes of objects, such as finite sized objects in free space, these s-plane singularities are limited to poles and possible singularities at infinity [6,36,82].

In the singularity expansion method the electromagnetic interaction with objects is characterized in terms of quantities directly identifiable with various characteristics of resulting interaction waveforms. Some characteristics are associated with the object characteristics including the presence of neighboring objects. Other characteristics are associated with the waveform of the incident field. Yet others are associated with the spatial distribution of the incident fields, such as specified by the direction of incidence and polarization. What is in effect accomplished through this technique is a decomposition of the interaction problem into various quantities which depend on different variables of the problem. The dependence of the interaction on different variables can then be separately considered resulting in a considerable simplification in understanding how the resulting electromagnetic interaction can vary over all possible variations of the parameters of a particular problem being considered. This effectively extends the complexity of the object geometries one may be willing to consider for detailed calculations.

Based on the fact that the electromagnetic interaction problem could be decomposed into various quantities which depend on different variables of the problem, some schemes for detection and discrimination of radar targets have been proposed [47,63,83]. Moffatt and Mains [63] have recently suggested the concept of using the complex natural resonance of objects [i.e.singularities of the object response waveform in the complex frequency plane] as a tool in target discrimination. They make use of the fact that the positions of the natural resonances in the complex frequency plane are excitation invariant,i.e., they are not a function of aspect angle, and that in general only the first few low frequency poles are necessary to characterize an object [61]. Their identification scheme uses a fitting technique to achieve a quantitative evaluation of the correlation between a measured transient waveform synthesized from multiple frequency scattering data [63] and a calculated difference equation waveform using difference coefficients (obtained from complex natural resonant frequencies) for a particular scatterer. Examples of discrimination results obtained for two wire geometries over a wide range of aspects in two principal planes using complete (10 frequencies) backscatter data has been reported [63]. The same procedures were also applied using incomplete backscatter data, i.e., with amplitude and phase data at certain frequencies arbitrarily set to zero. With minimal backscatter data requirements established, discrimination results were presented when the minimal data are taken from different target orientations [55, 63]. The results have demonstrated the possibility of drastic reduction in the bandwidth requirements for a multiple frequency discrimination radar and also that the backscatter data required can be obtained using near-conventional radar systems.

A similar radar target recognition technique that makes use of the fact that the complex natural frequencies of a target are intrinsic only to the body geometry, was reported by Van Blaricum and Mittra [83]. This scheme makes use of a technique which numerically extracts the complex resonances of a target from a time signature [84]. The recognition technique suggested by Van Blaricum and Mittra [83] applies this method to reduce the digitized backscattered time signature to a collection of complex frequencies which, as shown by Mains and Moffatt [55,63], characterizes the scatterer. Then these frequencies serve as the input to a pattern recognition algorithm which compares these extracted poles to those in a catalog to identify the target. The basic distinction between this scheme and the Mains and Moffatt [55] scheme is the form in which measured data are compared with target dictionary information. Mains and Moffatt generate a given transient waveform based both on the measured waveform and a given dictionary entry. This waveform is compared with the measured waveform. The scheme reported in Van Blaricum and Mittra [83] extracts the natural frequency content directly from the measured waveform, and the natural frequencies themselves are compared with dictionary entries.

Again all these target recognition schemes based on the singularity expansion method are simply signature comparison techniques. Thus their application is limited to a restricted class of objects whose characteristic scattering behaviour is known *a priori*. Furthermore polarization-depolarization aspect of the singularity expansion method has not been exploited in these techniques.

1.7 POLARIZATION UTILIZATION

The problem of polarization and depolarization have gained a considerable amount of attention in recent years; in optics, due to the advent of the laser and coherent light; in radio physics, due to space communication and the more exacting requirements on theoretical predictions for scattering by rough surfaces and radar targets. The possible application of the phenomenon of depolarization in the inverse scattering theory for better target identification/discrimination under various difficult situations needs to be investigated. Rigorous equations describing the depolarized echo of radar reflectors as a function of their physical shape and the polarizational state of the incident wave are known [7,8,77]. These relations could possibly be used in recovery of target shape and material information from known depolarization characteristics of the target. An exhaustive treatment of the depolarization caused by flat or rough surfaces [7,8] reveals that physical optics predicts a cross-polarized component in the backscattered direction whereas geometrical optics fails to uncover it. Starting with the Stratton-Chu-Silver integral [75] and by applying proper boundary conditions and resolving the scattered field into parallel and cross-polarized components, integral representations for the depolarization ratio are obtained. This expression is a function of the shape and material composition of the scattering object.

To the best of the author's knowledge, so far, the application of the depolarization characteristics to the inverse scattering problem (although with a limited scope) was attempted only by Erteza and Doran [32,33]. Although they called it "application of the concept of differential reflectivity", however essential to the determination of the unknown parameters was the measurement of the ratio of the power densities in two cross-polarized components of the scattered field. Erteza and Doran [32,33] presented a method for the determination of the permittivity and permeability of a large (compared with wavelength), smooth convex body, using a ray tracing technique [26] for vector fields. Implementation of the method involved the measurement of the ratio of two components of a reflected field for two distinct source-target-scattered field point configurations, with monochromatic, linearly polarized illumination of the target. This differential reflectivity technique essentially circumvented the boundary-value problem and led directly to the integral expressions for the scattered fields. Although a large number of simplifying assumptions were made in order to accomplish evaluation of these integrals [32], the resulting field and power expressions contain as first-order terms identical expressions to those that would be obtainable by a straightforward geometrical-optics approach. This provides a check for the Erteza and Doran [32,33] approach and also implies the feasibility of the use of the depolarization characteristics for the solution of a larger class of inverse scattering problems.

A possibility of incorporating the depolarization ratio in the scattering matrix (SM) representation [15,23,34,39] has been investigated. Inversion of the scattering matrix is expected to yield target information as function of the depolarization ratio and the aspect angle. Some special radar target scattering matrices are listed by Huynen [39], and their application to rough surface scattering is presented. This approach might provide a better understanding of the physical aspects of the target/clutter problem. A study of depolarized backscatter by Chytil [28, 29] showed that for curved surfaces the depolarization ratio D_p decreases as ka^{-n} (where $k = 2\pi/\lambda$) with "a" as the characteristic dimension of the scatterer (i.e.,width of strip, radius of circular cylinder, etc.) and $1 \leq n \leq 4$. Various investigations [40,56,74] have revealed that the polarization characteristics of the radar return signals from the atmospheric formation (i.e., clouds or atmospheric precipitation) contain information about the phase state of the water as well as shape and orientation of the particles in the formation. This property of the polarization is already in use for radio meteorological investigations of the shape and orientation of cloud and precipitation particles and also to analyze their phase state [74]. Finally it is pointed out that the targets differ from the "interference-reflectors" in the medium through their characteristic shape and structure. Therefore the polarization-transforming properties of the targets should provide an adequate means for the identification of the said shapes buried under clutter. This makes the study of the correlation between the depolarization power and the shape characteristics of reflectors even more desirable when dealing with inverse scattering solutions.

1.8 UTILIZATION OF DIFFERENTIAL GEOMETRY IN INVERSE SCATTERING PROBLEMS

Besides polarization-depolarization characteristics, another aspect, i.e., differential geometry as related to the surface profile inversion has been given very little importance in inverse scattering investigations. It is to be noted that for the vector treatment of the scattering at the surface of a convex three-dimensional object, as is the case here, differential geometry provides additional insight to the physical phenomenon that governs the interaction between the object and the electromagnetic fields. In differential geometry there are classical problems concerning closed convex surfaces in three-dimensional space which can be intimately related to the electromagnetic problem of profile inversion of closed convex shaped scatterers. In fact one such problem, the so called "Minkowski problem" [38,64] is being studied in the context of the present investigation. It appears to be possible to combine the mathematical concepts of the Minkowski problem with the polarization-depolarization aspects of the electromagnetic scattering concepts to set up a system of equations for the recovery of the surface of the scatterer.

In this investigation the fundamental link between electromagnetic theory and the differential geometry is provided by the Gaussian curvature of the scatterer at the point of interest (i.e., specular point). The Gaussian curvature, being an important parameter in differential geometry and at the same time related to the backscattered cross-section at a sufficiently high frequency [41], allows one to relate the results of differential geometry to the electromagnetic problem of inverse scattering. A detailed discussion of this aspect of the investigation is provided in Chapter Two.

In summary, though there exists a large body of literature dealing with the direct scattering problem, the number of treatises dealing with the inverse problem are relatively few. This is due primarily to the complexities associated with the inverse problem. For one thing, it would be a lot simpler to extract the quantitative information regarding the properties of a scattering body from the scattered signals if these scattered signals were derivable in closed form. Unfortunately, even the simplest of scattering problems tends to yield solution in the form of slowly converging infinite series, from which the desired information can hardly be obtained. Secondly, many of the inverse problems do not lend themselves to a formulation in terms of linear matrix- or integral-equations; and, consequently, sophisticated techniques such as polarization-depolarization characteristics and other systems approaches are required to resolve them. It is to be noted that even when it is possible to describe the inverse problem in terms of a linear matrix equation, the resulting equation is often ill-conditioned, and its inverse is unstable as was pointed out earlier in this chapter regarding the Bojarski-Lewis inverse problem. Special techniques are again necessary to handle these cases.

chapter two

MINKOWSKI'S PROBLEM AS RELATED TO ELECTROMAGNETIC INVERSE SCATTERING

2.1 INTRODUCTION

For the vector treatment of the scattering at the surface of a convex three-dimensional object, as is the case here, differential geometry provides additional insight to the physical phenomenon that governs the interaction between the object and the electromagnetic fields. However, differential geometry as related to the surface profile inversion has been given very little importance in inverse scattering investigations.

In differential geometry there are classical problems concerning closed convex surfaces which can be intimately related to the electromagnetic problem of profile inversion of closed convex shaped scatterers. In the context of the proposed investigation there are two such problems in differential geometry concerning closed convex surfaces in three-dimensional space, i.e., surfaces which are the full boundaries of bounded convex sets in three-dimensional space. In these cases the parameter surface is the entire unit sphere and the surface in space is its topological image [64, 80]. These problems concerning such surfaces can be formulated as follows [64]:

(i) Minkowski's problem: The Gaussian curvature K is given as a positive function of the direction of the normal to the surface, i.e., the spherical image of the surface is arbitrarily prescribed. The existence and uniqueness of a closed convex surface having the prescribed spherical image is required to be proved.

(ii) Christoffel-Hurwitz's problem: This problem is the same as the Minkowski problem except that the sum of the principal radii of curvature (or, stated otherwise, the ratio of the mean curvature to the Gaussian curvature), instead of the Gaussian curvature, is prescribed as a positive function of the direction of the surface normal. The existence and uniqueness of the convex surface having this property are required to be proved.

This chapter deals with the concepts of differential geometry and the Minkowski problem in particular. In Section 2.2, the transformation of the object surface onto the unit sphere via Minkowski's support function [64,80], which is an important step towards the formulation of the Minkowski problem, has been discussed. The mathematical statement and some curvature related formulas of the problem itself have been developed in Section 2.3. The geometrical optics relationship [26,42] between the scattering cross-section and the Gaussian curvature, along with its application in linking up the Minkowski problem to the inverse scattering problem, has been pointed out in Section 2.4. Finally, an example of a two-dimensional case, where it is possible to obtain an explicit solution of the inverse electromagnetic problem directly from the concepts of geometrical considerations, has been presented in Section 2.5. At this point it is to be noted that in the present investigation no attempt has been made to actually solve the Minkowski problem, but the related differential equations have been used in Chapter Four to derive a condition which relates the surface parameter of the scatterer to the radar measureables.

2.2 MINKOWSKI'S SUPPORT FUNCTION [52,64]

In Fig. 2.1, let $\hat{X}(x,y,z)$ be a closed convex surface (Gaussian curvature $K > 0$) containing the origin in its interior. The inner unit normal (ξ,η,ζ) defines the spherical image of the surface. Let $p'(\xi,\eta,\zeta)$ represent the distance from the origin to the plane tangent to the surface at the point where the inner normal is (ξ,η,ζ) (see Fig.2.1). $p'(\xi,\eta,\zeta)$ is defined in this manner for all values of ξ,η,ζ, satisfying $\xi^2 + \eta^2 + \zeta^2 = 1$.

The extension of this function to all variables ξ,η,ζ as a homogeneous function of degree one is called the Minkowski support function. i.e.,

$$M(\xi,\eta,\zeta) = (\xi^2+\eta^2+\zeta^2)^{1/2}\cdot p'\left[\frac{\xi}{(\xi^2+\eta^2+\zeta^2)^{1/2}}, \frac{\eta}{(\xi^2+\eta^2+\zeta^2)^{1/2}}, \frac{\zeta}{(\xi^2+\eta^2+\zeta^2)^{1/2}}\right] \quad . \tag{2.1}$$

It satisfies the Euler relations [80] for homogeneous function of degree one, i.e.,

$$\xi M_\xi + \eta M_\eta + \zeta M_\zeta = M \quad , \tag{2.2}$$

$$\xi M_{\xi\xi} + \eta M_{\xi\eta} + \zeta M_{\xi\zeta} = 0 \quad , \tag{2.3}$$

$$\xi M_{\xi\eta} + \eta M_{\eta\eta} + \zeta M_{\eta\zeta} = 0 \quad , \tag{2.4}$$

$$\xi M_{\zeta\xi} + \eta M_{\zeta\eta} + \zeta M_{\zeta\zeta} = 0 \quad , \tag{2.5}$$

where the subscript denotes partial differentiation with respect to ξ,η,ζ. The function M is very useful in the treatment of Minkowski's problem, therefore some of its properties are noted next.

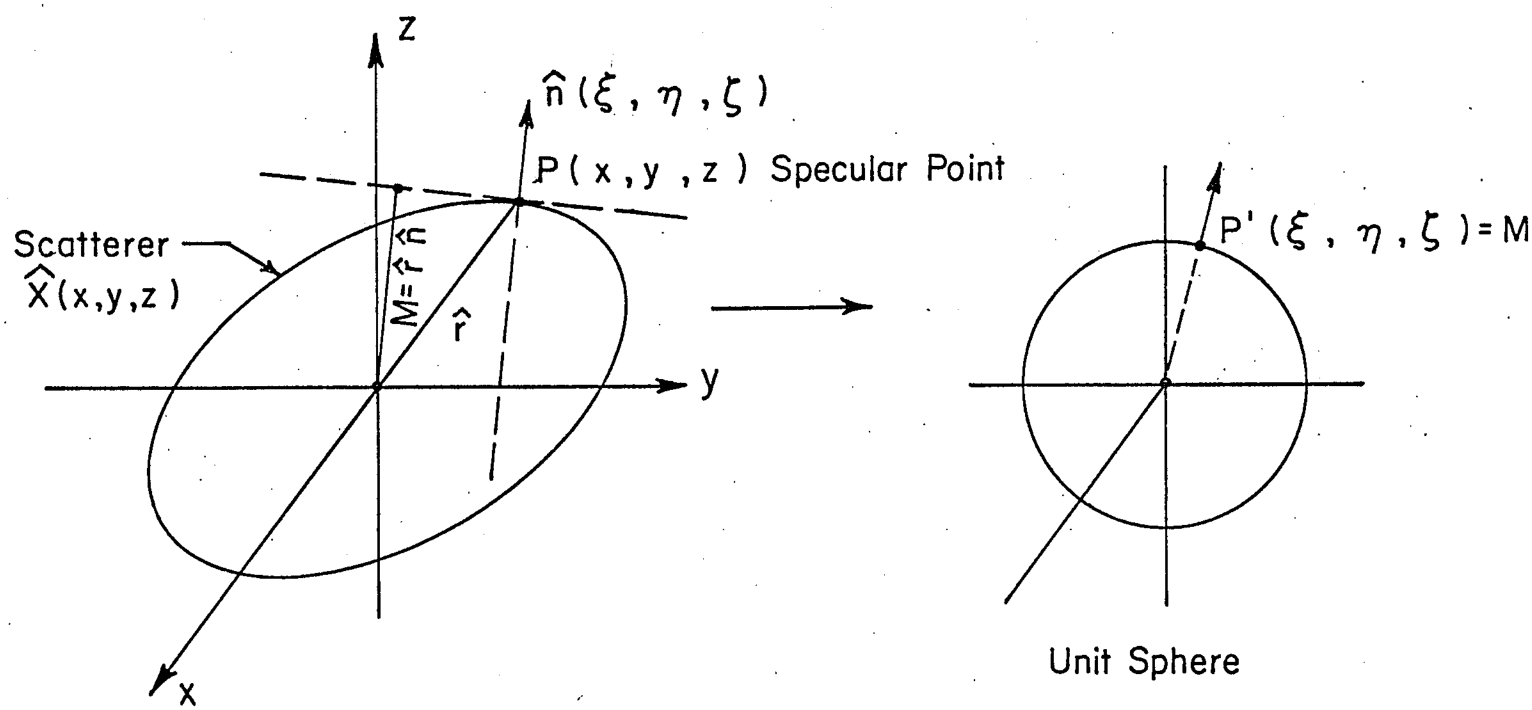

Fig. 2.1 Transformation of the specular point unto the unit sphere by Minkowski's support function.

Since the Gaussian curvature of the surface is positive, there corresponds to each point on the unit sphere exactly one point on the surface having this point as its spherical image. So the coordinates x,y,z of the surface may be considered as functions of ξ,η,ζ within the restriction $\xi^2+\eta^2+\zeta^2 = 1$. From the definition of M given above it is evident that (see Fig.2.1)

$$\overline{r} \cdot \hat{n} = M(\xi,\eta,\zeta) \qquad .$$

But since $\hat{n}\cdot d\overline{r} = 0$ because $\hat{n}$ is a normal to $\hat{X}(x,y,z)$, it follows that

$$\overline{r} \cdot d\hat{n} = dM(\xi,\eta,\zeta)$$

with $d\hat{n} = (d\xi,d\eta,d\zeta)$, or, in coordinate form

$$x = M_\xi \; , \; y = M_\eta \; , \quad z = M_\zeta \tag{2.6}$$

Thus, once the Minkowski support function is given over the entire unit sphere, the corresponding closed convex surface is known. Another important observation which follows from (2.6) is that if two support functions differ by a linear function, the corresponding surfaces differ by at most a translation.

2.3 MATHEMATICAL STATEMENT OF THE MINKOWSKI PROBLEM

In this section the derivation of various formulae which yield the curvature properties of the surface $\hat{X}$ are presented. For this purpose, the formula of Rodrigues [80] which holds along a line of curvature is used:

$$d\hat{X} + Dd\hat{n} = 0 \qquad .$$

Here D is the principal radius of curvature, and $\hat{n}$ the unit normal. In components, this may be written in the form:

$dx + Dd\xi = 0 \quad ; \quad dy + Dd\eta = 0 \quad ; \quad dz + Dd\zeta = 0$

with $\hat{X} = (x,y,z)$ and $\hat{n} = (\xi,\eta,\zeta)$. It is assumed that the surface is determined by the support function M through (2.6), and hence all quantities associated with the surface are likewise determined by M as homogeneous functions of an appropriate degree, i.e., from (2.6)

$$dx = M_{\xi\xi}d\xi + M_{\xi\eta}d\eta + M_{\xi\zeta}d\zeta$$
$$dy = M_{\eta\xi}d\xi + M_{\eta\eta}d\eta + M_{\eta\zeta}d\zeta$$
$$dz = M_{\zeta\xi}d\xi + M_{\zeta\eta}d\eta + M_{\zeta\zeta}d\zeta$$

Thus Rodrigues' formula may be rewritten as

$$(M_{\xi\xi}+D)d\xi + M_{\xi\eta}d\eta + M_{\xi\zeta}d\zeta = 0 \tag{2.7a}$$

$$M_{\eta\xi}d\xi + (M_{\eta\eta}+D)d\eta + M_{\eta\zeta}d\zeta = 0 \tag{2.7b}$$

$$M_{\zeta\xi}d\xi + M_{\zeta\eta}d\eta + (M_{\zeta\zeta}+D)d\zeta = 0 \tag{2.7c}$$

It is to be noted that the variables ξ,η,ζ are to be treated as independent variables in the above equations and in all the subsequent formulae involving the support function.

The homogeneous linear set of equations (2.7a) to (2.7c) for the quantities $d\xi$, $d\eta$ and $d\zeta$ have a non-trivial solution since principal directions exist, and the principal radii of curvature D_1 and D_2 are thus roots of the following determinantal equation

$$\begin{vmatrix} M_{\xi\xi} + D & M_{\xi\eta} & M_{\xi\zeta} \\ M_{\eta\xi} & M_{\eta\eta} + D & M_{\eta\zeta} \\ M_{\zeta\xi} & M_{\zeta\eta} & M_{\zeta\zeta} + D \end{vmatrix} = 0 \quad . \tag{2.8}$$

From (2.3), (2.4) and (2.5) it is evident that the determinant of the matrix of the M_{ik} (where $i,k = \xi,\eta,\zeta$) vanishes because that system of equations [i.e., (2.3) to (2.5)] is satisfied for at least some sets of values of the (ξ,η,ζ) which do not all vanish simultaneously. Using this fact, the above determinantal equation can be written as a quadratic equation, i.e.,

$$D^2 + (M_{\xi\xi} + M_{\eta\eta} + M_{\zeta\zeta})D + S[M] = 0 \quad .$$

The quantity $S[M]$ is the following sum of diagonal minors:

$$S[M] = (M_{\xi\xi}M_{\eta\eta}-M^2_{\xi\eta}) + (M_{\xi\xi}M_{\zeta\zeta}-M^2_{\xi\zeta}) + (M_{\eta\eta}M_{\zeta\zeta}-M^2_{\eta\zeta}) \quad .$$

From this quadratic equation for D, relations for the sum D_1+D_2 and the product $D_1 \cdot D_2$ of the principal curvature of the surface as functions of the direction of the normal to the surface are obtained as

$$M_{\xi\xi} + M_{\eta\eta} + M_{\zeta\zeta} = -(D_1 + D_2) \quad , \tag{2.9}$$

$$S[M] = D_1 \cdot D_2 = 1/K \quad . \tag{2.10}$$

Here K is the Gaussian curvature of the surface at the point where the surface normal is $\hat{n}(\xi,\eta,\zeta)$. The equations (2.9) and (2.10) can now be viewed as differential equations for the support function M when the values of (D_1+D_2) and D_1D_2 are given as functions of the variables ξ, η and ζ. It is evident from the statement of the Minkowski problem and the Christoffel-Hurwitz problem given in the introduction to this chapter that (2.9) pertains to the Christoffel-Hurwitz problem, whereas (2.10) pertains to Minkowski's problem. Thus based on (2.10) and (2.6), Minkowski's problem can be stated as: *Given the function* $K(\xi,\eta,\zeta)$, *find the functions* $x(\xi,\eta,\zeta)$, $y(\xi,\eta,\zeta)$, $z(\xi,\eta,\zeta)$.

2.4 MINKOWSKI'S PROBLEM AND THE INVERSE ELECTROMAGNETIC PROBLEM

From the statement of the Minkowski problem, given in the previous section, it is clear that if the Gaussian curvature of a scatterer can be related to the electromagnetic field quantities this problem of differential geometry is exactly the same as the problem of recovery of the surface profile of a scatterer from the known far-field data. It is known [42] that in the geometrical optics region the scattering cross-section σ in the direction of any reflected ray is equal to $R_e/4K$ where K is the Gaussian curvature at the point of reflection and R_e is the energy reflection coefficient [26]. Making use of this relationship, Minkowski's problem can directly be used to analyze the inverse problem. It is clear that when σ and R_e are known for all values of their arguments, [i.e., θ,ϕ] in the geometrical optics region, the Gaussian curvature K is determined over the hemisphere $0 \leq \theta < \pi/2$ of the unit sphere. This unit sphere, on which each point corresponds to the direction of the normal at one point on the scatterer's surface, is called the spherical image of that surface. As mentioned earlier, Minkowski's problem is the determination of the surface when its Gaussian curvature is given on the entire surface of the spherical image. It has one and only one solution for any sufficiently smooth positive function $K(\theta,\phi)$ which satisfies the condition [64,78]

$$K^{-1}(\theta,\phi)n(\theta,\phi)d\Omega = 0 \tag{2.11}$$

Here $\hat{n}(\theta,\phi)$ is the unit normal at the point θ,ϕ ; $d\Omega$ is the differential surface of the unit sphere, and integration extends over the whole sphere. Thus, corresponding to the Gaussian curvature K given by the geometrical optics approximation [42] on one half of the unit sphere and by arbitrary [subject to (2.11)], smooth continuation over the remainder of the sphere, there exists exactly one scatterer. The scatterer shape is determined by the solution of an elliptic partial differential equation involving $K(\theta,\phi)$. Therefore, it is concluded that the shape of all parts of the scatterer are affected by the arbitrary continuation of K. Consequently, the Gaussian curvatures K provided over the hemisphere $0 \leq \theta < \pi/2$, do not suffice to determine the shape of the scatterer nor any part of it. The resulting inverse problem has too large a family of solutions. However, if two functions $\sigma_+(\theta,\phi)$ and $\sigma_-(\theta,\phi)$ are given, corresponding to two different incident waves coming from opposite directions, and also if R_e is known, then geometrical optics determines K over the whole sphere. If this K satisfies (2.11) (as it must if it actually corresponds to a surface), then the inverse problem has a unique solution. Unfortunately the calculation of this solution, in the general case, requires the solution of an elliptic partial differential equation whose solution is extremely difficult and does not lend itself to numerical computational techniques. Thus, in this investigation, no attempt has been made to actually solve the Minkowski problem, rather the differential equation of the Minkowski problem has been used to derive a set of equations which relate the surface parameters to the radar measurables. In this context, it is pointed out that in the case of a two-dimensional convex body of revolution, (2.10) could be reduced to an ordinary differential equation. Thus in the next section an example of a two-dimensional convex body of revolution is presented, where the Minkowski problem has been used directly to yield explicit solutions to the inverse electromagnetic problem.

2.5 SOLUTION FOR CONVEX BODIES OF REVOLUTION (TWO-DIMENSIONAL CASE)[91]

As mentioned earlier, for a smooth, perfectly conducting, convex body of revolution, and in the high-frequency limit, the radar cross-section is given by the geometrical-optics approximation [42]. The monostatic radar cross-section is given by [normalized so that the radar cross-section of a sphere is given by $\sigma = \pi \cdot (\text{radius})^2$].

$$\sigma(u) = \pi K^{-1}(u) \quad , \tag{2.11}$$

where, as shown in Fig. 2.2, u describes the direction of the incident plane wave and $K(u)$ is the Gaussian curvature at the specular point.

For an axi-symmetric body, whose geometry is shown in Fig. 2.2, two principal radii of curvature at any point on the surface are given by

$$\rho_1 = f(x) \quad \text{and} \quad \rho_2 = \frac{[1+(df/dx)^2]^2}{d^2f/dx^2} \quad . \tag{2.12}$$

The expression for ρ_1 can be obtained straight from Fig. 2.2 (by virtue of the fact that it is a body of revolution), and the expression for ρ_2 is obtained by using the known definition of the radius of curvature at any point of a curve in differential geometry [31,53,68]. Thus, the reciprocal of the Gaussian curvature is given by

$$K^{-1} = \rho_1 \cdot \rho_2 = \frac{f(x)[1+(df/dx)^2]^2}{d^2f/dx^2} \quad . \tag{2.13}$$

Making use of the fact that

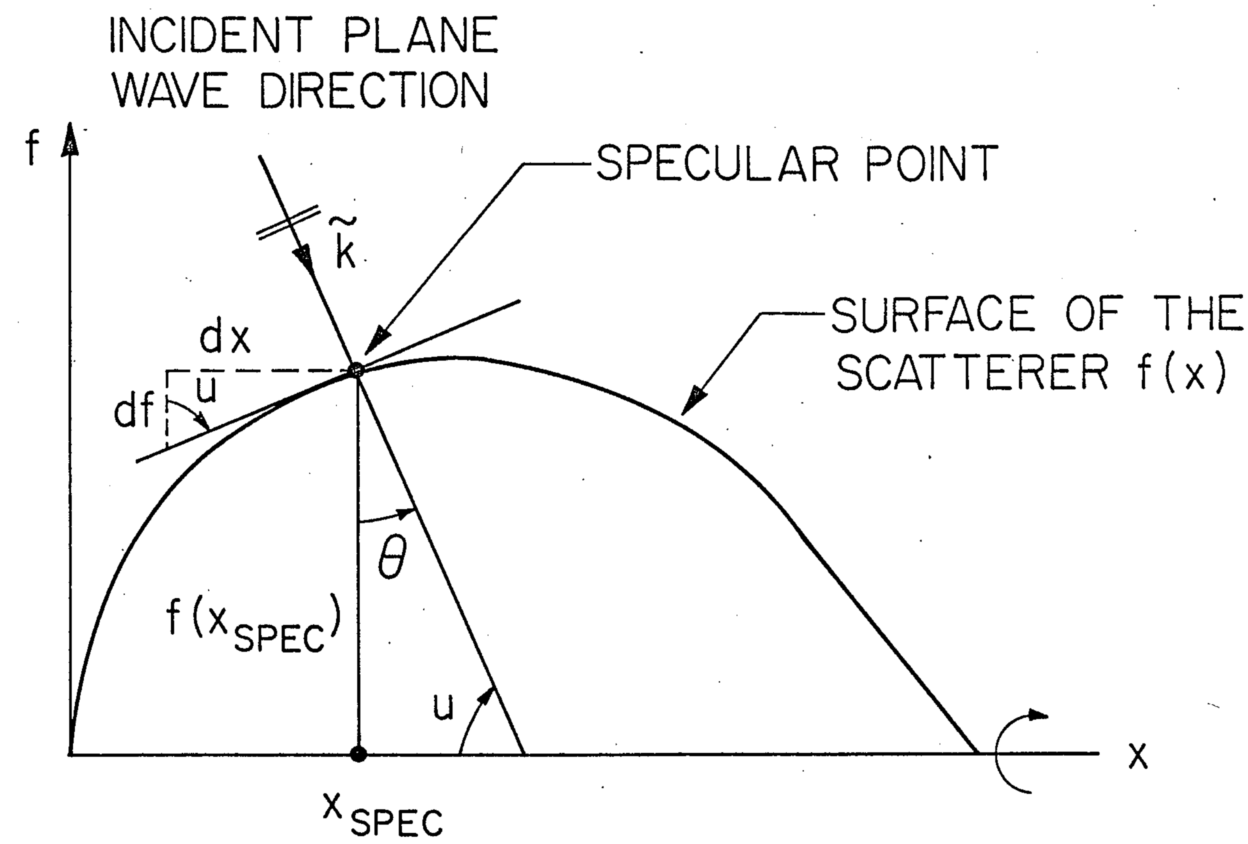

Fig. 2.2 Geometry Used For The Profile Inversion Of A Body Of Revolution

$$\frac{d^2f}{dx^2} = \frac{d}{dx}\left[\frac{df}{dx}\right] = \frac{d}{df}\left[\frac{1}{dx/df}\right] \cdot \frac{df}{dx}$$
$$= -\left(\frac{df}{dx}\right)^3 \frac{d^2x}{df^2}$$

Substituting this into (2.13), the reciprocal of the Gaussian curvature can be rewritten as

$$K^{-1} = \frac{f(x)[1+(dx/df)^2]^2}{(dx/df)(d^2x/df^2)} \quad . \tag{2.14}$$

Using (2.11) and (2.14), the expression relating the monostatic radar cross-section to the scatterer surface parameter is

$$\sigma(u) = \pi f(x) \frac{[1+(x')^2]^2}{x'(d/df)(x')} \quad , \tag{2.15}$$

where $\quad x' = \frac{dx}{df} \quad .$

Eq.(2.15) can be solved for f

$$\int_{f=o}^{f} f df = \frac{1}{2} f^2 = \frac{1}{\pi} \int_{x'=o}^{x'} \sigma \frac{x' dx'}{[1+(x')^2]^2} \quad .$$

With the substitution $x' = \tan u$ (see Fig. 2.2), the solution for f in terms of the angle u is obtained as

$$f(u) = \left\{ \frac{1}{\pi} \int_o^u \sigma(u) \frac{\tan u \; d(\tan u)}{[1+\tan^2 u]^2} \right\}^{1/2}$$
$$= \left\{ \frac{1}{\pi} \int_o^u \sigma(u) \sin(2u) du \right\}^{1/2} \quad . \tag{2.16}$$

Thus, (2.16) gives the f coordinate of the unknown shape as a function of a third parameter, u. A complete solution would require a similar equation for $x(u)$. This can be accomplished by considering the alternate form for the Gaussian curvature, i.e., (2.13), which along with (2.11) gives

$$\sigma = \frac{\pi f[1+(f')^2]^2}{(d/dx)(f')} \quad ,$$

where $f' = \dfrac{df}{dx}$.

Solving for dx and integrating

$$\int_{x=o}^{x} dx = x = \frac{1}{\pi}\int_{f'=\infty}^{f'} \frac{\sigma df'}{f[1+(f')^2]^2}$$

with the substitution, $f' = 1/\tan u$ (see Fig. 2.2) yields

$$x(u) = \frac{1}{\pi}\int_{o}^{u} \frac{\sigma(u)}{x(u)} \cdot \frac{d(1/\tan u)}{[1+(1/\tan u)^2]^2}$$

$$= \frac{1}{\pi}\int_{o}^{u} \frac{\sigma(u)}{f(u)} \sin^2 u \, du \qquad (2.17)$$

Thus, (2.16) and (2.17) provide the circular cylindrical coordinates of the scattering body [(2.16) must be applied first] as a function of the parameter u. In order to recover the complete shape of the scatterer, the radar cross-section must be known for the whole range of the aspect angles $0 \le u \le \pi$. An application [91] of this explicit solution for computing some numerical results suggests that a large variety of body sizes and shapes can be solved with this two-dimensional solution of the Minkowski problem.

As mentioned earlier, the Minkowski problem and the Christoffel-Hurwitz problem reduce to questions concerning nonlinear differential equations of elliptic character. Consequently, various properties of (2.9) and (2.10) including existence and uniqueness of their solutions are concerned with questions related to the field of elliptic differential equations. The first uniqueness proof for the Minkowski problem was given by Minkowski himself [48]. Under the assumption that the solution is analytic, Lewy [72] gave a uniqueness proof of the relevant Minkowski problem. His work on the existence of a solution is discussed in detail by Stoker [78] who also gave a particularly simple proof of a uniqueness theorem which requires merely a few derivatives of the surface.

In the context of the present investigation, where the main aim is to incorporate in (2.9) and (2.10) as boundary conditions on the scattering surface, the mathematical details of the existence and uniqueness of the solution of (2.9) and (2.10) are not important. Thus the detailed mathematical treatment of these problems are not included here, However, an excellent analysis of the solutions of (2.9) and (2.10) has been provided by Stoker [78].

chapter three

A TIME DOMAIN APPROACH TO ELECTROMAGNETIC SCATTERING

3.1 INTRODUCTION

The classical approach to the electromagnetic scattering problem is an analysis based on the differential equations for the fields, together with the boundary conditions at the scatterer. In general this approach has been confined to a single, but arbitrary, frequency. In the last seventy years, a number of valuable results have been produced by this method, however, only a very restricted class of canonical shapes had been treated. Moreover, extension of this approach to other target shapes is becoming more and more difficult.

Contrary to this, there has been relatively little work done on scattering problems with general time variation although the most common radar signature of objects is the time variation of the scattered signal. Therefore, a fundamental and useful method for the computation of the field scattered by an arbitrary shape would be the treatment of an impulsive incident wave. The primary conceptual time domain model, i.e., the impulse and related transient response waveforms of a scattering object, first proposed by Kennaugh and Cosgriff [44], has been discussed in Section 3.2. Furthermore, the interpretation and application of such a primary conceptual model for electromagnetic scattering is also presented in this section. Another efficient technique, making use of the space-time integral equation which is known as the "Impulse response augmentation technique" for obtaining the far-field electromagnetic response of scattering objects [9,12,13] will be discussed in Section 3.3. In this context, a brief derivation of the space-time integral equation for induced surface currents on the scatterer will also be presented in this section. In the impulse response augmentation technique, in order to obtain an estimate of the leading edge (or equivalently, the high frequency) response of the target, the physical optics currents have been assumed. This assumption leads to polarization independence by virtue of the fact that the impulse response which results may be written as the second derivative of the target's projected area as shown in Fig. 1.2. It is then required to determine as to whether or not the polarization dependent effects appear as singularity functions at the leading edge of the impulse response. It is the finding of the investigation by Bennett and co-workers [12] that these effects indeed do appear and, to a first approximation for smooth convex bodies, are functions of the difference in the principal radii of curvature at the specular point and have the form of the first derivative of the projected area. These results along with their possible application in the problem of profile inversion of smooth, convex, perfectly conducting objects will be discussed in Section 3.4.

3.2 THE CONCEPT OF THE TIME DOMAIN MODEL IN ELECTROMAGNETIC SCATTERING PROBLEMS

In time domain modeling, the scattering process is modeled by a passive linear two-port with time-invariant parameters. The input is $E(t)$, the output $F(t)$, and the two-port has an impulse response function $F_I(t)$. The input and output are related through the convolution integral as

$$F(t) \doteq \int_{t_1}^{\infty} F_I(\tau)E(t-\tau)d\tau \tag{3.1}$$

The coordinate frame, for defining the various quantities in (3.1) and to explain the scalar treatment of the electromagnetic fields, is shown in Fig. 3.1. With plane wave incidence of intensity $E(t)$, transverse components of the scattered field with intensity $F(t)$ (normalized) are produced at an arbitrary location in the far-field of the scattering object. In order to remove the time delay between scatterer and observer, a new time scale $t' = t-R/c_0$ is introduced. Here R is the distance of the observer from the origin of the coordinate system and c_0 is the free space propagation velocity. The input $E(t')$ is simply $E(t)$ with t replaced by t'. For the output $F(t')$, t is replaced by t' in $F(t)$. The impulse response waveform $F_I(t')$ is the response when the input $E(t')$ is impulsive, i.e., $E(t') = \delta(t')$. The lower integration limit t_1' in (3.1) is the initial value of t' at which the impulse response waveform $F_I(t')$ departs from zero. This limit is, in general, not zero since the initial contribution need not arrive at a time $t = R/c_0$. The conceptual two-port model has a frequency-dependent phasor response $G(j\omega)$ which is related to the radar cross-section of the scatterer as

$$\sigma(\omega) = \pi|G(j\omega)|^2 \tag{3.2}$$

The frequency-dependent phasor response $G(j\omega)$ and the time-dependent impulse response waveform $F_I(t')$ form a Laplace transform pair

$$G(j\omega) = c_0 \int_0^{\infty} F_I(t')e^{-j\omega t'}dt' \tag{3.3a}$$

$$F_I(t') = \frac{1}{2\pi j c_0} \int_{-\infty}^{+\infty} G(j\omega)e^{t'j\omega}d\omega \tag{3.3b}$$

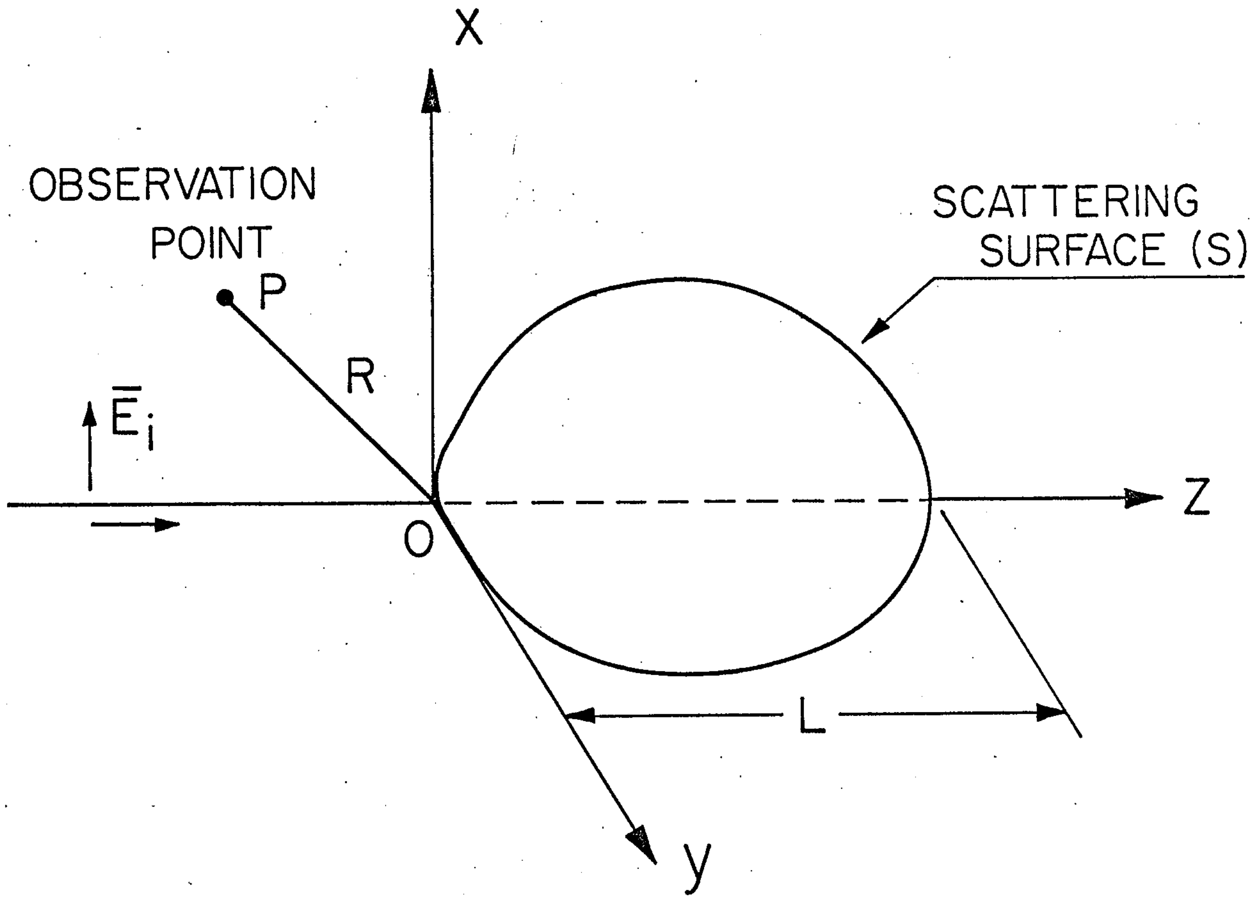

Fig. 3.1 Coordinates For Time Domain Scattering Problem

or using s notation $(s = j\omega)$

$$G(s) = c_0 \int_0^{\infty} F_I(t')e^{-st'}dt' \tag{3.4a}$$

$$F_I(t') = \frac{1}{2\pi j c_0} \int_{-j\infty}^{+j\infty} G(s)e^{t's}ds \quad . \tag{3.4b}$$

The impulse response waveform $F_I(t')$ is the time-dependent electromagnetic field strength produced at the output terminals when the input $E(t')$ is an impulsive plane electromagnetic wave, i.e., $E(t') = \delta(t')$. This impulse response of the two-port conceptual model is dependent on the orientation of the scattering object, the observation angle (but not range) and the particular transverse component of the scattered field selected. Once $F_I(t')$ is known, the response waveform for any incident waveform is determined by (3.1). Two other particular response waveforms of interest in the time domain study of electromagnetic scattering are defined as follows:

the step response

$$F_U(t') = \int_{t_1'}^{\infty} F_I(\tau)u(t'-\tau)d\tau \tag{3.5}$$

and the ramp response

$$F_R(t') = \int_{t_1'}^{\infty} F_I(\tau)(t'-\tau)u(t'-\tau)d\tau = \int_{t_1'}^{t'} F_U(\tau)d\tau \tag{3.6}$$

The Laplace transform relations in (3.3) and (3.4) state that $F_I(t')$ and $G(j\omega)$ can be derived from one another. But $G(j\omega)$ is known exactly for only one finite three-dimensional shape - the sphere, and even for this shape, the transformation to obtain $F_I(t')$ cannot be achieved exactly. Thus, a study of the scattering problem in the time domain consists mainly of the development of a reasonable estimate for the impulse response waveform $F_I(t')$. A number of distinct advantages of the time domain approach, as well as some disadvantages have been pointed out in recent investigations [9,12,45,61,67]. In the opinion of the author, the following remarks justify the use of the time domain approach in the present investigation:

(i) The impulse and transient response waveforms of a scattering object must be related in a rather direct way to the geometry and to the constitutive parameters of the object. It has been shown [44,61], for example, that the area beneath the ramp response waveform is proportional to the Rayleigh coefficient and hence, to the volume of the scatterer. More fundamentally, however, as the impulsive or transient illumination moves across the object, only that portion of the object which has been illuminated can possibly contribute to the scattered field waveform. Therefore, until the time when the transient illumination has passed completely over the object, there is a direct correlation between the response waveform at a given time and a specific portion of the object. Furthermore, two objects which present initially identical geometrical and physical properties over a given region must produce identical response waveforms up to the time corresponding to complete illumination of this region, regardless of their geometrical and physical properties beyond this point.

(ii) It is thought that, at least in principle, it is possible to incorporate into an estimate of the waveform $F_I(t')$ all of the best features of various approximate or asymptotic estimates of $G(s)$ while at the same time utilizing certain unique features of the time-dependent waveform. If certain estimates of $G(s)$, whose validity is restricted to particular portions of the spectrum, are known, it is far from clear how a consideration of these estimates can be used to approximate a $G(s)$ corresponding to the remainder of the spectrum. In the time domain, however, the estimates of $G(s)$ become time-limited portions of the waveform, and it is known that these pieces must combine with other pieces to produce a single waveform. Certain conditions on this total waveform are known from low-frequency derived moment conditions [45,61]. Even very crude estimates of how the pieces are combined add some new knowledge concerning $G(s)$. This feature of the time domain approach has been utilized in Chapter Five to generate input data for testing the proposed inverse scattering model. There, an approximate model for the impulse response waveform of a prolate spheroid has been synthesized by mainly using the high-frequency estimates.

The low frequency scattering properties of any finite, three-dimensional object provide interesting and useful conditions on the impulse and transient response waveforms. At sufficiently low frequencies, the phasor response, $G(s)$, of a scattering object can be expanded in a Taylor series about the origin $s = 0$ as

$$G(s) \simeq \sum_{n=0}^{\infty} a_n s^n \quad . \tag{3.7}$$

According to Rayleigh's scattering theory [4,65], the coefficients a_0 and a_1 in such an expansion are zero, while the coefficient a_2 is proportional to the scatterer volume. It is to be noted that the coefficient a_2 depends upon the shape, orientation, and constitutive parameters of the scatterer as well as the polarization of the incident and scattered fields. Expanding $e^{-st'}$ in the definition integral in (3.4a) in a Taylor series about the origin $s = 0$, and comparing the resulting series with the series in (3.7) yields,

$$\int_0^\infty F_I(t')dt' = a_0 = 0 \quad , \tag{3.8a}$$

$$\int_0^\infty t'F_I(t')dt' = a_1 = 0 \quad , \tag{3.8b}$$

$$\int t'^2 F_I(t')dt' = \frac{2a_2}{c_0} \quad , \tag{3.8c}$$

$$\int_0^\infty t'^n F_I(t')dt' = \frac{(-1)^n n! a_n}{c_0^n} \quad . \tag{3.8d}$$

These are known as the moment conditions on the impulse response waveform $F_I(t')$. The first three moment conditions have been used successfully in various investigations [59-61] of the time domain scattering problem. These three moment conditions have been interpreted [61] as requiring that the net area beneath the impulse and the step response waveforms be zero, and that the net area beneath the ramp response waveform be proportional to the Rayleigh coefficient, a_2, of the scatterer.

The conditions imposed on the impulse and transient response waveforms by the high frequency scattering properties of any finite, three-dimensional object have brought forward important relationships between the electromagnetic field quantities and the shape profile of the scatterer. In order to derive this relationship, the high frequency estimate of $G(s)$ is obtained by using the well known physical optics approximation. In the geometry shown in Fig. 3.1, a surface current distribution $\vec{J}_S$ over the surface S produces a radiated field intensity E_x at a large distance R along the negative z axis, given by

$$E_x = -\frac{j\omega\mu}{4\pi R} e^{j(\omega t-kR)} \int_S (\vec{J}_S \cdot \hat{a}_x) e^{-jkz} dS \quad . \tag{3.9}$$

In the physical-optics approximation, it is assumed that $\vec{J}_S = 2\hat{n} \times \vec{H}_i$ over the illuminated portion of S, $\vec{J}_S = 0$ elsewhere. Under such an assumption, for a harmonic incident plane wave with $\vec{E}_i$ polarized in the x direction, traveling in the positive z direction, the x component of the backscattered field is given by

$$E_s^x(j\omega) = -\frac{j\omega}{2\pi R c_0} e^{j(\omega t-kR)} \int_{S_{i\ell\ell}} \hat{a}_x \cdot \hat{n} \times \hat{a}_y e^{-2jkz} dS \quad , \tag{3.10}$$

where $\vec{E}_i = \hat{a}_x e^{j(\omega t-kz)}$.

It is to be noted that in the above equations using the phasor notations, the real part of the complex expressions are implied for the actual time dependent fields. Thus the value of $G(j\omega)$, the normalized backscattered phasor response defined [45] as

$$\mathrm{Re}\{G(j\omega)e^{j\omega(t-R/c_0)}\} = (2R/c_0)E_s(t-R/c_0) \quad ,$$

is obtained by using (3.10) as

$$G(j\omega) = \frac{j\omega}{\pi c_0^2} \int_{S_{i\ell\ell}} e^{-2jkz} \hat{a}_z \cdot \hat{n} dS \quad . \tag{3.11}$$

From Fig. 3.1 it is evident that

$$\hat{a}_z \cdot \hat{n} dS = \hat{a}_z \cdot \overrightarrow{dS} = -dA(z) \quad ,$$

where $A(z)$ is the area of the scatterer surface between the $x-y$ plane and a cutting plane at z projected orthogonally on the $x-y$ plane. It follows from (3.11) that $G(s)$ $[s = j\omega]$ can be written

$$G(s) = -\frac{}{\pi c_0^2} \int_{z=o^-}^{z=\ell^+} e^{-2s(z/c_0)} [\frac{dA(z)}{dz}] \, dz \quad , \tag{3.12}$$

where $A(z)$ is a monotonic function of z, defined as zero for $z < 0$, reaching a constant value $A(\ell)$ at the shadow boundary and beyond, where $z \geq \ell$. $A(z)$ has been redefined as the projected area function of the scatterer later in this chapter. Integration by parts of (3.12), and the substitution of $t'=2z/c_0$, yields

$$G(s) = -\frac{1}{4\pi}\int_0^{\infty} e^{-ts}\frac{d^2A(z)}{dz^2}\, dt \quad . \tag{3.13}$$

In arriving at (3.13) use has been made of the fact that

$$\left.\frac{dA(z)}{dz}\right|_{z=o^-,\ell^+} = 0 \quad \text{and} \quad \frac{d^2A(z)}{dz^2} = 0 \quad \text{for} \quad z > \ell^+, z < 0^- \quad .$$

Comparing (3.13) with (3.4a) implies that

$$F_I(t\ ) = -\frac{1}{4\pi}\frac{d^2A(z)}{dz^2} \quad , \qquad z = \frac{c_0 t}{2} \tag{3.14}$$

Thus the impulse response predicted by physical optics is a simple waveform equal to a multiple of the second derivative of $A(z)$, plotted with a time scale such that the cutting plane used to determine $A(z)$ moves with one-half the velocity of the incident impulsive wave (see Fig. 1.2) starting at the nearest point of the scatterer, at $t = 0^-$, and reaching the shadow boundary at $t = 2\ell/c_0$. The multiplying factor $(1/4\pi)$ on the left-hand-side of (3.14) depends on the particular normalization reference followed. Thus, it may vary for different normalizations used although leaving the functional form of the relation (3.14) unaltered. The main advantage of this physical optics approximation, i.e., (3.14), is the ease with which the impulse response can be determined for any shape once the area function $A(z)$ has been obtained. In practice, as pointed out in the next section, substantial corrections must be made to the waveform predicted by physical optics; nevertheless the physical optics approximation serves as a good starting point.

3.3 SPACE-TIME INTEGRAL EQUATION APPROACH

In order to gain further insight into time domain scattering, a more direct approach to the problem, based on the space-time vector integro-differential equation for the current density on the surface of the scatterer, is adopted in this section. In the following, first the space-time integral equation for the current density on the scattering surface is discussed and then the impulse response augmentation technique [9,13] has been outlined briefly.

3.3.1 Derivation of the Space-time Integral Equation

The general scattering problem is shown in Fig. 3.2a. $\vec{H}_i$ is the magnetic field incident on a perfectly conducting body which may be viewed as the field that would exist if the scatterer were not present. This incident field sets up a current $\vec{J}_S$ on the surface of the scatterer as shown in Fig. 3.2b. These currents in turn radiate and produce the scattered magnetic field $\vec{H}_S$. Once the surface currents have been determined, the far-field may be calculated.

One way to obtain an expression for these surface currents is to start out with a general expression for the far-field at an arbitrary point in space and then move this point in space onto the surface of the conducting body where the boundary conditions are applied. For a perfectly conducting body, either the E-field boundary conditions can be applied

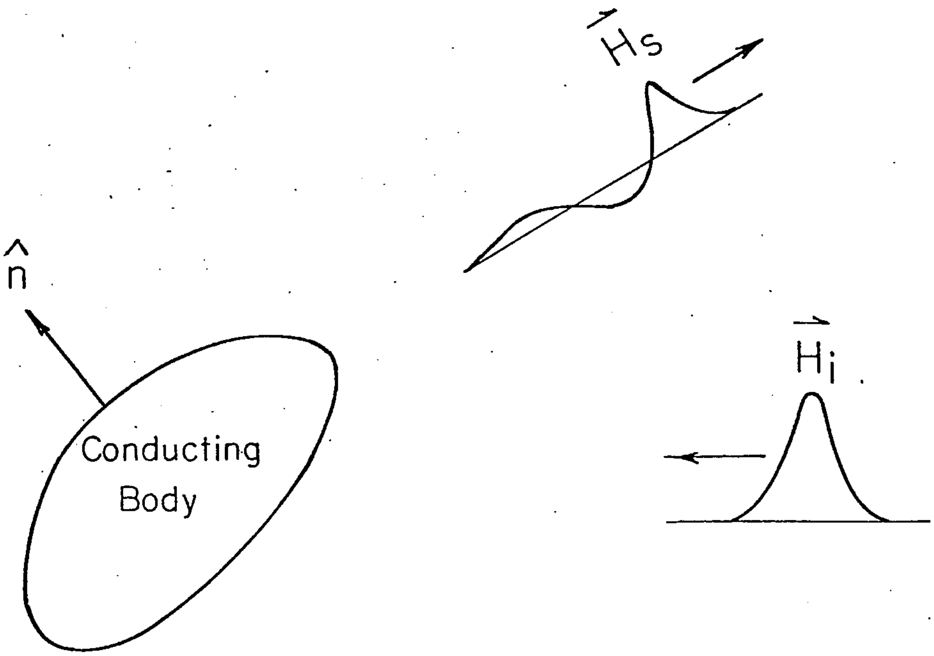

Fig. 3.2a General Scattering Problem

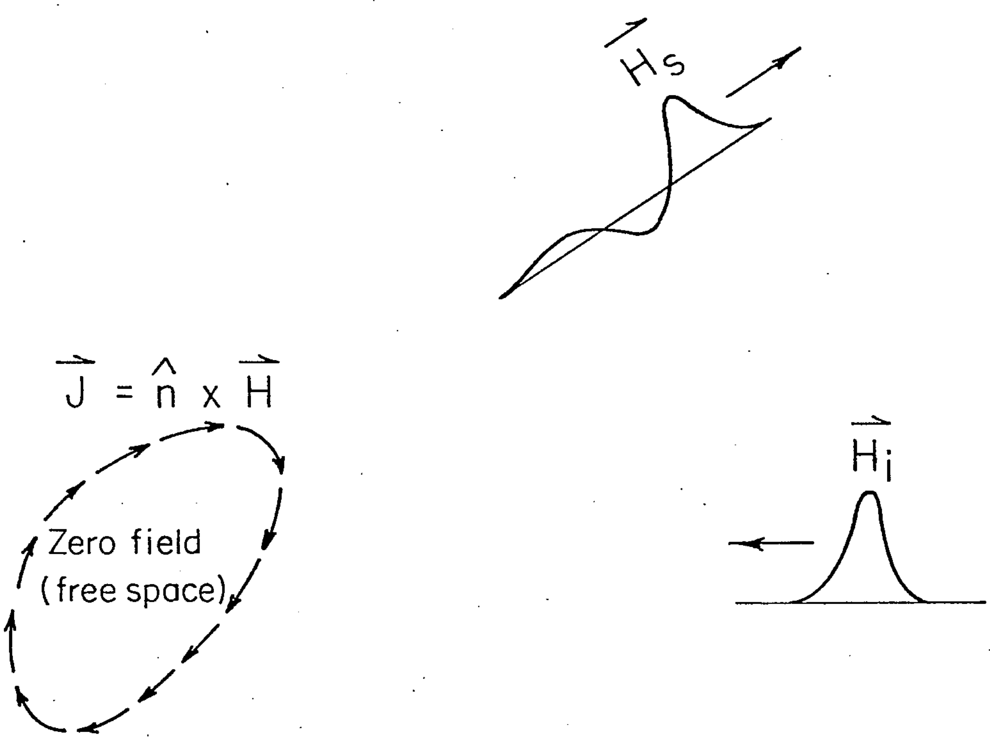

Fig. 3.2b Equivalent Of General Scattering Problem

which yield the E-field integral equation (EFIE), or alternately, the H-field boundary condition can be applied which yield an H-field integral equation (MFIE). However, it was found [9,10] that for the case of solid conducting bodies the EFIE formulation is less appropriate, because it requires that the numerical space derivative be taken on the surface of the body. Therefore, in this work the MFIE formulation is used.

The geometry for derivation of the MFIE for the induced surface current is shown in Fig. 3.3. The vector potential due to any current distribution on a surface S' is given by

$$\vec{A}_p(\vec{r},t) = \frac{1}{4\pi}\int_{S'} \frac{J_S(\vec{r}',t-R/c_0)}{R}\, dS' \quad .$$

The total magnetic field $\vec{H}$ is simply the sum of the incident field and the field produced by the induced current $\vec{J}_S$, i.e.,

$$\vec{H}(\vec{r},t) = \vec{H}_i(\vec{r},t) + \nabla \times \vec{A}_p(\vec{r},t) \quad .$$

Working out $\nabla \times \vec{A}_p$ [8], gives

$$\vec{H}(\vec{r},t) = \vec{H}_i(\vec{r},t) + \frac{1}{4\pi}\int_{S'} \Big[\frac{\vec{J}_S(\vec{r}',t')}{R^2} + \frac{1}{Rc_0} \cdot \frac{\partial \vec{J}(\vec{r}',t')}{\partial t'}\Big] \times \hat{a}_R dS' \quad ; \quad t' = t-R/c_0 \quad .$$

From this, $\vec{J}_S$ may be obtained by simply shrinking the observation point to a point on the surface of the scatterer and then applying the boundary conditions to express $\vec{H}$ in terms of $\vec{J}_S$. It is to be noted that alternatively an equation in terms of $\vec{H}$ can be obtained, however the numerical computation of the far-scattered field from $\vec{H}$ takes somewhat longer than it does using $\vec{J}_S$ [9,10]. Hence, the integro-differential equation was expressed in terms of $\vec{J}_S$. Shrinking the

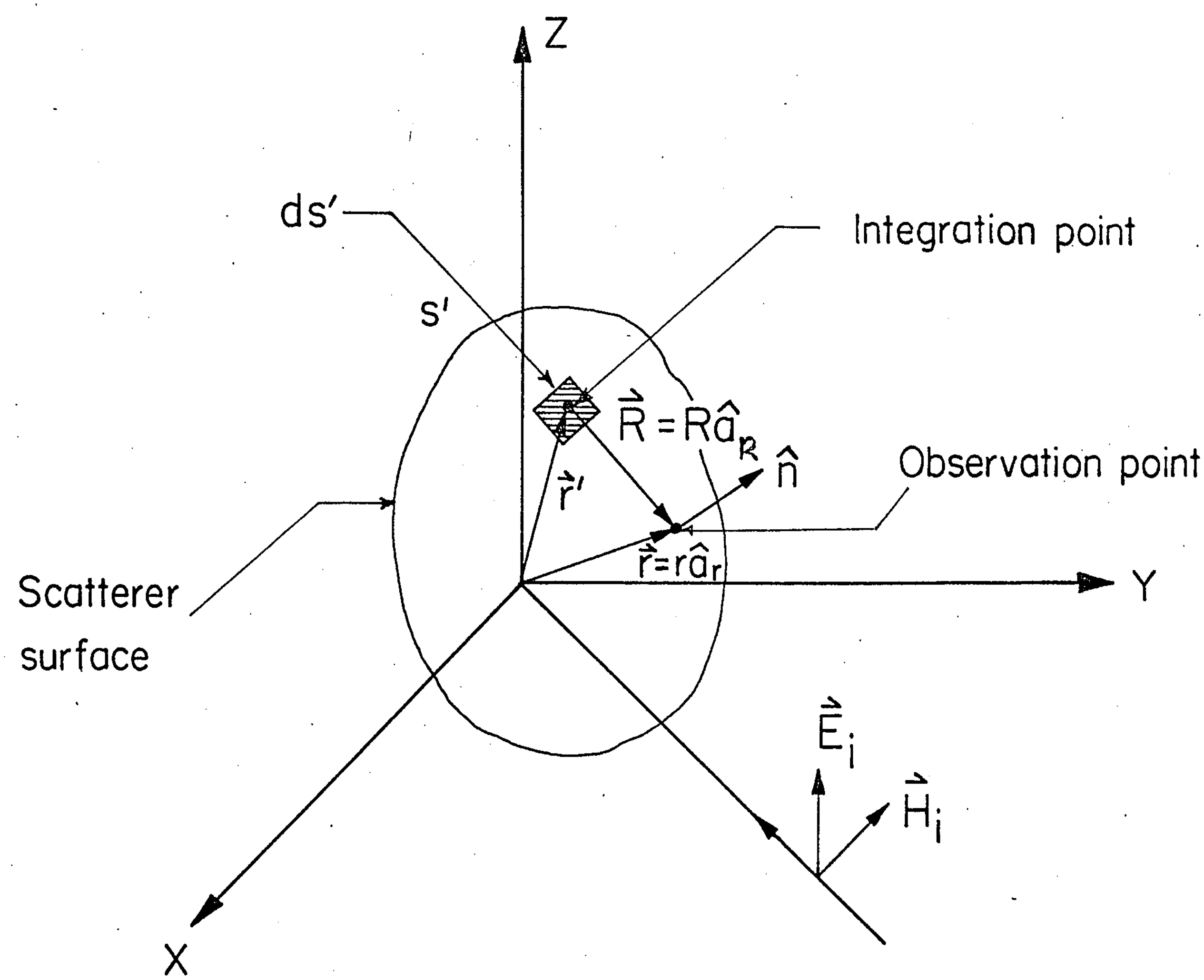

Fig. 3.3 Target Geometry For Derivation Of MFIE

observation point on the surface and carrying out the limiting procedure, one finds

$$\vec{H}(\vec{r},t) = 2\vec{H}_i(\vec{r},t) + \frac{1}{2\pi}\int_{S'} \left[\frac{\vec{J}_S(\vec{r}',t')}{R^2} + \frac{1}{Rc_0}\frac{\vec{J}_S(\vec{r}',t')}{\partial\tau}\right] \times \hat{a}_R dS' \quad ; \; t' = t - R/c_0$$

Finally, applying the H-field boundary condition, one obtains

$$\vec{J}_S(\vec{r},t) = \hat{n} \times \vec{H}(\vec{r},t)$$

or,

$$\vec{J}_S(\vec{r},t) = 2\hat{n} \times \vec{H}_i(\vec{r},t) + \frac{1}{2\pi}\int_{S'} \hat{n} \times \left\{\left[\frac{\vec{J}_S(\vec{r}',t')}{R^2} + \frac{1}{Rc_0}\frac{\partial\vec{J}_S(\vec{r}',t')}{\partial t'}\right] \times \hat{a}_R\right\} dS' \quad ; \; t' = t - R/c_0 \qquad (3.15)$$

This is the space-time vector integro-differential equation for the current density on the surface of the scatterer. Before proceeding to solve for the far-scattered field from $\vec{J}_S(\vec{r},t)$, it is worthwhile to comment on some of the features (3.15) exhibits.

It is evident that the equation for $\vec{J}_S$ represents a system of three coupled scalar integral equations for the three components of $\vec{J}_S$, but since

$$\hat{n} \cdot \vec{J}_S(\vec{r},t) = 0 \quad ,$$

it is possible to reduce the number of independent equations to two. It is also clear that the term $2\hat{n} \times \vec{H}_i(\vec{r},t)$ corresponds to the usual physical optics approximation on the illuminated portion of the scatterer. The integral term on the right-hand-side of the equation for $\vec{J}_S(\vec{r},t)$ represents the influence of currents at other surface points on the current at $(\vec{r},t)$. The important characteristic here is that the influence of other currents on the current at $(\vec{r},t)$ is delayed by R/c_0 which makes the numerical solution of the equation feasible. This retardation effect is especially important, since it allows the solution of the equation for the current without inverting a matrix as is required for the numerical solution of the frequency domain integral equation. Actually the surface current $\vec{J}_S$ may be determined by a "stepping on" procedure in time [9,67], since the current at time t is given in terms of the known incident field at that time and the current on other portions of the scatterer at prior times which have already been calculated. This in fact is a distinct advantage of the time domain approach over the frequency domain approach.

For obtaining expressions for the far-scattered field from the induced surface current density $\vec{J}_S(\vec{r},t)$, it is approximated that R is so large that the contribution of the first term in the square brackets to the integral in (3.15) is negligible. In addition the following assumption can be made (see Fig. 3.3)

$$\frac{1}{R} \longrightarrow \frac{1}{r}$$

$$\hat{a}_R \longrightarrow \hat{a}_r \quad .$$

With these approximations the expression for the far-scattered field is:

$$\vec{H}_S(\vec{r},t) = \frac{1}{4\pi r c_\sigma} \int_{S'} \left[\frac{\partial \vec{J}(\vec{r}',t')}{\partial t'}\right] \times \hat{a}_r dS' \quad ; \; t' = t - R/c_0 \qquad (3.16)$$

This shows that the far-field could be considered directly without trying to determine the detailed behaviour of the surface currents first, which would greatly simplify the problem.

3.3.2 The Impulse Response Augmentation Technique [12]

A new technique called "The impulse response augmentation technique" for obtaining the impulse response and frequency response of an arbitrary target over the entire spectrum was developed by Bennett and co-workers [12]. The impulse response augmentation technique utilizes the established computational procedure of determining the smoothed impulse response of an arbitrary target by numerical solution of the space-time integral equation and the known variation of the impulse response due to the specular return (high frequency portion). These two results provide, respectively, low and high frequency information exactly and are combined in a natural and rigorous manner to yield the frequency response over the entire spectrum and total impulse response with a minimum of uncertainty.

The space-time integral equation solves the scattering problem directly in the time domain where the unit of time is the light meter. (A light meter is defined as the time it takes an electromagnetic wave moving at the speed of light to travel one meter. It has the effect of normalizing the time by the speed of the light in meters/second.) The impulse excitation would yield the universal solution for a particular target. However, the present day computer limitations preclude the direct numerical solution of the space-time integral equation for the impulse excitation. The most useful excitation has been found to be a regularized (or smoothed) impulse of the form shown in Fig. 3.4a. The response $\vec{H}_S(t)$ due to this excitation is known as the regularized (or smoothed) impulse response and can be computed exactly with the space-time integral

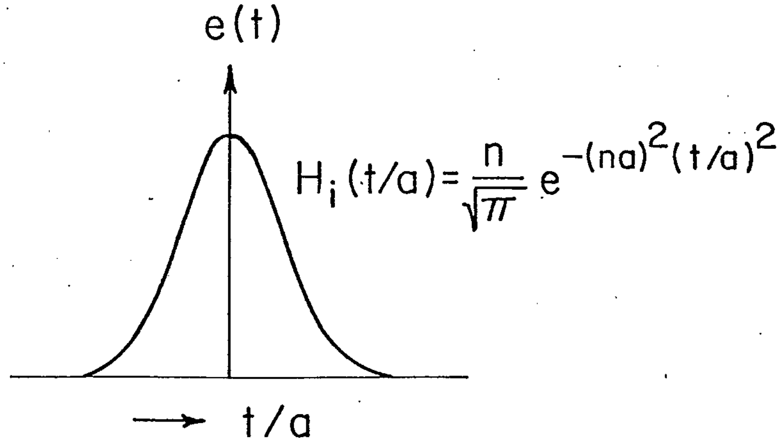

$H_i(t/a)$: is the incident magnetic field at the origin of the coordinate system.

a : is the characteristic linear dimension of the target.

n : is the parameter which controls the width of the pulse and chosen such that the product (na) is a constant.

Fig. 3.4a Regularized (Or Smoothed) Impulse Excitation

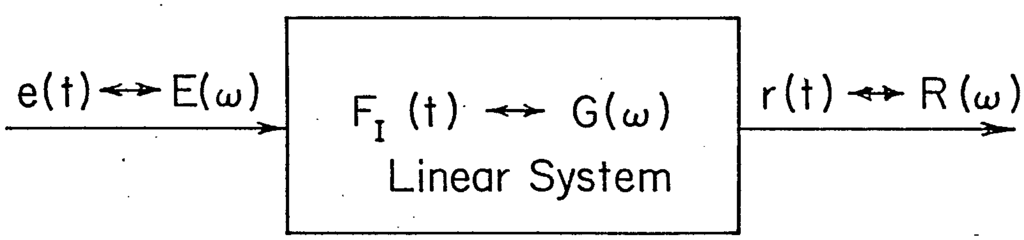

$$r(t) = h(t) * e(t)$$

$$R(\omega) = H(\omega) \cdot E(\omega)$$

Fig. 3,4b Functional Diagram Of The Linear System equation. The regions of slow variation in the smoothed impulse response remain the same in the exact impulse response; thus, it is only necessary to determine the structure of the singular regions and any other regions of fast variation. But the singular portions of the exact impulse response that results from scattering by specular points on smooth convex targets can be computed from the physical optics approximations and hence need not be computed by solving the space-time integral equation.

The impulse response augmentation technique has been explained [9] by considering the basic approach to the deconvolution (or system identification) problem. Fig. 3.4b shows the functional diagram of a linear system (in this case electromagnetic scattering by a target) that is characterized by its impulse response $F_I(t)$, or equivalently, its system function (or frequency response) $G(\omega)$. In the problem being considered here, $e(t)$ the incident Gaussian pulse is specified analytically and $r(t)$ is computed by solving the space-time integral equation. It is desired to find $F_I(t)$ and/or $G(\omega)$. However, the estimate of the system response $\tilde{r}(t)$ that is computed contains some uncertainty or noise. Thus, the transform of the computed or measured smoothed impulse response $R(\omega)$ also contains noise $N_0(\omega)$ and may be written as

$$\tilde{R}(\omega) = R(\omega) + N_0(\omega) \quad ,$$

and the corresponding system function $\tilde{G}(\omega)$ is

$$\tilde{G}(\omega) = G(\omega) + e^{(\omega/2n)^2} \cdot N_0(\omega) \quad .$$

Thus, the noise at high frequencies in the estimate of the system function increases exponentially. Physically this occurs because the interrogation signal is a smoothed impulse and its transform decays exponentially with frequency. Thus, this method by itself will not yield the system function at all frequencies.

How this defect is circumvented by the impulse response augmentation technique is displayed in the block diagram of Fig. 3.5. This technique first augments the smoothed impulse response to remove the contribution from singular portions (i.e., mainly the specular points) of the impulse response that are known from physical optics approximations. If $f_a(t)$ is a suitable augmentation function that contains the known singular portions of the impulse response, the augmented smoothed impulse response $r_a(t)$ is given as

$$r_a(t) = r(t) - e(t) * f_a(t) \quad .$$

Next the transform of the augmented smoothed impulse response $R_a(\omega)$ is computed and divided by the transform of the incident pulse to yield the augmented frequency response $H_a'(\omega)$. This function contains noise which increases exponentially at frequencies above some value. However, it is known that the augmented frequency response must go to zero with increasing frequency. Thus, an estimate of the high frequency behaviour of the augmented frequency response $\hat{H}_a(\omega)$ is of the form

$$\begin{aligned} \hat{H}_a(\omega) &= H_a'(\omega) \qquad ; \qquad \omega \leq \omega_c \\ &= P(\omega) \qquad ; \qquad \omega \geq \omega_c \end{aligned}$$

where ω_c is the boundary point and $P(\omega)$ is the high frequency estimate of $H_a(\omega)$. The inverse Fourier transform of $\hat{H}_a(\omega)$ then yields the estimate of the augmented impulse response $\hat{h}_a(t)$. Finally, the inverse of the augmentation procedure is performed on $\hat{h}_a(t)$, which yields the estimate of the impulse response $F_I(t)$. An estimate of the

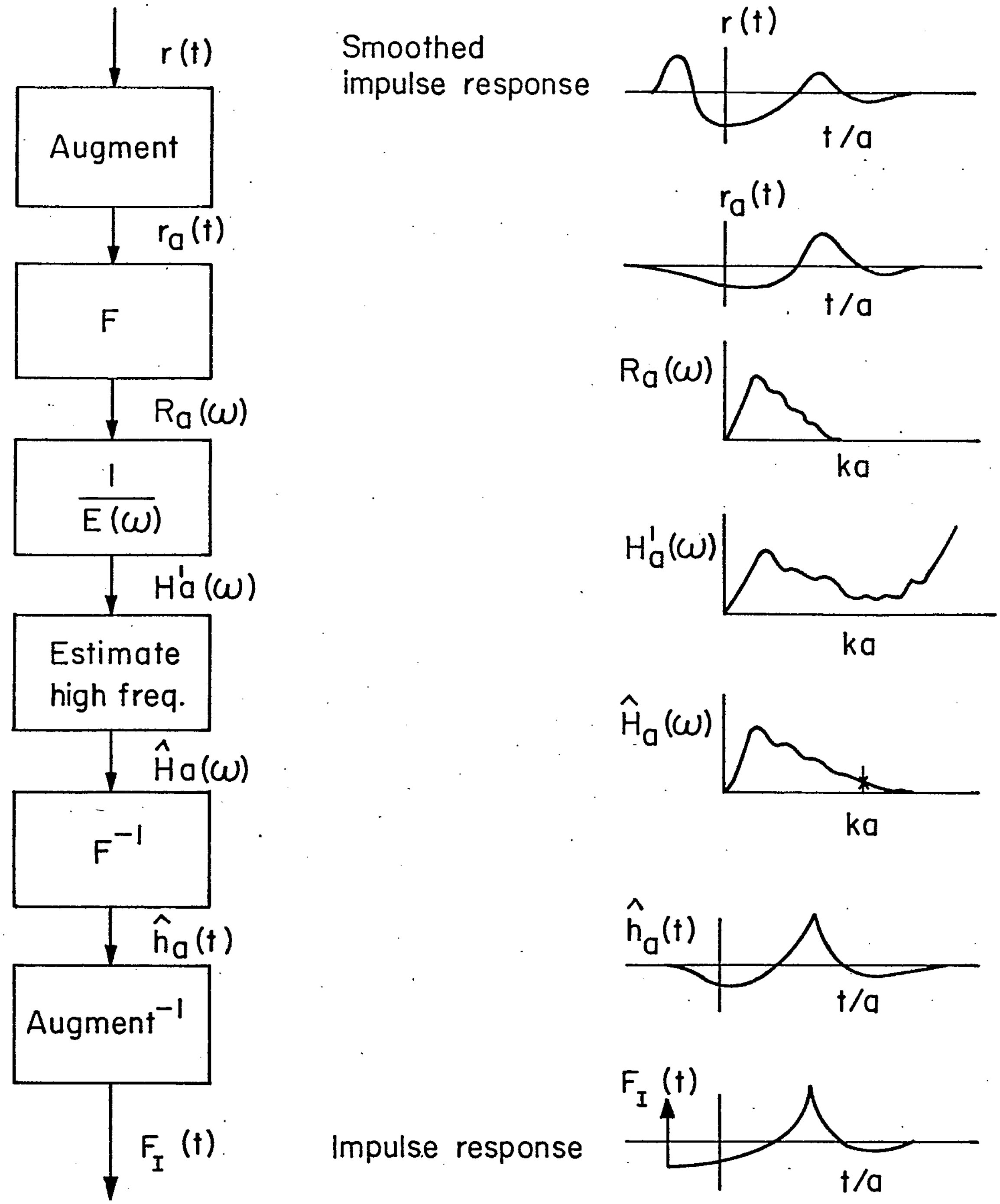

Fig. 3.5 Impulse Response Augmentation Technique [12]

system function $H(\omega)$ is obtained by applying the inverse of the augmentation procedure in the frequency domain to $H_a(\omega)$.

3.4 POLARIZATION CORRECTION IN THE LEADING EDGE OF THE IMPULSE RESPONSE

In the expression for the induced surface current density, i.e., (3.15), the first term on the right-hand side is the physical optics current, i.e.,

$$\vec{J}_{po} = 2\hat{n} \times \vec{H}_i \qquad \text{illuminated side}$$
$$= 0 \qquad \text{shadow side}$$

The corresponding physical optics approximation for the far-field impulse response, as was derived in Section 3.2, was found to be [12]

$$r_0 \vec{H}_{po}(\vec{r},t) = \frac{1}{2\pi} \frac{\partial^2 A(t)}{\partial t^2} \hat{a}_{Hi} \qquad , \qquad (3.17)$$

where $A(t)$ is the projected area function as shown in Fig. 1.2, and $\hat{a}_{Hi}$ is the unit vector in the direction of $\vec{H}_i$. It is to be noted that the scattered magnetic field has been weighted by r_0, the distance of the observer from the scatterer. Expression (3.17) is simply the physical optics approximation to the impulse response, and since it is only a function of the projected area, then as noted earlier, it is polarization independent.

The first order correction to the physical optics approximation is obtained by applying the more general results of Bennett et al [12] which provide an expression for the effects of local currents on the observer. The validity of the consideration here is restricted to the leading edge portion of the impulse response, i.e., this correction holds better towards the high frequency end of the phasor frequency response. To derive an analytic expression for the first order correction to the physical optics far-field, the physical optics currents are assumed on the surface of the scatterer. These physical optics currents, in turn, are substituted into the integral part of (3.15), which yields a first-order correction to the physical optics currents,

$$\vec{J}_{po1}(\vec{r},t) = \frac{1}{2\pi}\iint\limits_{S_\varepsilon} \hat{n} \times \{[\frac{1}{R^2} + \frac{1}{Rc_0}\frac{\partial}{\partial t'}]\vec{J}_{po}(\vec{r}',t') \times \hat{a}_R\}\, dS' \qquad (3.18)$$

where S_ε is the whole surface S' of the scatterer excluding the observation point. These first-order corrections to the physical optics currents are then used to compute the first-order correction to the physical optics far-field as shown in (3.16), i.e.,

$$r_0\vec{H}_{po1}(\vec{r},t) = \frac{1}{4\pi}\iint\limits_{S'} [\frac{\partial\vec{J}_{po1}(\vec{r}',t')}{\partial t'}] \times \hat{a}_r\, dS' \qquad (3.19)$$

Next the expansion of the triple cross-product in (3.18) yields

$$\vec{J}_{po1} = \frac{1}{2\pi}\iint\limits_{S_\varepsilon} [\hat{n} \cdot \hat{a}_R L(\vec{J}_{po}) - L(\hat{n} \cdot \vec{J}_{po})]\, dS'$$

where the operator L represents the operation $[\frac{1}{R^2} + \frac{1}{Rc_0}\frac{\partial}{\partial t'}]$. A circularly shaped patch for S_ε with radius ρ_0 could be assumed, because consideration is restricted here to leading edge effects and therefore only the current in the vicinity of the observation point need be accounted for. Using this fact and the various geometrical interpretations of the inner product terms in the above integral [12], an analytical expression for J_{po1} was derived [12]. This is given by

$$\vec{J}_{po1} = \hat{a}_1 \left(\frac{K_1 - K_2}{4\pi}\right) \left[\pi\rho_0 J_{1po} + \frac{\pi\rho_0^2}{2} \frac{\partial J_{1po}}{\partial t'}\right]$$

$$+ \hat{a}_2 \left(\frac{K_2 - K_1}{4\pi}\right) \left[\pi\rho_0 J_{2po} + \frac{\pi\rho_0^2}{2} \frac{\partial J_{2po}}{\partial t'}\right] \tag{3.20}$$

where $J_{1po} = -2H_{i2}$,

$J_{2po} = -2H_{i1}$.

ρ_0 is the radius of a circular integration patch about the observer, and could be estimated from the mean area illuminated as a function of time.

Here $\hat{a}_1$, $\hat{a}_2$ are unit tangent vectors to the principal lines of curvature at the specular point respectively, with K_1 and K_2 representing the corresponding curvatures. H_{i1} and H_{i2} denote the components of the incident magnetic field in a_1 and a_2 directions respectively.

Substituting the expression for $\bar{J}_{po}$ into (3.20) yields

$$\vec{J}_{po1} = 2\left(\frac{K_1 - K_2}{4\pi}\right)\left[\pi\rho_0 + \left(\frac{\pi\rho_0^2}{2}\right) \frac{\partial}{\partial t'}\right]\hat{n} \times H_{i1}\hat{a}_1$$

$$+ 2\left(\frac{K_1 - K_2}{4\pi}\right)\left[\pi\rho_0 + \left(\frac{\pi\rho_0^2}{2}\right) \frac{\partial}{\partial t'}\right]\hat{n} \times H_{i2}\hat{a}_2 \tag{3.21}$$

The relation for the first-order correction to the physical optics far-field is obtained by replacing $\vec{J}_{po1}$ in (3.19) with the expression in (3.21), which yields

$$r_0\vec{H}_{po1} = \frac{1}{2\pi}\frac{\partial}{\partial t}\{\hat{a}_1 \iint_{S'} \left(\frac{K_1 - K_2}{2}\right)\left[\pi\rho_0 + \left(\frac{\pi\rho_0^2}{2}\right) \frac{\partial}{\partial t'}\right]H_{i1}\, dA_{proj}$$

$$+ \hat{a}_2 \iint_{S'} \left(\frac{K_1 - K_2}{2}\right)\left[\pi\rho_0 + \left(\frac{\pi\rho_0^2}{2}\right) \frac{\partial}{\partial t'}\right]H_{i2}\, dA_{proj} \tag{3.22}$$

where dA_{proj} represents the incremental projected area function defined in Fig. 1.2. As a first approximation for ρ_0, the surface at the specular point is assumed to be spherical with curvature K', which gives [12]

$$\rho_0 = (t + z) - \frac{K'}{2} (t + z)^2 \tag{3.23}$$

where t and z are defined in Appendix II, and the coordinate surface is oriented so that the incident wave is propagating in the negative z direction and the specular point is located on the z axis at the origin. The effect of the second term in (3.23) is of second order, and thus it will be neglected for this consideration.

Substitution of (3.23) (with $K' = 0$) into (3.22), letting the incident field be an impulse, and carrying out the integration, yields for the first order correction [12]

$$r_0 \vec{H}_{p01} = \frac{1}{2\pi} \frac{\partial A(t)}{\partial t} [\hat{a}_1 H_{i1} - \hat{a}_2 H_{i2}] \left(\frac{K_1 - K_2}{2}\right) \quad . \tag{3.24}$$

Thus from (3.24) it is evident that the first order correction to the physical optics approximation is proportional to the difference between the principal curvatures at the specular point and it has the functional form of the first derivative of the projected area function $A(t)$. It should be noted that the validity of the analytic expression as a total correction to the physical optics approximation for the field is the function of the validity of the approximation used in deriving it. One questionable assumption during the derivation of (3.24) is that the difference in principal curvatures remains the same in the vicinity of the specular point. But, again to a first approximation, this assumption is certainly valid. Finally, it is felt that the correction terms presented here are valid to the extent of giving the functional form of the correction terms, the polarizational dependence they introduce, and their relationship to the difference of principal curvatures at the specular point. The inter-relationship between scatterer surface parameters and the scattered wave polarization characteristics predicted by this correction term will be utilized in the next chapter in proposing a scheme for the recovery of the surface of a smooth, convex closed, perfectly conducting object from far-field scattering data.

chapter four

A MONOSTATIC INVERSE SCATTERING MODEL BASED ON POLARIZATION UTILIZATION

4.1 INTRODUCTION

In this chapter the solution of the inverse problem of electromagnetic scattering by smooth, convex shaped, perfectly conducting, three-dimensional scatterers is analyzed. Certain high frequency approximations [27,42,47] were used in incorporating the concepts of the Minkowski problem into the space-time integral solution of electromagnetic scattering to yield a set of equations for the recovery of the surface profile of the scatterer from the scattered field data. The underlying assumption in this investigation was based on the fact [7,8,28] that the "depolarization characteristics" of the scattered field do necessarily contain information regarding the surface profile of the scatterer.

It has been established [47,88] that a knowledge of the scattered field's magnitude about the monostatic angle contains information on the curvature of the scatterer at the specular point. In order to elaborate on this fact, a brief derivation of the geometrical optics approximation for the reflected fields is presented in Section 4.2. For the three-dimensional cases, this stipulation about the scattered field's magnitude, permits one to assume that for any smooth, slowly and uniformly varying convex-shaped scatterer, an "equivalent ellipsoid", centered at the origin and of identical curvatures about the monostatic direction, gives rise to an identical backscattered field magnitude. This equivalent ellipsoid modeling of the scatterer's surface is discussed in detail in Section 4.3.

Representation of each point of the scatterer by such an equivalent model (see Fig. 4.1) makes it possible to combine the mathematical concepts of "Minkowski's problem" with the polarization-depolarization aspects of the electromagnetic scattering concepts to yield a system of equations for the recovery of the surface of the scatterer. This is achieved in Section 4.4 through 4.6.

4.2 HIGH FREQUENCY APPROXIMATION FOR THE SCATTERED FIELDS

The consideration here will be restricted to isotropic homogeneous media; thus, one is concerned with electric fields $\overline{E}$ (or magnetic fields $\overline{H}$) which are solutions of

$$\nabla^2\vec{E} + k^2\vec{E} = 0$$

subject to the condition that $\nabla \cdot \vec{E} = 0$.

The Luneberg-Kline asymptotic expansion for large ω [46,54] is

$$\vec{E}(\vec{r},\omega) = e^{-jk_0\psi(\vec{r})} \sum_{m=0}^{\infty} \frac{\vec{E}_m(\vec{r})}{(j\omega)m} , \tag{4.1}$$

where $k_0 = \omega/c_0$, with c_0 being the phase velocity in free space. ψ represents the phase function and it is evident that the surfaces ψ = constant are equiphase-surfaces or wavefronts. In the high frequency limit, the asymptotic expansion (4.1) for $\vec{E}$ reduces to [47]

$$\vec{E}(\ell,\omega) \sim e^{-j\omega k_0\psi(\ell)}\vec{E}_0(\ell) \tag{4.2}$$

where

$$\vec{E}_0(\ell) = \vec{E}_0(\ell_0)\exp[-\frac{1}{2}\int_{\ell_0}^{\ell} \nabla^2\psi d\ell'] , \tag{4.3}$$

with ℓ defined in a way such that

$$\frac{\partial}{\partial\ell} = \nabla\psi\cdot\nabla . \tag{4.4}$$

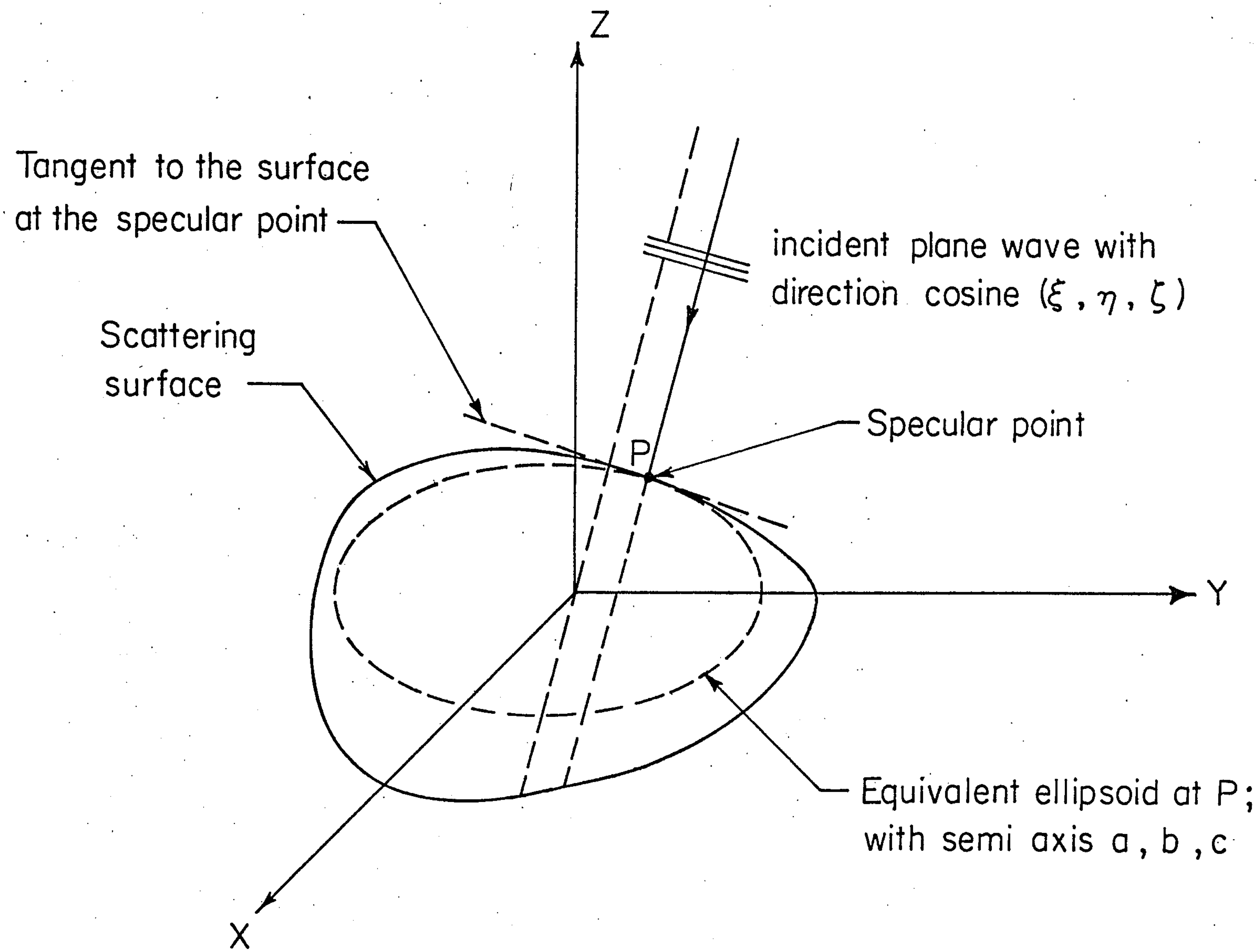

Fig. 4.1. "Equivalent ellipsoid" Model for specular point.

It is to be noted that $\nabla\psi$ has a direction perpendicular to the surface $\psi(\overline{r})$ = constant, so that ℓ specifies a position on a curve perpendicular to this surface. From (4.3) it is clear that $\vec{E}_\alpha(\ell)$ is determined if its value at the reference point ℓ_α is known.

For homogeneous media, the rays are straight lines, and, for isotropic media, the rays are perpendicular to the wavefronts; thus,

$$d\psi = |\nabla\psi|\,dh = n'dh \qquad , \tag{4.5}$$

where dh is an incremental distance along the ray path and n' is the refractive index of the medium. Integrating (4.5) yields

$$\psi = \psi_\alpha + n'h \qquad , \tag{4.6}$$

where ψ_α is the reference phase function. It also follows from (4.4), along with (4.5) and the fact that $|\nabla\psi|^2 = n'^2$ [47], that

$$dh = n'd\ell .$$

Introducing the Gaussian curvature of the wavefront $K = 1/D_1D_2$, where D_1 and D_2 are the principal radii of curvature of the wavefront surface ψ , it can be shown [47] that

$$\frac{dK}{dh} = -K\nabla^2\psi/n' \qquad .$$

Integrating this equation yields

$$K(\ell)/K(\ell_\alpha) = \exp[-\int_{\ell_\alpha}^{\ell} \nabla^2\psi d\ell'] \qquad . \tag{4.7}$$

Using (4.6) and (4.7), one may write (4.2) as

$$\vec{E}(\ell) \sim \vec{E}_\alpha(\ell_\alpha)e^{-jk_\alpha\psi_\alpha}[K(\ell)/K(\ell_\alpha)]^{1/2} \cdot e^{-jkh} \qquad , \tag{4.8}$$

where $k = n'k_0$. This expression for $\vec{E}$ is directly related to the geometrical optics approximation, as is shown next.

According to classical geometrical optics, the flux of light energy between the points P_1 and P_2 is governed by Fermat's principle, i.e., it follows a ray path which satisfies

$$\delta \left[\int_{P_1}^{P_2} n' dh \right] = 0 \qquad (4.9)$$

The wave follows a curve which makes the optical distance between P_1 and P_2 (given by the above integral) stationary. Usually the ray path minimizes this distance.

The intensity of the geometrical optics field is governed by the conservation of the energy flux in a tube of rays, such as the astigmatic tube of rays shown in Fig. 4.2. Let I^2 be the intensity of the field at P_2 and I_α^2 the intensity at the reference point P_1, then for an isotropic, homogeneous medium

$$I^2 d\Sigma = I_\alpha d\Sigma_\alpha$$

where $d\Sigma$ and $d\Sigma_\alpha$ are the cross-sections of the tube of rays at P_2 and P_1, respectively. It follows from differential geometry [47] that

$$\frac{d\Sigma}{d\Sigma_\alpha} = \frac{K}{K_\alpha} \quad , \qquad \text{hence,}$$

$$I = I_\alpha \sqrt{K/K_\alpha} \qquad (4.10)$$

with $K = K(\ell)$ and $K_\alpha = K_\alpha(\ell_\alpha)$.

From (4.9) and (4.10) it is clear that classical geometrical optics

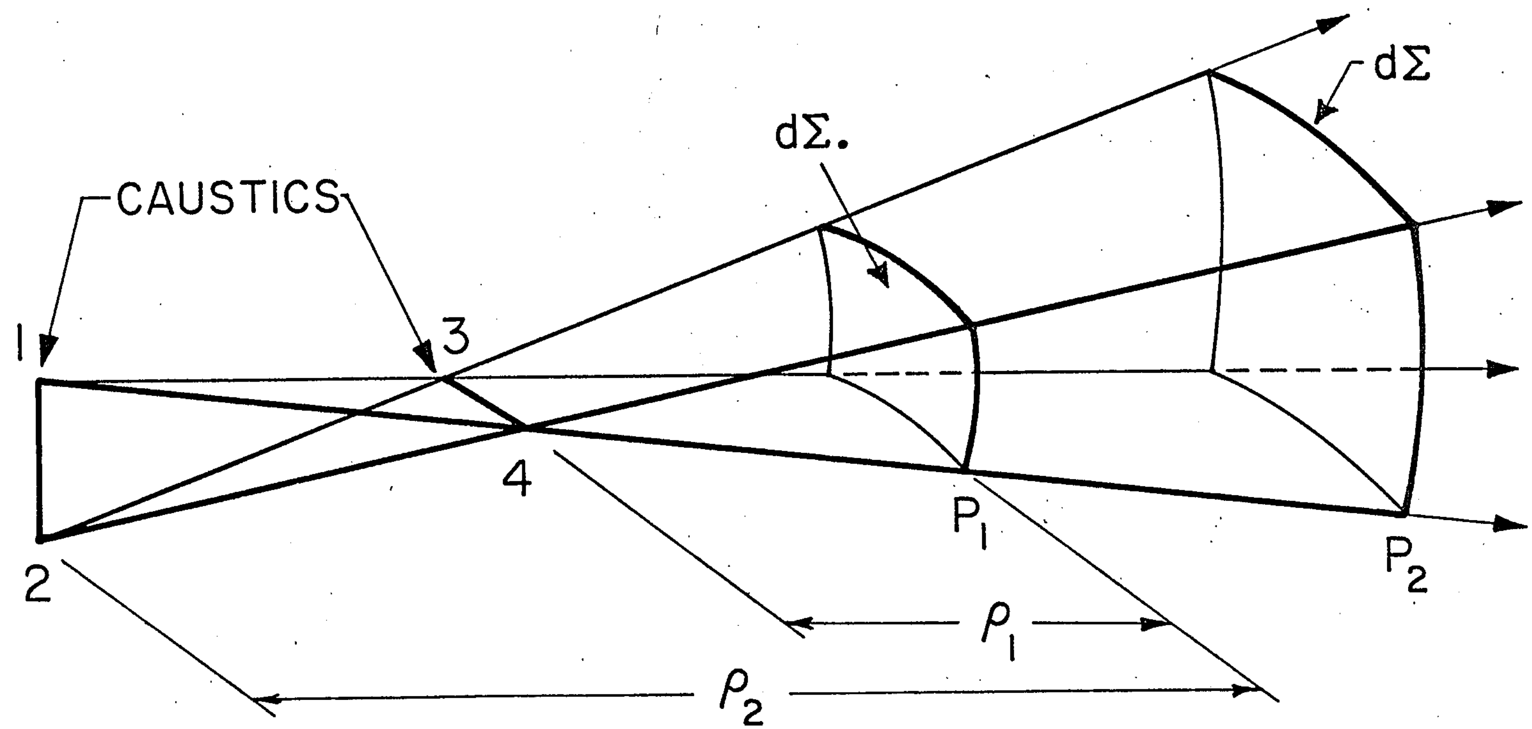

Fig. 4.2 Astigmatic Bundle Of Rays

correctly describes the path along which the high frequency field, given by (4.8), propagates and also the manner in which the field intensity varies with position. However, the description of the electromagnetic field in the limit of large ω by the Luneberg-Kline asymptotic expansion, i.e. (4.8), is superior to the one by the classical geometrical optics, i.e. (4.10). This is because classical geometrical optics ignores the polarization and wave nature of the light, hence while predicting the directions of reflection and refraction at a boundary surface, it cannot account for the intensities of the reflected and refracted waves. In order to overcome this shortcoming, most investigators have included artificially [47] polarization and phase information so that the classical geometrical optics field is modified to the form given by (4.8). Thus, the field represented by (4.8) has commonly been referred to as the geometrical optics field.

The ratio K/K_0 has been found [47] in terms of h and ρ_1, ρ_2, the radii of curvature of the reference wavefront shown in Fig. 4.2. When this expression for (K/K_0) is substituted into (4.8), one obtains

$$\vec{E}(\ell) \sim \vec{E}_0(\ell_0)e^{-jk_0\psi_0} \sqrt{\frac{\rho_1\rho_2}{(\rho_1+h)(\rho_2+h)}} \; e^{-jkh} \quad . \tag{4.11}$$

It is to be noted that, when $h = -\rho_1$ or $-\rho_2$, the field becomes infinite and the geometrical optics field is invalid. The congruence of rays at the lines 1-2, 3-4 in Fig. 4.2 is called a caustic. As one passes through a caustic line, the sign of $(\rho+h)$ changes, i.e.,

$$(\rho+h)^{-1/2} = |(\rho+h)^{-1/2}| \; e^{j(\pi/2)} \quad ,$$

and thus the correct phase shift of $\pi/2$ is introduced naturally.

In order to find the high-frequency approximation for the reflected field $\vec{E}_r$ from the point P on a perfectly conducting, smoothly curved surface, the following boundary condition is applied

$$\hat{n} \times (\vec{E}_i + \vec{E}_r) = 0 \quad . \tag{4.12}$$

Here $\hat{n}$ is the outward directed unit normal vector to the scattering surface at the point P , and $\vec{E}_i$ is the incident electric field. It follows from (4.2) and (4.12) [47] that

$$\vec{E}_{r_0}(P)e^{-jk_0\psi} = [\hat{n}\hat{n} - \hat{b}\hat{b}] \cdot \vec{E}_i(P) \tag{4.13}$$

where $\hat{b}$ is a unit vector tangent to the surface and is defined by

$$\hat{b}(\hat{b} \cdot \vec{E}_i) = -\hat{n} \times (\hat{n} \times \vec{E}_i) \quad .$$

The quantity in the bracket in (4.13) is a dyadic reflection coefficient which changes the direction but not the magnitude of $\vec{E}_i(P)$. It simplifies to scalar -1 when $\vec{E}_i(P)$ is tangent to the surface, which is the case for backscatter. In the far zone, the quantity under the square root in (4.11) reduces to $\sqrt{\rho_1\rho_2}/R$, where R is the distance from P to the observation point. Silver [75] has determined $\sqrt{\rho_1\rho_2}$ for an incident spherical wave. For the case of plane wave incidence

$$\sqrt{\rho_1\rho_2} = \sqrt{D_1D_2}/2 \tag{4.14}$$

where D_1 and D_2 are the principal radii of curvature of the reflecting surface at P. It is to be noted that if D_1 or D_2 become infinite, as in the case of a flat plate or cylindrical scatterers, the geometrical optics approximation becomes invalid.

Thus (4.11) along with (4.14) show that the assumption made at the beginning of this chapter, namely that a knowledge of the scattered field's magnitude about the monostatic angle contains information on the curvature of the scatterer at the specular point is a valid one. This fact is used in the next section in developing an equivalent ellipsoid model for the surface of a smooth, convex, closed scatterer.

4.3 EQUIVALENT ELLIPSOID MODEL

It has been established by various investigators that a knowledge of the scattered field's magnitude about the monostatic angle contains information on the curvature of the scatterer at the specular point [88]. As it has been shown in Section 4.2 this dependence is dominating in the high-frequency region, i.e., when the wavelength is much smaller than the dimension of the target (exact bounds on the region are not defined, primarily because body shape and complexity to some extent determine which scattering laws apply to a given situation). This stipulation for the three-dimensional case permits one to assume that at sufficiently high frequencies for any smooth, slowly and uniformly varying convex shaped scatterer, an "equivalent ellipsoid", centered at a prefixed origin and of identical principal curvature about the monostatic direction, gives rise to an identical backscattered field magnitude (see Fig. 4.1). Representing each point of the scatterer by such an equivalent model, changes the problem of recovery of the specular points with respect to the preassigned origin, i.e., recovery of x, y, z, to that of recovery of a, b, c – the semi axes of the equivalent ellipsoid for each monostatic direction. Stating it differently, in this model it is assumed that the specular point (or the point of reflection) instead of being on the unknown object is on an object whose shape and orientation is known (i.e., the ellipsoid centered at the preassigned origin) but the size (i.e., a, b, c) is unknown.

An application of a similar "equivalent curvature" modeling of the specular point for two-dimensional convex, smooth scatterers has been reported by Vandenberghe and Boerner [88]. However, they did not develop any analytic expression, relating the curvature at the specular point to the backscattered field, instead they applied known techniques of system synthesis. An iterative averaging method, they had introduced, compares the averaged magnitude of the backscattered field, given off by the unknown scatterer with that resulting from a known rotationally symmetric scatterer (e.g., a circular cylinder) which can easily be calculated. The agreement they obtained between the results and the exact values certainly validates the equivalent ellipsoid assumption for the three-dimensional case encountered in the present investigation.

Although there may be many different ellipsoids which will satisfy the criteria of having identical curvature about the specular point, there can only be one such ellipsoid which will be centered at the prefixed origin and oriented as shown in Fig. 4.1. In other words, for a given monostatic direction, by fixing the origin and the orientation of the equivalent ellipsoid, a one-to-one correspondence between the set of unknowns (x, y, z) and (a, b, c) is obtained. Obviously there will be degenerate cases whenever the specular point corresponds to the point of symmetry of the equivalent ellipsoid as shown in Fig. 4.3a and Fig. 4.3b. However, the coordinates (x, y, z) of the specular point, corresponding to these two degenerate cases, will be identical and thus the uniqueness of the solution is preserved. Therefore, if a sufficient number of equivalent ellipsoids, corresponding to the different monostatic directions and the same preassigned orientation and origin, are recovered from the knowledge of the backscattered field data, then with these recovered equivalent ellipsoids and known directions of incidence, the corresponding specular points with respect to the preassigned origin will be known uniquely. Thus, instead of solving for the coordinates of the specular point, (x, y, z), the ellipsoid's equivalent semi-axes (a, b, c) are recovered. In the following sections, the space-time integral equation and the Minkowski problem have been utilized to obtain three independent equations involving the unknowns a, b, c of the equivalent ellipsoid corresponding to the unknown specular point coordinates (x, y, z) of the target and the known backscattered field data.

4.4 UTILIZATION OF THE SPACE-TIME INTEGRAL EQUATION

The space-time integral equation for currents on the surface of a perfectly conducting body is given by (3.15). It is to be understood here that all the results obtained in the time domain can simply be converted into the frequency domain by use of Fourier transformation and appropriate scaling [12]. As pointed out earlier, the first term on the right-hand side of (3.15) is the physical optics current, and this yields the physical optics approximation to the far-field impulse

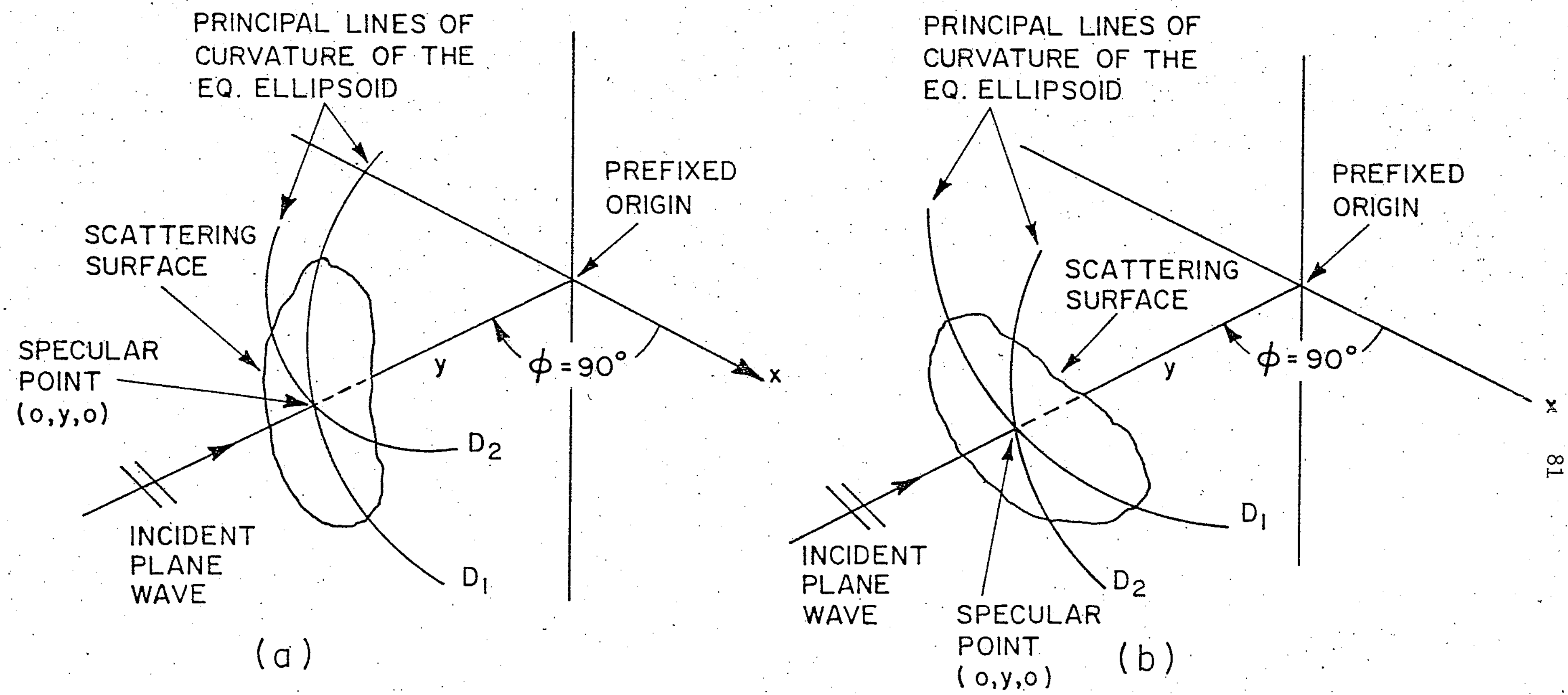

Fig. 4.3 Example Of A Degenerate Case Of The Equivalent Ellipsoid,
(a) Principal Line Of Curvature, With Radius D_1, Normal To The x–y Plane.
(b) Principal Line Of Curvature, With Radius D_1, In The x–y Plane.

response. The integral term on the right-hand side of (3.15) gives the first-order correction to the physical optics approximation of the backscattered far-field. Thus at sufficiently high frequencies the total backscattered far-field may be represented as

$$r_\alpha \vec{H}_S(\vec{r},t) = r_\alpha \vec{H}_{p\alpha}(\vec{r},t) + r_\alpha \vec{H}_{p\alpha 1}(\vec{r},t) \quad . \tag{4.15}$$

Substituting values from (3.17) and (3.24) for $\vec{H}_{p\alpha}$ and $\vec{H}_{p\alpha 1}$, yields

$$r_\alpha \vec{H}_S(\vec{r},t) = \frac{1}{2\pi}\frac{\partial^2 A(t)}{\partial t^2}\hat{a}_{H_i} + \frac{1}{2\pi}\frac{\partial A(t)}{\partial t}\left(\frac{K_1-K_2}{2}\right)\cdot[H_{i_1}\hat{a}_1 - H_{i_2}\hat{a}_2] \ . \tag{4.16}$$

If the direction $\hat{a}_{H_i}$ of the incident magnetic field is represented in terms of its component H_{i_1} along the $\hat{a}_1$ direction and H_{i_2} along the $\hat{a}_2$ direction, then the expression for the backscattered far-field is written as

$$\begin{aligned} r_\alpha \vec{H}_S(\vec{r},t) &= \frac{1}{2\pi}\left[\frac{\partial^2 A(t)}{\partial t^2} + \frac{\partial A(t)}{\partial t}\left(\frac{K_1-K_2}{2}\right)\right] H_{i_1}\hat{a}_1 \\ &+ \frac{1}{2\pi}\left[\frac{\partial^2 A(t)}{\partial t^2} - \frac{\partial A(t)}{\partial t}\left(\frac{K_1-K_2}{2}\right)\right] H_{i_2}\hat{a}_2 \quad , \end{aligned} \tag{4.17}$$

where the magnitude of the incident magnetic field $|\vec{H}_i|$ has been assumed to be unity. It is to be noted that for an arbitrary, linearly polarized incident field $\vec{H}_i$, the polarization angle α with respect to the $\hat{a}_1$ direction is assumed to be unknown and for the purpose of the present investigation needs to be determined in terms of radar measurables.

For the recovery of each specular point, the semi axes a, b, c of the corresponding equivalent ellipsoid need to be determined. Thus a system of three independent equations involving a, b, c, the direction cosines

ξ, η, ζ of the incident wave, and at least three independent radar measurables are required.

Consider a monostatic situation, where the incident wave and the normal to the surface at the specular point have the same direction cosines (ξ,η,ζ). Then, if $\vec{H}_i$ is of unit magnitude and makes an angle α with $\hat{a}_1$ at the specular point, the unit vector in the direction of the incident magnetic vector may be written as

$$\hat{a}_{H_i} = H_{i_1}\hat{a}_1 + H_{i_2}\hat{a}_2 \quad . \tag{4.18a}$$

A unit vector perpendicular to $\hat{a}_{H_i}$ and in the plane of $\hat{a}_1$ and $\hat{a}_2$ is

$$\hat{a}_{cr} = H_{i_2}\hat{a}_1 - H_{i_1}\hat{a}_2 \quad . \tag{4.18b}$$

Now the magnitude of the co-polarized component of the backscattered far-field (i.e., the component which is parallel to the incident wave polarization) results from (4.17) and (4.18a) as

$$\begin{aligned} |r_\alpha \vec{H}_{1p}(\vec{r},t)| &= r_\alpha \vec{H}_S(\vec{r},t) \cdot \hat{a}_{H_i} \\ &= \frac{1}{2\pi}\left[\frac{\partial^2 A(t)}{\partial t^2} + \left(\frac{K_1-K_2}{2}\right)(H_{i_1}^2 - H_{i_2}^2)\frac{\partial A(t)}{\partial t}\right] \quad . \end{aligned} \tag{4.19}$$

Similarly, the magnitude of the cross-polarized component (i.e., the component which is perpendicular to the incident wave polarization) is

$$|r_\alpha \vec{H}_{1c}(\vec{r},t)| = r_\alpha \vec{H}_S(\vec{r},t) \quad \hat{a}_{cr} = \frac{1}{\pi}\left(\frac{K_1-K_2}{2}\right)(H_{i_1} \cdot H_{i_2})\frac{\partial A(t)}{\partial t} \quad . \tag{4.20}$$

Next, consider another incident wave with the same direction of incidence, but the incident magnetic field now encloses an angle $(\alpha-\pi/2)$ with the $\hat{a}_1$ direction. The corresponding co-polarized component of the scattered field is

$$|r_\alpha \vec{H}_{2p}(\vec{r},t)| = \frac{1}{2\pi}\left[\frac{\partial^2 A(t)}{\partial t^2} - \left(\frac{K_1-K_2}{2}\right)(H_{i_1}^2 - H_{i_2}^2)\frac{\partial A(t)}{\partial t}\right] \quad , \tag{4.21}$$

and the cross-polarized component is

$$|r_\alpha \vec{H}_{2c}(\vec{r},t)| = \frac{1}{\pi}\left(\frac{K_1-K_2}{2}\right)(H_{\hat{i}_1} \cdot H_{\hat{i}_2}) \frac{\partial A(t)}{\partial t} \quad . \tag{4.22}$$

Since $H_{\hat{i}_1} = |H_{\hat{i}}|\cos\alpha$ and $H_{\hat{i}_2} = |H_{\hat{i}}|\sin\alpha$, hence from (4.19), (4.20) and (4.21), one finds that

$$D_e = \frac{|r_0\vec{H}_{1p}(\vec{r},t)| - |r_0\vec{H}_{2p}(\vec{r},t)|}{|r_0\vec{H}_{1c}(\vec{r},t)|}$$

$$= \frac{1}{\tan\alpha} - \tan\alpha \quad . \tag{4.23}$$

Eq.(4.23) expresses the polarization angle α in terms of the backscattered field as desired for the purpose of the present investigation, i.e.,

$$\alpha_{1,2} = \tan^{-1}\left[-\frac{D_e}{2} \pm \sqrt{\left(\frac{D_e}{2}\right) + 1}\ \right] \tag{4.24}$$

Two values of α *are complimentary to each other and the choice of a 'plus' or 'minus' sign in (4.24) does not affect the final system of equations for the profile inversion as will be shown later.*

An interesting outcome of this analysis is that the cross-polarized component of the backscattered far-field, i.e., (4.20) and (4.22), are identical for the incident polarization of α and $\alpha - \pi/2$. This is to be expected and can easily be verified from the theory of reciprocity [70]. In Fig. 4.4, let $\hat{i}_1$ be the polarization direction of the incident wave and $\hat{i}_2$ be the polarization direction of the response waveform (in the present case cross-polarized backscattered wave). The reciprocity theorem then implies that by retaining the above conditions

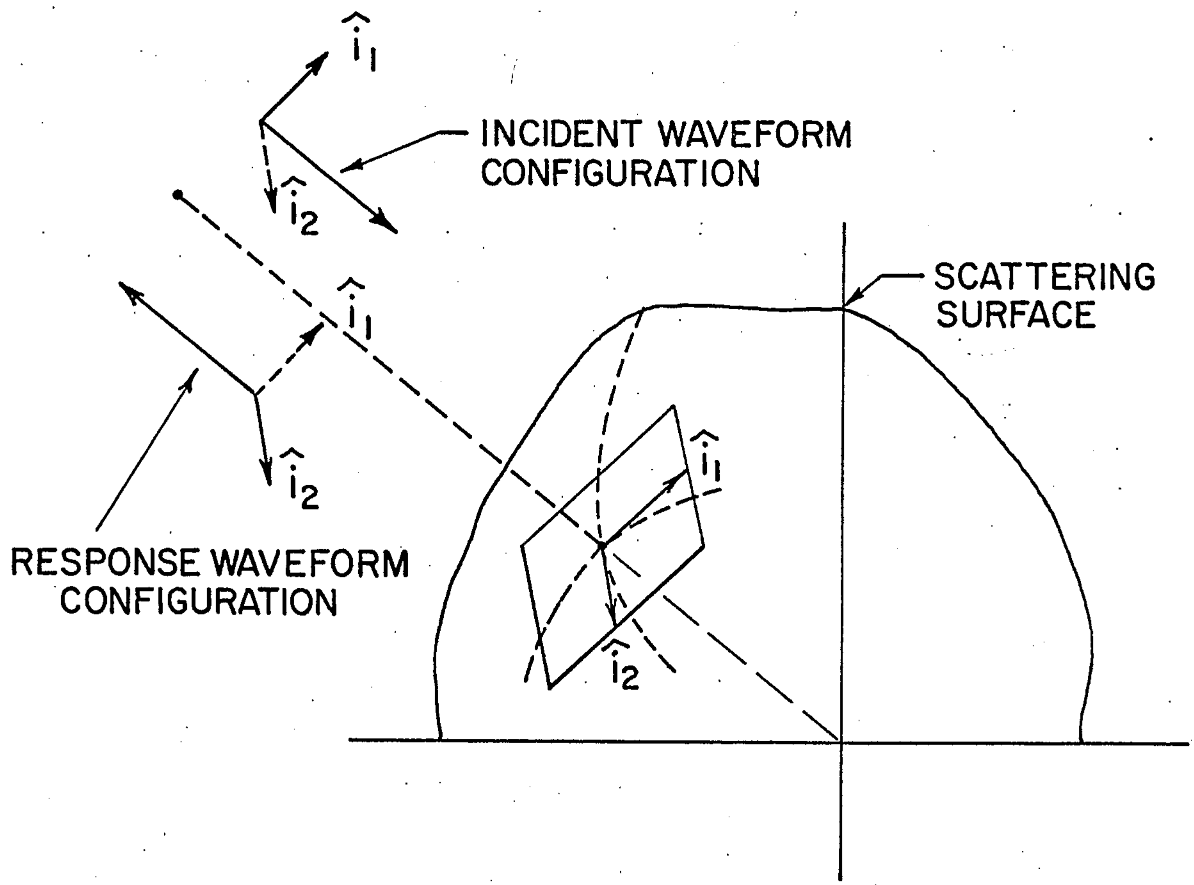

Fig. 4.4 Geometry For The Application Of The Reciprocity Theorem

and by changing the polarization direction of the incident wave from $\hat{i}_1$ to $\hat{i}_2$, the corresponding response waveform (with polarization direction $\hat{i}_2$) will remain identical to the previous response waveform. However, once the creeping wave considerations are introduced in (4.20) and (4.22), the two cross-polarized components $\vec{H}_{1c}$ and $\vec{H}_{2c}$ will differ from one another considerably. This is mainly because the creeping wave path in the shadow zone of the scatterer will be different for different polarizations. Thus, it is concluded that the cross-polarization terms, i.e., (4.20) and (4.22), are identical in the high-frequency limits only and they will differ from each other as the low frequency region is approached.

Using (4.19) to (4.21), the expression for the first and second derivatives of the projected area function are obtained as

$$\frac{\partial^2 A(t)}{\partial t^2} = \pi[\,|r_0 \vec{H}_{1p}(\vec{r},t)| + |r_0 \vec{H}_{2p}(\vec{r},t)|\,] \tag{4.25}$$

and

$$\left(\frac{K_1 - K_2}{2}\right) \frac{\partial A(t)}{\partial t} = \frac{\pi}{\cos\alpha \cdot \sin\alpha} \, |r_0 \vec{H}_{1c}(\vec{r},t)| \quad . \tag{4.26}$$

It is to be noted that the right-hand-side of (4.25) and (4.26) both contain only the backscattered field data since α can be represented in terms of the scattered field as given in (4.24).

4.5 UTILIZATION OF MINKOWSKI'S PROBLEM

As discussed earlier in Chapter Two, the problem of determining a surface, when its Gaussian curvature $K(\hat{n})$ is given on the entire surface of the spherical image, is known as Minkowski's problem. Geometrical optics predicts that if σ , the monostatic scattering cross-section, is known all over a perfectly conducting, smooth, convex, three-dimensional surface, then $K(\hat{n})$ is determined over the entire surface of the unit sphere (i.e., the spherical image of the scatterer). In the present investigation all the points on the surface of the equivalent ellipsoid (corresponding to the specular point of interest on the scattering surface) are transformed onto the unit sphere using Minkowski's support function M which satisfies the partial differential equations (2.9) and (2.10). The support function M of this equivalent ellipsoid, with semi axes a, b, c was obtained in Appendix I as

$$M(\xi,\eta,\zeta) = [(a\xi)^2 + (b\eta)^2 + (c\zeta)^2]^{1/2} \quad , \tag{4.27}$$

where $-1 \leq \xi,\eta,\zeta \leq 1$. The substitution of this expression for M into (2.9) and (2.10) yields two equations involving a, b and c for known values of the direction cosines (ξ,η,ζ). It is to be noted that the right-hand side of (2.10) could be related to radar measurables, and therefore (2.10) constitutes one equation involving a, b and c as the unknowns. The other two independent equations, i.e., (4.25) and (4.26) were obtained by analyzing the space-time integral equation for scattering in Section 4.4.

From the above discussion it is now clear that no attempt has been made here to actually solve the Minkowski problem, but (2.10) has been used as a condition which must be satisfied by the surface parameters of the object in order to have a given value of the backscattered radar-cross-section. In the next section, (4.27) along with (4.25) and (4.26) will be used in proposing a system of equations for the recovery of the surface profile of a perfectly conducting, closed convex, smooth object from the knowledge of the far scattered field.

4.6 SYSTEM OF EQUATIONS FOR THE RECOVERY OF SURFACE PROFILE

If the projected area function $A(t)$, and the difference between the principal curvatures at the specular point, (K_1-K_2), are expressed in terms of the unknown semi axes a, b, c of the equivalent ellipsoid and the known direction cosines (ξ,η,ζ) of the incident wave, then (4.25) and (4.26) will represent two independent equations of the desired system of equations for the recovery of the specular point. Furthermore, from (4.26) it is evident that the choice of the sign in (4.24) is not important for the recovery as $(\cos\alpha \sin\alpha)$ has the same value for $\alpha = \alpha_1$ and $\alpha = \alpha_1 - \pi/2$.

The difference between the principal curvatures at the specular point, (K_1-K_2), has been expressed in the desired form in Appendix I, and $A(t)$ has been obtained in terms of (a,b,c), (ξ,η,ζ) and time t in Appendix II. The third and the final relation for the system of equations is obtained by substituting the value of $M(\xi,\eta,\zeta)$ into (2.10) as shown in Appendix I, and by relating the Gaussian curvature K at the specular point to the backscattered radar-cross-section using the geometrical optics approximation [27,42,47]. As mentioned earlier, this approximation implies that the differential scattering cross-section in the direction of any reflected ray is equal to $R_e/4K$, where R_e is the reflection coefficient. Finally, by transforming the expressions from the time (t) to the frequency (ω) domain by appropriate scaling and

Fourier transformation [12] as discussed in (3.3) and (3.4), the following system of equations for the recovery of the equivalent ellipsoid, and hence the coordinates of the specular point, is arrived at

$$\left|\frac{K_1-K_2}{2}\right| \left| \mathcal{F}\left[\frac{\partial A(t)}{\partial t}\right]\right| = \frac{\pi}{\cos\alpha\sin\alpha} \cdot \left|r_0 H_{1c}(\omega)\right| \tag{4.28}$$

$$\left| \mathcal{F}\left[\frac{\partial^2 A(t)}{\partial t^2}\right]\right| = \pi\left|r_0 H_{1p}(\omega) + r_0 H_{2p}(\omega)\right| \tag{4.29}$$

$$\frac{(a\ b\ c)^2}{[(a\xi)^2+(b\eta)^2+(c\zeta)^2]^{1/2}} = 1/K = 4\sigma \quad ; \quad \text{perfectly conducting case} \tag{4.30}$$

Here, $\mathcal{F}$ represents the Fourier transform and σ is the backscattered radar cross-section. Substituting the expression for the magnitude of $\left[\frac{\partial A(t)}{\partial t}\right]$ in (4.28) and for $\left[\frac{\partial^2 A(t)}{\partial t^2}\right]$ in (4.29) from Appendix II, gives

$$\left|K_1-K_2\right| \left[\left(\frac{G}{\omega^2}\right)^2 + \left(\frac{2\Gamma G}{\omega}\right)^2\right]^{1/2} = \frac{\left|H_{1c}\right|}{\cos\alpha\sin\alpha} \tag{4.31}$$

$$2[(2\Gamma G)^2 + (G/\omega)^2]^{1/2} = [|H_{1p}|^2+|H_{2p}|^2+2|H_{1p}|\cdot|H_{2p}| \cdot \cos(\phi_{1p}-\phi_{2p})] \quad . \tag{4.32}$$

Here, $(\phi_{1p}-\phi_{2p})$ is the relative phase of H_{1p} compared to that of H_{2p}, and Γ and G are defined in Appendix II. Weighting of the field magnitudes with respect to r_0 is understood in (4.31) and (4.32). The left-hand-side of (4.28), (4.29) and (4.30) consist of the unknowns a, b, c and their right-hand-sides consist of only the backscattered far-field data. Thus, as mentioned earlier, the final system of equations for the profile inversion consists of (4.28), (4.29) and (4.30). Once the semi axes a, b, c are recovered from the above system of equations, using expressions for M in (4.27) with known (ξ,η,ζ), the coordinates (x,y,z) of the specular point are determined by (2.6) as

$$x = \frac{\xi a^2}{[(a\xi)^2+(b\eta)^2+(c\zeta)^2]^{1/2}} , \tag{4.33a}$$

$$y = \frac{\eta b^2}{[(a\xi)^2+(b\eta)^2+(c\zeta)^2]^{1/2}} , \tag{4.33b}$$

$$z = \frac{c\zeta^2}{[(a\xi)^2+(b\eta)^2+(c\zeta)^2]^{1/2}} . \tag{4.33c}$$

Application of the inverse scattering model developed here to various test cases will be undertaken in Chapter Six . There, as an example of the application of the proposed inverse scattering model, the test case of a perfectly conducting prolate spheroid will be presented. The major difficulty in performing this test is that the kind of input data needed is not readily available for most of the scatterer shapes. To circumvent this difficulty, an approximate solution for the back-scattered co- and cross- polarized field given off by a prolate spheroid is developed in the next chapter.

chapter five

APPROXIMATE CO- AND CROSS- POLARIZED BACKSCATTERED FIELD OF A CONDUCTING PROLATE SPHEROID

5.1 INTRODUCTION

In order to utilize (4.28) and (4.29) for the recovery of the prolate spheroid, the scattered field quantities on the right-hand-side of these equations must be known. However, to the best of the author's knowledge these input data required for the proposed inverse scattering model are not readily available for most of the scatterer shapes. To circumvent this difficulty, an approximate solution for the backscattered field given off by a prolate spheroid is developed in this chapter. Starting with the vector integro-differential equation for the induced current on the surface of the scatterer, and applying the physical optics approximations [45], the time domain representation for the co- and cross-polarized backscattered far-field has been obtained.

The frequency domain treatments of electromagnetic scattering by a conducting prolate spheroid have been reported by Andreasen [5], Oshiro [65], and Waterman [90]. However, most of these solutions do not cover the entire frequency spectrum and also do not take into account the depolarization of the electromagnetic wave after the scattering from the surface. The approach to the problem via the application of the time domain concepts have been undertaken successfully by Moffatt and co-workers [59,60, 62] and by Bennett and co-workers [9,10,12]. Although these solutions do cover the entire frequency domain, they do not account for the depolarization effects of electromagnetic waves at the surface of the scatterer.

Compared to the above mentioned results, computational results based on the model derived in this chapter are elementary, nevertheless they do yield data for the co- and cross- polarized component of the backscattered field and are quite reliable towards the high frequency end of the spectrum (which is the region of interest as far as this investigation is concerned).

In Section 5.2 certain features of the time domain concepts, which have been exploited in developing the model here, are discussed. In order to get better insight into these features of the time domain concept, an impulse response model synthesized with these concepts by Moffatt [61, 62] has been discussed in Section 5.3. In Section 5.4 the impulse response model developed for the purpose of the present investigation is discussed and finally the computational results based on this model are presented in Section 5.5.

5.2 SOME RELEVANT BASIC FEATURES OF TIME DOMAIN CONCEPTS

The convolution integral in (3.1), relating the response waveform to the interrogating signal, provides an understanding of the relationship between the contributions to $G(s)$ from various portions of the spectrum and the response waveform $F_I(t')$. If the input signal is a monochromatic continuous wave, then the graphical interpretation of convolution is that of reversing one of the signals with respect to time and then sliding one over the other. At any given time, the response is given by the integral of the product of the two waveforms over that time interval where they coincide. For the monochromatic input, this consists of sliding a sinusoid of a given period across the reverse waveform $F_I(-t')$. It follows that at relatively low frequencies, the response can be influenced little by the minute details of the waveform. Therefore, the response at low frequencies is basically dependent on the general size and shape of the waveform. As the input frequency increases, more and more of the waveform details become important whereas slowly varying portions of the waveform become less important since the contributions from these are effectively cancelled by the positive and negative portions of the sinusoid. Two conclusions were drawn from these observations:

(i) The general shape and the size of the impulse response waveform $F_I(t')$ is dictated by the low-frequency response of the object.

(ii) The fine structure and detail of the waveform is controlled by the high-frequency response of the object.

The impulse response as predicted by physical optics has been discussed for the general case in Chapter Three. There, the physical optics approximation to the time-function is simply derived from the cross-sectional area as a function of distance along the line of wave travel. It has been experienced [44] that the impulse response predicted by physical optics is very simple and it is possible to improve on these approximations with a little effort.

In order to correct the physical optics impulse approximation to yield the Rayleigh limit (i.e., the low frequency limit), it has been suggested that an additional time-function may be added to the impulse response so as to give the proper value for the first three moments of the resultant corrected impulse response. This correction function may be formed in many ways, but two simple methods, which have been found useful [44], are the "staircase" and the "polynomial" approximations.

In the "staircase approximation", as shown in Fig. 5.1a, two rectangular pulses are added to the physical optics response. The amplitude of the first pulse is the same as the final value of the physical optics pulse, while the amplitude of the second pulse and the duration of both pulses are determined from the first three moment equations, i.e.,(3.8a),(3.8b) and (3.8c).

A second method of correcting the physical optics impulse response consists of adding a polymonial function of time, starting at the final value of the physical optics time response, choosing the polymonial coefficients and its duration from the three moment equations. This results in a quadratic correction function as shown in Fig. 5.1b.

It is obvious that these two methods for correcting the physical optics impulse response are crude and empirical. These methods have been extended and modified [61] to make use of higher order approximations to the low-frequency scattering properties as well as improved approximations [61] to the high-frequency response. However, these simple examples clearly demonstrate that a first order approximation to the impulse response can be made, using only the Rayleigh scattering coefficient and the physical optics approximation.

To sum up, in general, the physical optics approximation is used to predict the short time behaviour of the response waveform. Latter portions of the waveform are selected either from a knowledge of the character of the response corresponding to specific geometrical features of

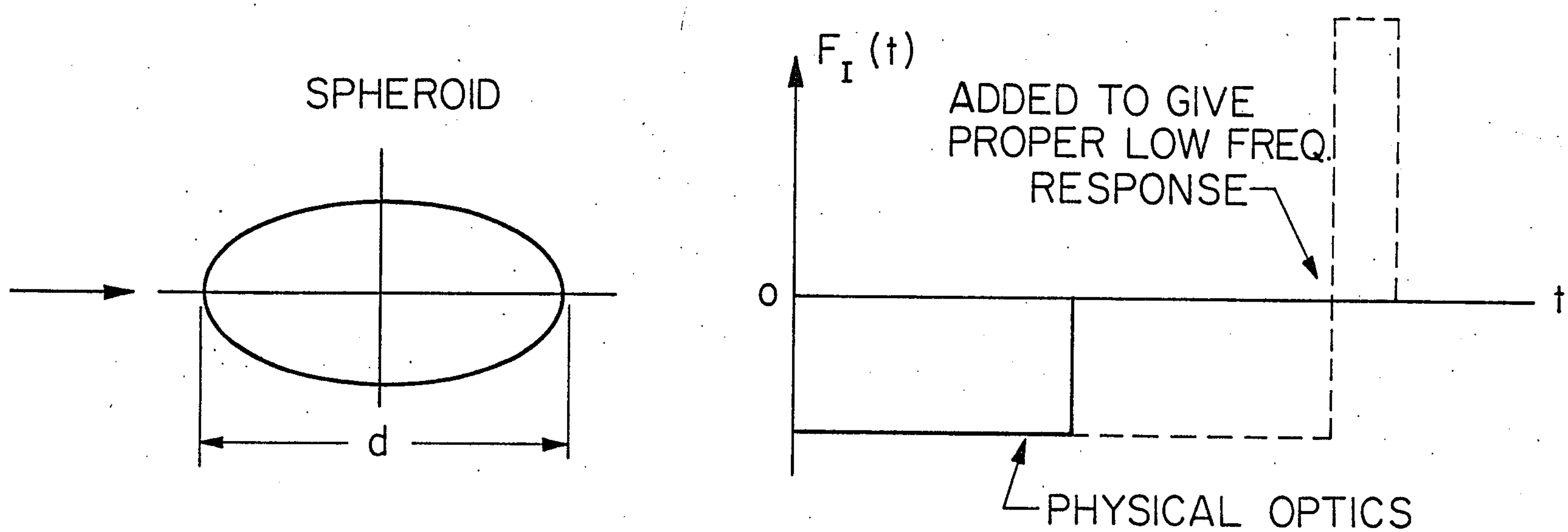

Fig. 5.1a "Staircase Approximation" To The Impulse Response Waveform

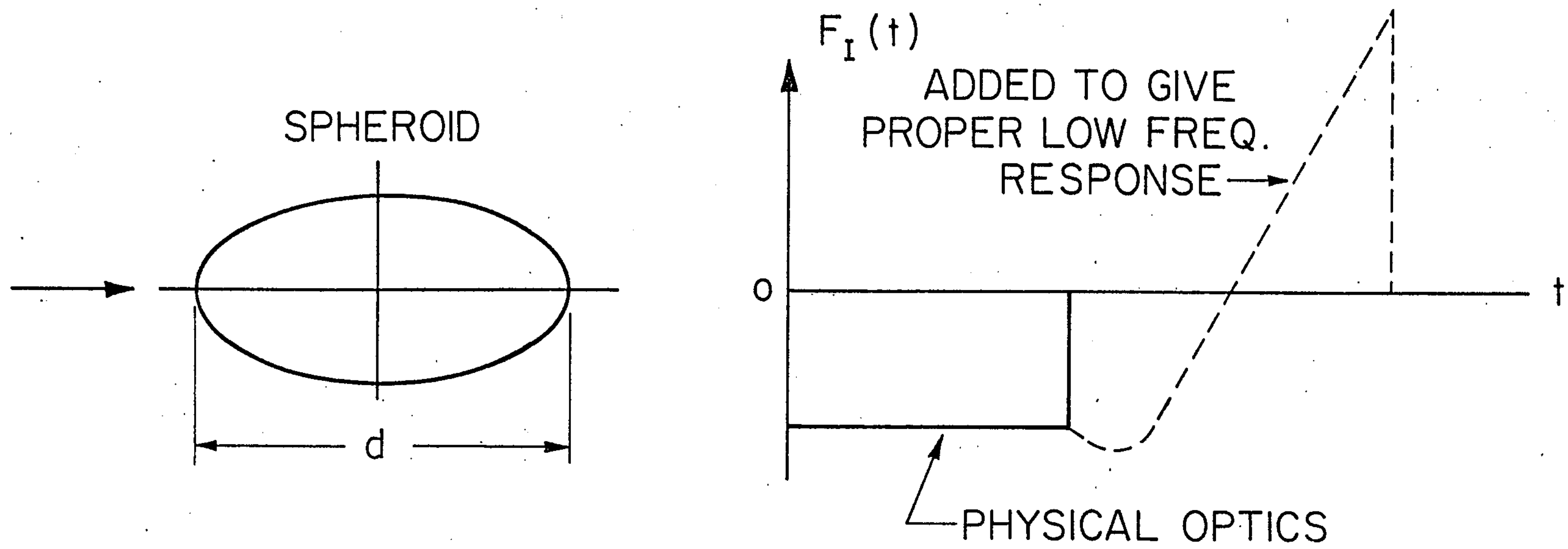

Fig. 5.1b "Polynomial Approximation" To The Impulse Response Waveform

the object or simply from a rough guess of its probable form. These various pieces of the waveform are then joined with sufficiently undetermined parameters to permit the known moment conditions to be satisfied. As an example, in the next section an approximate general solution for the electromagnetic backscattering by a perfectly conducting prolate spheroid is presented [61], without taking depolarization effects into account.

5.3 IMPULSE RESPONSE MODEL FOR ELECTROMAGNETIC BACKSCATTERING BY A PROLATE SPHEROID [61,62]

The prolate spheroid and the coordinates for this problem are shown in Fig. 5.2. Without loss of generality the direction of propagation of the incident plane wave is restricted to the $y-z$ plane, and the incident direction is specified by the angle θ. Two principal polarizations defined for the incident wave are:

TE, where the incident electric-field vector is normal to the y-z plane, and

TM, where the incident electric-field vector lies in the $y-z$ plane.

With each of these principal polarizations a path length is associated which corresponds to the line of sight up to the shadow boundary and a geodesic in the shadow region (see Fig. 5.2). It is to be noted that these paths are measured from an initial reference plane perpendicular to the line of sight.

At this point, certain useful simplifying approximations, made in the

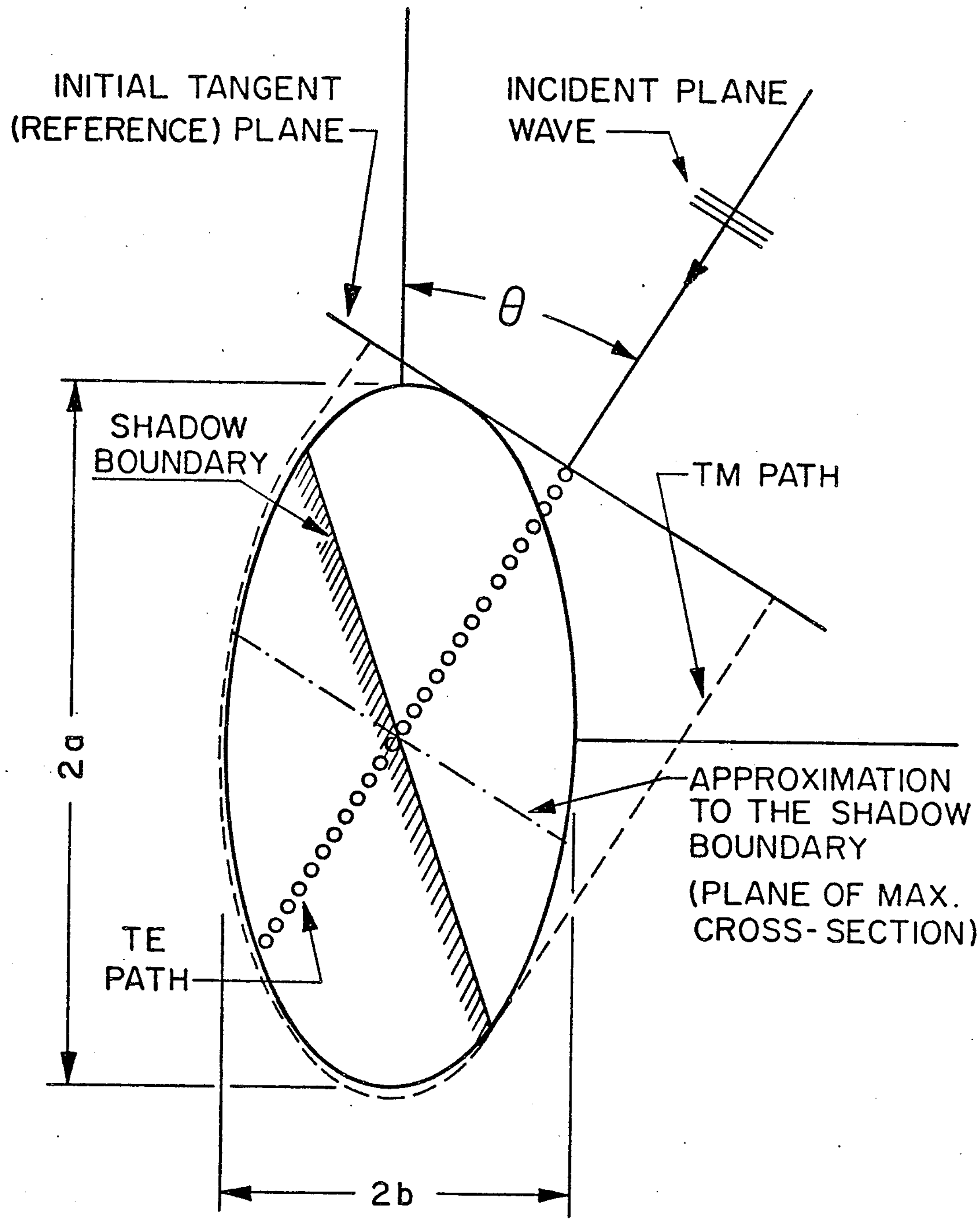

Fig. 5.2 Coordinates Of A Prolate Spheroid For Impulse Response Waveform [61]

course of development of the impulse response model, need to be discussed. The first of these simplifications involves the point of termination in time and the influence of the shadow boundary on the physical optics approximation. For the sphere the shadow boundary is always normal to the direction of propagation of the incident field. However, for a spheroid this only occurs for axial and broadside incidence. Moffatt [61,62] simplified this situation by ignoring the inclination of the shadow boundary and terminating the physical optics approximation at the point corresponding to the peak transverse cross-section encountered by the cutting plane. A second approximation was made in the measurement of path lengths on the shadow side of the spheroid. For either one of the principal polarizations, this distance should be evaluated along the perimeter of an ellipse, i.e., by an incomplete elliptic integral. These integrals are tabulated, but to obtain a simple closed-form expression, the creeping wave path length on the spheroid was calculated with the assumption that an ellipse of semi-major axis 'a' and semi-minor axis 'b' has a circumference given by

$$cir \simeq 2\pi \sqrt{\frac{a^2+b^2}{2}}$$

The impulse response waveform of the spheroid for arbitrary orientation and linear polarization (TE or TM) was written as the sum of two terms

$$F_I(t') = F_{I_1}(t') + F_{I_2}(t') \tag{5.1}$$

where $F_{I_1}(t')$ is used to enforce the desired character of the waveform and $F_{I_2}(t')$ is used to satisfy the known moment conditions [45,61]. With the knowledge of the character of the axial incidence model [60, 61], the high frequency portion of the basic impulse response waveform [i.e., the portion of the impulse response which contributes most to the high frequency end of the phasor response (see discussion in Section 5.2)] for the spheroid was assumed to be of the form[61,62]

$$F_{I_1}(t') = -A_1\delta(t') + (A_2 - A_3 e^{\alpha' t'})[u(t') - u(t' - Tt_0) + A_4 e^{-\alpha' t'} \cdot u(t' - Tt_0)] \quad , \tag{5.2}$$

where

$$A_1 = \frac{ab}{2(a^2\cos^2\theta + b^2\sin^2\theta)} \tag{5.3a}$$

$$A_2 = \frac{ab^2}{2(a^2\cos^2\theta + b^2\sin^2\theta)^{3/2}} \tag{5.3b}$$

$$\alpha' = \left[\frac{\dfrac{-\beta A_1^2}{2A_2}}{\dfrac{-A_1^3}{3A_2^2} - \dfrac{K_r}{2} - \dfrac{A_1^2}{2\beta A_2}} - \beta^2 \right]^{1/2} \tag{5.3c}$$

and $t_0 = 2b/c_0 \quad , \quad \beta = \dfrac{\pi/2}{T - \dfrac{A_1}{A_2}}$.

Here, K_r is the Rayleigh coefficient and u denotes the unit step. The quantity T depends on the principal polarization. It is determined from the geometry of the spheroid and as explained earlier corresponds to the line of sight up to the point of maximum cross-section for the cutting plane, and a geodesic creeping wave path length in the shadow region of the spheroid. Two conditions are imposed on the waveform in (5.2), they are,

$$A_3 \lll A_2$$

and

$$(A_2 - A_3 e^{\alpha' T t_0}) = A_4 e^{-\alpha' T t_0} = P_1 \quad ; \text{ a constant.}$$

This gives

$$A_4 = \frac{1}{A_3} [P_1 A_2 - P_1^2]$$

and

$$\alpha' = \frac{1}{2Tt_0} \ln \left[\frac{A_4}{A_3} \left(\frac{A_2}{P_1} - 1\right)\right]$$

From this, it is clear that P_1 and A_3 are not specified. Thus, with these two parameters, it is possible to achieve a degree of control on the character of the creeping wave contribution. For example, with the peak creeping wave contribution P_1 fixed, A_3 controls the slope of the waveform prior to the peak. It is to be noted that no attempt has been made to utilize the low-frequency derived moment condition to determine the constants P_1 and A_3 or, for that matter, include additional parameters to satisfy higher order moments. Such an approach was found [61] to be ineffective because it is difficult to maintain simultaneously the desired character of the impulse waveform. Even for the simple case, the moment condition may lead to a very complicated set of simultaneous nonlinear integral equations.

Next Moffatt [61] proposed to superimpose a second waveform ensuring the correct low-frequency behaviour of the response. This is an exponentially damped sinusoid which is written in the form

$$F_{I_2}(t') = E[e^{-\phi_1 t'} - e^{-\phi_2 t'}]\ u(t') \qquad (5.4)$$

where E, ϕ_1 and ϕ_2 can be complex. Let the first three moments of $F_{I_1}(t')$, the high frequency portion of the waveform, be I_1, I_2 and I_3, i.e.

$$\int_0^\infty F_{I_1}(t')\ dt' = I_1 \qquad (5.5a)$$

$$\int_0^\infty t' F_{I_1}(t')\,dt' = I_2 \tag{5.5b}$$

$$\int_0^\infty t'^2 F_{I_1}(t')\,dt' = I_3 \quad . \tag{5.5c}$$

Imposing the zero, first and second moment conditions on the total impulse response waveform of the spheroid, i.e., $F_I(t')$, yields the following set of simultaneous non-linear equations

$$E[\phi_2 - \phi_1] = -I_1 \phi_1 \phi_2 \quad , \tag{5.6a}$$

$$E[\phi_2^2 - \phi_1^2] = -I_2 \phi_1^2 \phi_2^2 \quad , \tag{5.6b}$$

$$2E[\phi_2^3 - \phi_1^3] = (K_r - I_3)\phi_1^3 \phi_2^3 \quad . \tag{5.6c}$$

It has been shown[61,62] that if

$$\frac{4}{(I_2/I_1)^2 + (K_r - I_3)/2I_1} \leq \frac{I_2^2}{I_1^2 + (I_2/I_1)^2 + (K_r - I_3)/2I_1} \quad ,$$

then ϕ_1, ϕ_2, E are real and given by

$$\phi_2 = \frac{I_2/I_1}{2[(I_2/I_1)^2 + (K_r - I_3)/2I_1]}$$

$$+ \frac{1}{2}\left\{ \frac{(I_2/I_1)^2}{[(I_2/I_1)^2 + (K_r - I_3)/2I_1]^2} - \frac{4}{[(I_2/I_1)^2 + (K_r - I_3)/2I_1]} \right\}^{1/2} \quad ,$$

$$\phi_1 = \frac{1}{\phi_2[(I_2/I_1)^2 + (K_r - I_3)/2I_1]} \quad ,$$

$$E_1 = \frac{-I_1 \phi_1 \phi_2}{\phi_2 - \phi_1} \quad .$$

If the above cited inequality is not satisfied, ϕ_1 and ϕ_2 become complex conjugates

$$\phi_{1r} = \phi_{2r} = \frac{I_2}{2I_1[(I_2/I_1)^2+(K_r-I_3)/2I_1]} ,$$

$$\phi_{1i} = -\phi_{2i} = \frac{1}{2}\left\{ \frac{4}{(I_2/I_1)^2+(K_r-I_3)/2I_1} - \frac{I_2^2}{I_1^2+(I_2/I_1)^2+(K_r-I_3)/2I_1} \right\}^{1/2} ,$$

$$E = -\frac{j}{2}\left\{ \frac{I_1}{\phi_{1i}[(I_2/I_1)^2+(K_r-I_3)/2I_1]} \right\} ,$$

where I_1, I_2 and I_3 were found to be

$$I_1 = -A_1 + A_2 T - \frac{A_3 e^{\alpha' T}}{\alpha'} + \frac{A_4 e^{-\alpha' T}}{\alpha'} ,$$

$$I_2 = \frac{A_2 T^2}{2} - \frac{A_3 T e^{\alpha' T}}{\alpha'} + \frac{A_3 e^{\alpha' T}}{\alpha'^2} + \frac{A_4 T e^{-\alpha' T}}{\alpha'} + \frac{A_4 e^{-\alpha' T}}{\alpha'^2}$$

$$I_3 = \frac{A_2 T^3}{3} + \frac{T^2}{\alpha'}[A_4 e^{-\alpha' T} - A_3 e^{\alpha' T}] + \frac{2T}{\alpha'^2}[A_3 e^{\alpha' T} + A_4 e^{-\alpha' T}] + \frac{2}{\alpha'^3}[A_4 e^{-\alpha' T} - A_3 e^{\alpha' T}] .$$

Thus, except for A_3 and P_1 the remainder of the parameters of the impulse response waveform are known. It has been felt [61] that very little is gained by introducing sophisticated procedures and techniques for establishing the two parameters A_3 and P_1 above, particularly when they are expected to change with aspect angle. Also such sophistication would be achieved at the expense of a much more complicated model. The purpose here is to develop a simple model and, hopefully, one whose constant parameters are invariant for a given axial spheroid ratio regardless of orientation and incident polarization. Thus, a rough estimate of the parameter A_3 was obtained from the axial waveform results [60,61], and the invariance of the creeping wave peak with respect to the axial ratio, obtained in [60], was accepted.

It has been shown [61,62] that the impulse response model described in this section is in reasonable agreement with measured data for a spheroid of 2 : 1 axial ratio. The minor disagreement between calculated and measured data has been attributed to the enforced simplicity of the model, achieved at the expense of numerous approximations and estimates, which possibly could be corrected with a more completed model. Based on the insight gained from this example, in the next section, in a somewhat similar fashion, an impulse response model for the co- and the cross-polarized components of the backscattered field (at least for the high frequency case) off a prolate spheroid is developed.

5.4 APPROXIMATE IMPULSE RESPONSE MODEL FOR CO- AND CROSS-POLARIZED BACKSCATTERED FIELD

Since the main aim is to generate input data for the inverse scattering model of Chapter Four at sufficiently high frequencies, the waveform synthesized here is deliberately made as simple as possible. This impulse response model is merely the physical optics approximation for short times and a creeping wave contribution consisting of the extension of the physical optics approximation beyond the shadow boundary (with a time scale stretching to account for the fact that the wave travels along the surface of the scatterer beyond the shadow boundary) and an exponential decay beyond the object.

In order to derive a general expression for the initial time portion of the prolate spheroid impulse response, an expression for the area function $A(t)$ for arbitrary direction of incidence needs to be known. For a general direction of incidence, ϕ (the value of θ does not matter because this is a two-dimensional case), on a prolate spheroid, Bennett and co-workers [12] obtained an expression for the area function. The calculations needed are identical to that presented in Appendix II, except that here only one coordinate transformation (two-dimensional case) is required. Consider a prolate spheroid with semi-major axis 'a' and semi-minor axis 'b' which are centered at the origin of the coordinate system. With x' representing the distance from the origin along the direction of incidence(see Fig.A.II.1),$A(x')$gives the projected area of the scatterer as delineated by the incident impulse as it moves across the scatterer at one-half the free space velocity of light (this has been discussed in detail in Chapter Three). For a given direction of incidence $\bar{\phi}$, $A(x')$ is given as [12]

$$A(x') = \frac{\pi ab^2}{\Gamma^3(\phi)} \, [\Gamma^2(\phi) - x'^2] \, u \, [\Gamma(\phi) - x'] \quad , \qquad (5.7)$$

where

$$\Gamma(\phi) = \left[\frac{a^2b^2B_1(\phi)}{B_1(\phi)E_1(\phi) - C_1^2(\phi)} \right]^{1/2} \qquad (5.8)$$

with

$$B_1(\phi) = a^2\cos^2\phi + b^2\sin^2\phi \quad ,$$

$$C_1(\phi) = (a^2-b^2)\sin\phi\cos\phi \quad ,$$

$$E_1(\phi) = a^2\sin^2\phi + b^2\cos^2\phi \quad .$$

In this case, as discussed in (3.14)

$$x' = -\frac{c_0 t}{2} = -t/2$$

which, on substitution into (5.7), yields the expression

$$\frac{1}{2\pi} A(t) = \frac{G'}{2} [4\Gamma^2(\phi) - t^2] \; u \; [t + 2\Gamma(\phi)] \tag{5.9}$$

where $$G' = \frac{ab^2}{\Gamma^3(\phi)} \quad .$$

It has been shown in Chapter Three that the ramp response is given by the projected area function, i.e.,

$$\textit{ramp response} = \frac{1}{2\pi} A(t) \quad .$$

This is a physical optics approximation and conventionally holds true only up to the shadow boundary. However, in the present model, this approximation has been extended beyond the shadow boundary and has been modified in a manner such that the time beyond the shadow boundary is calculated according to the distances measured along the surface of the scatterer rather than along line-of-sight in free space, i.e.,

$$\begin{aligned} \textit{ramp response} &= A(t)[u(t+2\Gamma) - u(t)] \\ &\quad + A(\frac{2\Gamma}{T_c} t)[u(t) - u(t-T_c)] \end{aligned} \tag{5.10}$$

where

$$T_c = Tt_0 - 2\Gamma$$

with T being the total path length as discussed in Section 5.2. It is to be noted that in (5.10) the consideration of the path length beyond the shadow boundary has been simplified by just scaling the time t by a factor $(2\Gamma/T_c)$, i.e., by assuming a linear deformation of the path length beyond the shadow boundary. In the present consideration, the location of the shadow boundary has been simplified in a manner similar to Moffatt [61], where the inclination of the shadow boundary was ignored and, instead, the shadow boundary was located at the point corresponding to the peak transverse cross-section encountered by the cutting plane (see Fig. 5.2). With this definition of the shadow boundary, for a prolate spheroid centered at the origin (as is the case here), (5.9) indicates that the shadow boundary is always located at $t = 0$ on the time scale, and the distance between the shadow boundary and the specular point along the direction of the incident wave is given by $\Gamma(\phi)$ (see Fig. 5.2). Using (5.9) and (5.10), the expression for the projected area function of the scatterer is obtained as

$$\frac{1}{2\pi} A(t) = \frac{G'}{2} [4\Gamma^2(\phi) - t^2][u(t+2\Gamma) - u(t)]$$
$$+ \frac{G'}{2} [4\Gamma^2(\phi) - \frac{4\Gamma^2(\phi)}{T_c^2} t^2][u(t) - u(t-T_c)] \quad . \qquad (5.11)$$

A sketch of the projected area function given by (5.11) is shown in Fig. 5.3. There, the stretching of the time scale beyond the shadow boundary, in order to take care of creeping-wave path length (at least to a first approximation), has been clearly demonstrated. Taking the derivative of (5.11) with respect to time yields

$$\frac{1}{2\pi} \frac{\partial A(t)}{\partial t} = -G't[\{u(t+2\Gamma)-u(t)\} - (\frac{4\Gamma^2}{T_c^2}) \{u(t)-u(t-T_c)\}]$$
$$+ \frac{G'}{2} [(4\Gamma^2-t^2)\delta(t+2\Gamma) - (4\Gamma^2-t^2)\delta(t)$$
$$+(4\Gamma^2 - \frac{4\Gamma^2}{T^2} t^2)\delta(t)+(4\Gamma^2 - \frac{4\Gamma^2}{T_c^2} t^2)\delta(t-T_c)] \quad . \qquad (5.12a)$$

Using the properties of the delta function, it can easily be shown that the quantity inside the second square bracket of (5.12a) is zero, thus

$$\frac{1}{2\pi} \frac{\partial A(t)}{\partial t} = -G't[\{u(t+2\Gamma) - u(t)\} - \frac{4\Gamma^2}{T_c^2} \{u(t)-u(t-T_c)\}] \qquad (5.12b)$$

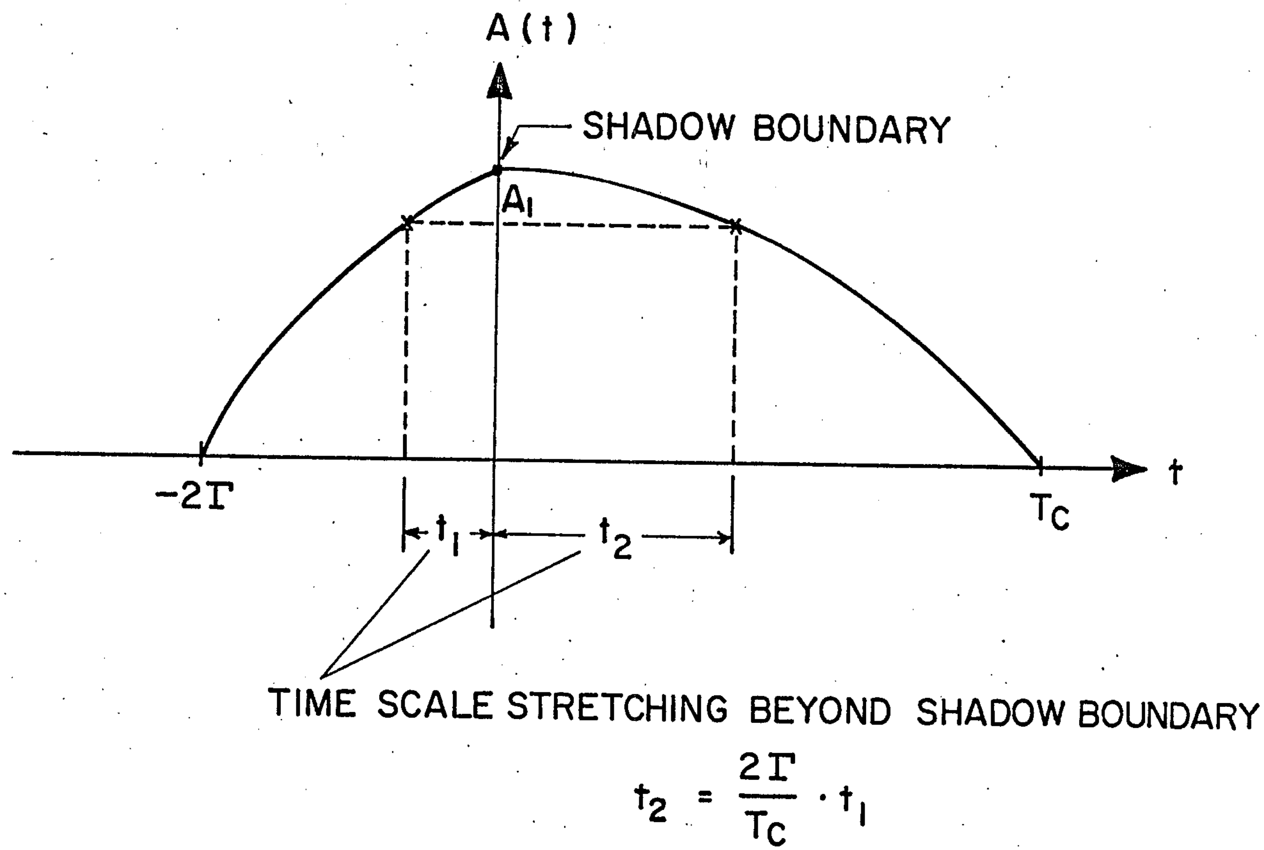

Fig. 5.3 Extension Of The Physical Optics Approximation Beyond Shadow Boundary

Differentiating (5.12b) with respect to time and using the properties of the delta function again, yields

$$\frac{1}{2\pi}\frac{\partial^2 A(t)}{\partial t^2} = 2\Gamma G'\delta(t+2\Gamma) - \frac{4\Gamma^2}{T_c}G'\delta(t-T_c)$$
$$-G'[\{u(t+2\Gamma)-u(t)\} - \frac{4\Gamma^2}{T^2}\{u(t)-u(t-T_c)\}] \qquad (5.13)$$

Now, substituting the values of $\frac{\partial A(t)}{\partial t}$ and $\frac{\partial^2 A(t)}{\partial t^2}$ from (5.12b) and (5.13) into (4.19), the high frequency approximation to the backscattered co-polarized field yields

$$|r_0\vec{H}_{c0}(\vec{r},t)| = 2\Gamma G'\delta(t+2\Gamma) - \frac{4\Gamma^2}{T_c}G'\delta(t-T_c)$$
$$-G'[1+t(\cos 2\alpha)(\frac{K_1-K_2}{2})][u(t+2\Gamma)-u(t)]$$
$$-G'[\frac{4\Gamma^2}{T_c^2}+\frac{4\Gamma^2}{T_c^2}t(\cos 2\alpha)(\frac{K_1-K_2}{2})][u(t)-u(t-T_c)] \quad . \qquad (5.14)$$

Here, it has been assumed that the incident magnetic field $\vec{H}_i$ is of unit magnitude and its polarization angle is α (see Chapter Four for the definition of the polarization angle). Thus H_{i_1} and H_{i_2} were replaced by $\cos\alpha$ and $\sin\alpha$ respectively in (5.14).

A sketch of the approximate impulse response model is shown in Fig. 5.4. From a knowledge of the axial impulse response waveform [60,61] and the experience of the previous investigators [9,12,45,61,67], it is clear that the impulse response waveform in (5.14) has two primary faults:

Firstly, the erroneous jump occuring at the shadow boundary ($t = 0$), and secondly, the form of the response waveform at the creeping wave peak ($t = T_c$).

In the first case, there is no evidence that in the neighborhood of the

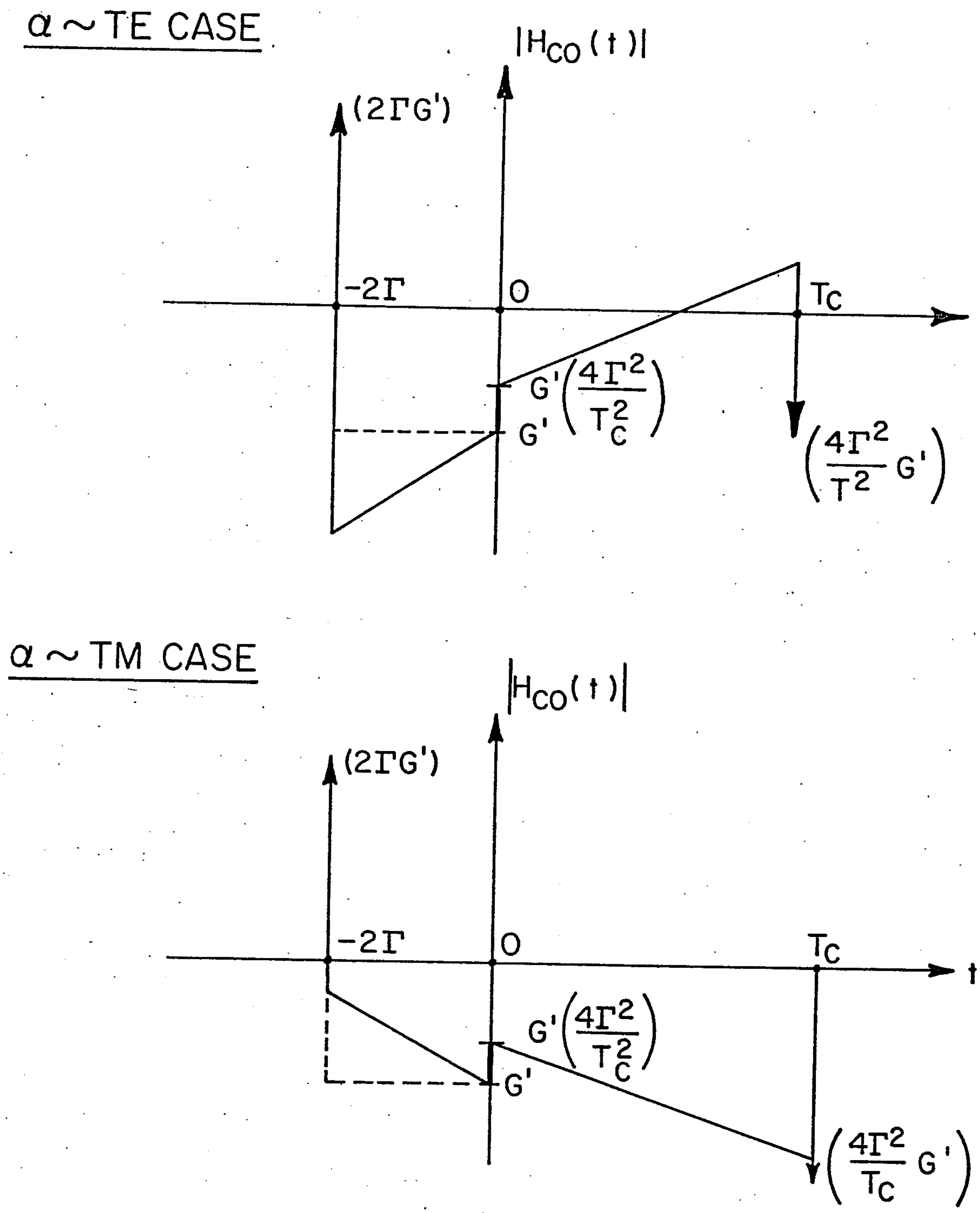

Fig. 5.4 Impulse Response Waveform Corresponding To (5.14)

shadow boundary a discontinuity should occur in the waveform. In the second case, although a sharp creeping wave peak is expected at $t = T_c$, this peak cannot be impulsive in nature. For the case of a smooth object, the delta function contribution to the impulse response waveform can only come from the specular point. In a similar approach to the problem (i.e., using the ramp response as the starting point) Moffatt [61,62] also encountered similar defects, and concluded that these defects arise because of the assumption made in calculating the creeping wave path length and in locating the shadow boundary on the surface. There, it was also pointed out that, in principle, it should be possible to correct the ramp-response-derived model. However, the additional parameters required would exceed the known conditions on the waveform. This is the type of problem one encounters when starting with an analytic approximation of the ramp response waveform. Since this waveform is smoother than its first or second derivatives, it can be estimated with fewer parameters. But in the impulse response waveform, i.e., when differentiated twice, the type of functional dependence assumed is extremely critical.

In order to overcome the above mentioned defects of the impulse response waveform of (5.14), a direct model of the impulse response waveform is proposed. In this model all the desired properties of (5.14) have been retained and the erroneous jump at the shadow boundary is simply eliminated. Although this elimination of the jump is based on somewhat empirical reasoning, it is expected to be valid for the high frequency end of the spectrum, which is the region of interest as far as this investigation is concerned. The creeping wave peak term (i.e., delta function at $t = T_c$) is not included for the time being and it will be considered with the terminating term which will be added later. With these above mentioned adjustments to (5.14), the approximate model for the impulse response waveform for the co-polarized backscattered field is

$$
\begin{aligned}
|r_0 \vec{H}_{c0}(\vec{r},t)| &= 2\Gamma G'\delta(t+2\Gamma) \\
&\quad -G'[1+t(\cos 2\alpha)(\frac{K_1-K_2}{2})][u(t+2\Gamma)-u(t)] \\
&\quad -G'[1+\frac{4\Gamma^2}{T_c^2}t(\cos 2\alpha)(\frac{K_1-K_2}{2})][u(t)-u(t-T_c)] \quad . \qquad (5.15)
\end{aligned}
$$

Substitution of the value of $\frac{\partial A(t)}{\partial t}$ from (5.12b) into (4.20) along with $H_{i_1} = \cos\alpha$, $H_{i_2} = \sin\alpha$ yields an expression for the impulse response waveform corresponding to the cross-polarized backscattered field as

$$
\begin{aligned}
|r_0 \overline{H}_{cr}(\overline{r},t)| &= -G't(\frac{K_1-K_2}{2})\sin 2\alpha[u(t+2\Gamma)-u(t)] \\
&\quad -\frac{4\Gamma^2 G'}{T_c^2}t(\frac{K_1-K_2}{2})\sin 2\alpha[u(t)-u(t-T_c)] \quad . \qquad (5.16)
\end{aligned}
$$

An undesirable characteristic of the model presented in (5.15) and (5.16) is the abrupt termination of the waveform at $t = T_c$. From a physical point of view the time domain backscattered field should die out smoothly after the incident impulse has passed beyond the scattering object [9,61]. Thus, for the times after the plane moves beyond the spheroid, the waveforms in (5.15) and (5.16) are extended continuously and multiplied by an exponentially damped term. As mentioned earlier, the damping factor could be chosen in such a manner that the resulting waveform is forced to satisfy the second moment condition. However, it has been shown [61] that such an approach might prove quite cumbersome, and even for very simple waveforms, the integration indicated by the moment conditions can lead to a very complicated set of simultaneous nonlinear equations. Since here the interest is restricted to the high frequency end of the spectrum, the impulse response waveform is kept simple by choosing the same damping factor α' as given in (5.3c) and derived by Moffatt [61]. Thus, with the new termination term added, the impulse response model is given as

$$
\begin{aligned}
|r_0 \vec{H}_{c0}(\vec{r},t)| = \; & 2\Gamma G'\delta(t+2\Gamma) \\
& - G'[1+t(\cos 2\alpha)(\tfrac{K_1-K_2}{2})][u(t+2\Gamma)-u(t)] \\
& - G'[1+\frac{4\Gamma^2}{T_c^2}\,t(\cos 2\alpha)(\tfrac{K_1-K_2}{2})][u(t)-u(t-T_c)] \\
& - G'[1+\frac{4\Gamma^2}{T_c}\,(\cos 2\alpha)(\tfrac{K_1-K_2}{2})]e^{\alpha'(T_c-t)}\,u(t-T_c)
\end{aligned}
\qquad (5.17)
$$

$$
\begin{aligned}
|r_0 \vec{H}_{cr}(\vec{r},t)| = \; & -G't(\tfrac{K_1-K_2}{2})\sin 2\alpha[u(t+2\Gamma)-u(t)] \\
& - \frac{4\Gamma^2 G'}{T_c^2}\,t(\tfrac{K_1-K_2}{2})\sin 2\alpha[u(t)-u(t-T_c)] \\
& - \frac{4\Gamma^2}{T_c^2}\,G'(\tfrac{K_1-K_2}{2})(\sin 2\alpha)e^{\alpha'(T_c-t)}\,u(t-T_c)
\end{aligned}
\qquad (5.18)
$$

The sketch of the impulse response wave corresponding to (5.17) is given in Fig. 5.5 for the cases where the incident wave polarization is close to the TE and TM cases. Comparison of these two sketches with the impulse response waveform reported by Bennett and co-workers [12] brings out the fact that the basic nature of the singularities in both cases are identical. It is to be noted that these are the portions of an impulse response waveform which contribute to the high frequency end of the phasor response in a major way. In the next section, using (5.17) and (5.18), computational results for the phasor response of a prolate spheroid of axial ratio of 2 : 1 are presented.

$\alpha \sim$ TE CASE

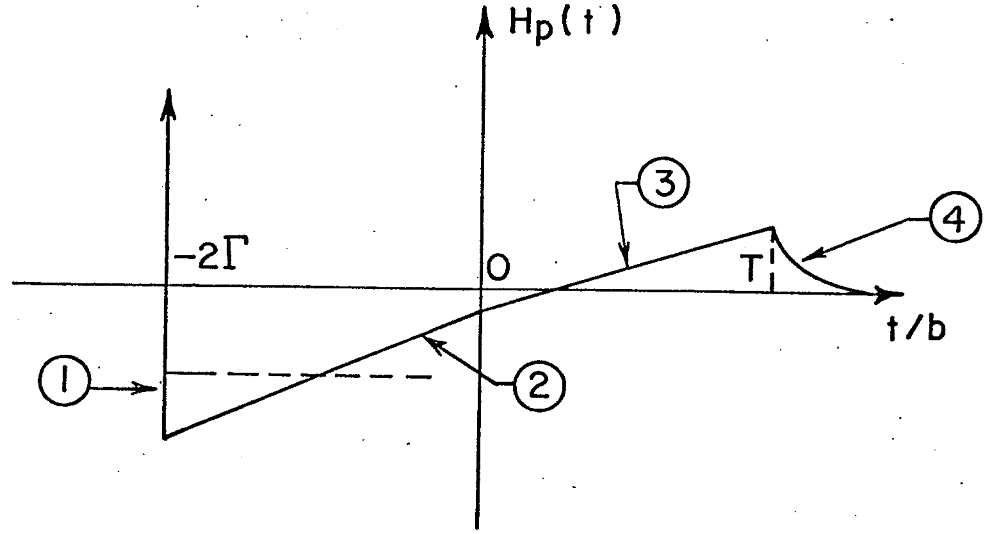

$\alpha \sim$ TM CASE

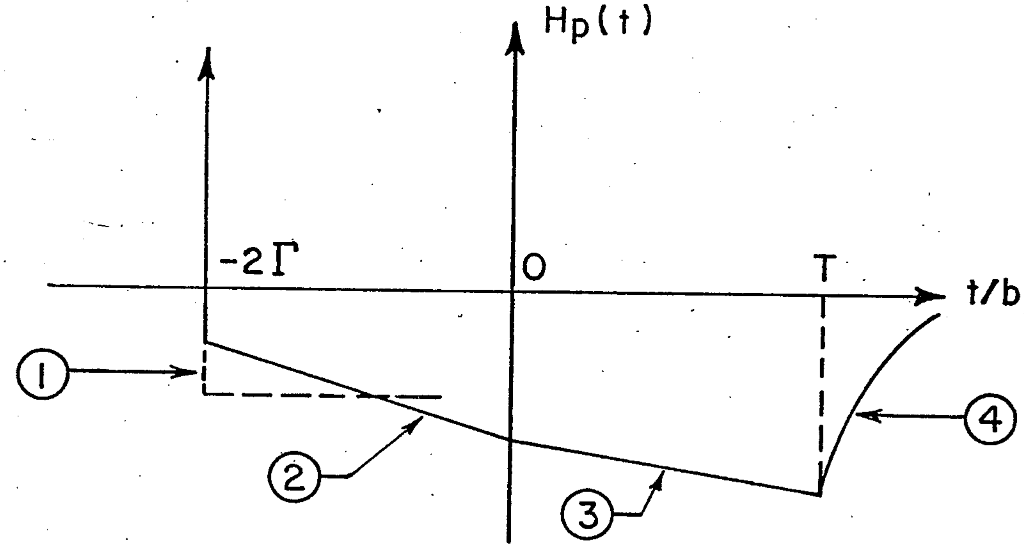

(1) PHYSICAL OPTICS APPROX.

(2) POLARIZATION CORRECTION [BENNETT et al ; 1973]

(3) ACCOUNTS FOR THE FACT THAT WAVE TRAVELS ALONG THE SURFACE OF THE OBJECT BEYOND THE SHADOW BOUNDARY (i.e. POINT OF MAX. CROSS SEC.)

(4) EXPONENTIAL DECAY BEYOND T*

*T; CORRESPONDS TO LINE OF SIGHT TO THE POINT OF MAX. CROSS SEC. & A GEODESIC CREEPING WAVE PATH LENGTH BEYOND [MOFFATT ; 1969]

Fig. 5.5 Approimate model for the input data.

5.5 COMPUTATIONAL RESULTS

The frequency-dependent co- and cross- polarized phasor responses can be obtained directly from (5.17) and (5.18) by making use of the Fourier transformation pairs defined in Appendix III. However, before this transformation could be performed, values of various parameters in (5.17) and (5.18) must be known for arbitrary polarization of the incident wave. Except for T_c and α', all other parameters are independent of the incident wave polarization and could easily be calculated from the known size of the prolate spheroid and the known direction of incidence ϕ. T_c, the creeping wave path length is directly dependent on the incident wave polarization as can be easily seen from Fig. 5.2. The factor α', as defined in (5.3c), is polarization-dependent as it involves the Rayleigh coefficient K_r.

An approximate analytical expression for the total path length T (which corresponds to the line-of-sight up to the point of maximum cross-section for the cutting plane and a geodesic creeping wave path length in the shadow region), for two extreme cases of the incident wave polarization (i.e., TE and TM), has been reported by Moffatt [61,62]. Based on the approximation that the circumference of an ellipse of semi-major axis 'a' and semi-minor axis 'b' is given by $\pi\sqrt{2(a^2+b^2)}$, the path length T corresponding to the two principal polarizations, has been obtained [62] as follows

$$T(TM) = \frac{\sin\phi\cos\phi(a^2-b^2)}{2b\sqrt{a^2\sin^2\phi+b^2\cos^2\phi}} + \frac{1}{2b}\sqrt{a^2\cos^2\phi+b^2\sin^2\phi}$$

$$+ \frac{\pi}{2b}\sqrt{\frac{a^2+b^2}{2}} + \frac{1}{2b}\left| \frac{\sin\phi\cos\phi(a^2-b^2)}{\sqrt{a^2\sin^2\phi+b^2\cos^2\phi}} - \sqrt{a^2\cos^2\phi+b^2\sin^2\phi}\right| \tag{5.19}$$

$$T(TE) = \frac{\sin^2\phi\cos^2\phi(a^2-b^2)^2}{b\sqrt{a^2\cos^2\phi+b^2\sin^2\phi}\,(a^2\sin^2\phi+b^2\cos^2\phi)}$$

$$+ \frac{\sqrt{a^2\cos^2\phi+b^2\sin^2\phi}}{b} + \frac{\pi}{2b}\sqrt{\frac{c_1^2+c_2^2}{2}}\ , \tag{5.20}$$

where

$$c_1^2 = b^2 \ \{1 - \frac{\sin^2\phi\cos^2\phi(a^2-b^2)^2}{a^2b^2}$$

$$+ [\ \frac{\sin^2\phi\cos^2\phi(b^2-a^2)(a^2-b^2)}{ab(a^2\cos^2\phi+b^2\sin^2\phi)}\ ]^2\ \}$$

and

$$c_2^2 = \frac{a^2b^2-\sin^2\phi\cos^2\phi(a^2-b^2)^2}{a^2\sin^2\phi+b^2\cos^2\phi}$$

$$+ [\ \frac{\sin^2\phi\cos^2\phi(a^2-b^2)(b^2-a^2)}{\sqrt{a^2\cos^2\phi+b^2\sin^2\phi}\ (a^2\sin^2\phi+b^2\cos^2\phi)}\ ]^2$$

As α varies from one extreme to the other (i.e., 0 to $\pi/2$) the creeping wave path length T must vary from $T(TE)$ to $T(TM)$. An empirically suggested analytic expression for this variation is

$$T(\alpha) = T(TE)\cos^2\alpha + T(TM)\sin^2\alpha \tag{5.21}$$

This expression was arrived at mainly from two considerations. First, when $\alpha = 0$, $T(\alpha)$ should become $T(TE)$; and when $\alpha = \pi/2$, $T(\alpha)$ should represent $T(TM)$. Secondly, in case of a sphere, where the creeping wave path length is identical for the TE and the TM polarization (see

Fig. 5.2), the path length $T(\alpha)$ is independent of the polarization of the incident wave and, therefore, in this degenerate case $T(\alpha)$ should remain constant for an arbitrary value of α . Although the approximation in (5.21) appears to be unsophisticated, it certainly is a valid first order approximation from the physical surface geometry point of view (especially for a 2 : 1 prolate spheroid).

Next, in order to obtain a value of the damping factor α' from (5.3c) for an arbitrary value of the polarization angle α , an expression for the value of the Rayleigh coefficient for an arbitrary value of α was developed. Moffatt [61] has presented values of the Rayleigh coefficient for TE and TM cases for various axial ratios of the prolate spheroid. There, a general solution for the coefficients in a power series expansion of the scattered field in terms of the wave number (ka) [61] has been utilized to obtain the Rayleigh term for the case of prolate and oblate spheroids. The Rayleigh coefficient $K_r(\alpha)$ is defined in a manner such that

$$E_s(\alpha) = K_r(\alpha)\cdot(ka)^2 \tag{5.22}$$

where $E_s(\alpha)$ denotes the normalized scattered field for an incident polarization angle α. For TE and TM cases, (5.22) will yield

$$E_s(TE) = K_r(TE)(ka)^2 \tag{5.23a}$$

and

$$E_s(TM) = K_r(TM)(ka)^2 \quad . \tag{5.23b}$$

For an arbitrary linearly polarized, incident wave, where the incident magnetic field $\vec{H}_i$ makes an angle α with the $\hat{a}_1$(TM) direction (see Fig. 5.6), the magnitude of the component of the electric field in the $\hat{a}_2$ direction is $E_i\cos\alpha$; and the component in the $\hat{a}_1$ direction is

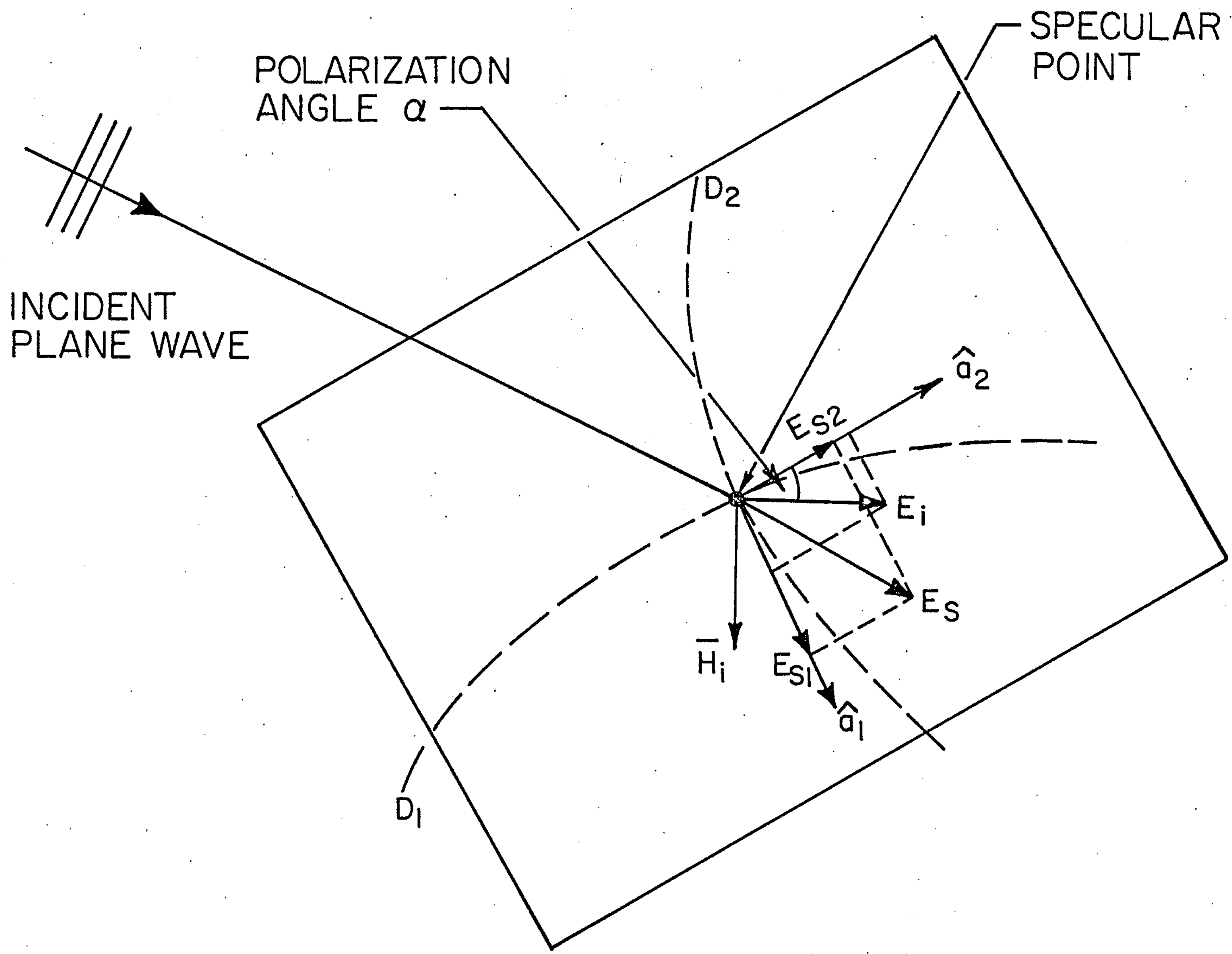

Fig. 5.6 Geometry Around The Specular Point For Derivation Of The Expression For Rayleigh Coefficient

$E_i \sin\alpha$. From (5.23a) and (5.23b) the corresponding components of the scattered field are

$$E_{s_2}(\mathrm{TE}) = K_r(\mathrm{TE})\cos\alpha(ka)^2 \qquad \text{and}$$

$$E_{s_1}(\mathrm{TM}) = K_r(\mathrm{TM})\sin\alpha(ka)^2 \quad .$$

Therefore, the total scattered field is

$$|E_s(\alpha)| = K_r(\alpha)(ka)^2 = \{[K_r(\mathrm{TE})\cos\alpha]^2+(K_r(\mathrm{TM})\sin\alpha]^2\}^{1/2}(ka)^2 \; . \tag{5.24}$$

Thus, from (5.24), the expression for the Rayleigh coefficient for an arbitrary value of α is given by

$$K_r(\alpha) = \{[K_r(\mathrm{TE})\cos\alpha]^2 + [K_r(\mathrm{TM})\sin\alpha]^2\}^{1/2} \quad . \tag{5.25}$$

With the values of $K_r(\mathrm{TE})$ and $K_r(\mathrm{TM})$ for arbitrary direction of incidence ϕ for a prolate spheroid as documented in [61], (5.25) provides the value of the Rayleigh coefficient for arbitrary direction of incidence ϕ with arbitrary polarization α.

Now, with all the parameters in (5.17) and (5.18) specified for the arbitrary linearly polarized incident wave and for an arbitrary direction of incidence, the frequency-dependent phasor response has been computed using the Fourier transformation pair given in (3.3). For the two extreme cases (TE and TM) of the incident wave polarization (i.e., when the cross-polarized return vanishes), the frequency-domain results are available in the published literature [12]. Therefore, for the quasi TE and quasi TM (i.e., almost TE and almost TM)cases, the approximate solutions developed here were converted to the frequency domain by

Fourier transformation, and compared with the available published results (see Figs. 5.7a to 5.7f). As expected, the agreement in nature of variation and general shape between the two sets of results was good towards the high frequency end (i.e., $\omega \gtrsim 5.0$). Towards the low frequency end the approximate solution differs much from the established solutions published in the literature [12]. This was to be expected, as very little low frequency information was included in the time domain representations in Fig. 5.5. *Note, that exact values of the field cannot be compared as the y axis of [12] is the total field and not the co-polarized field. (Also, note that Fig. 5.7 provides approximations for the quasi TE ($\alpha = 5°$) and quasi TM ($\alpha = 85°$) cases, but not for the exact TE and TM solutions.)* It is to be noted that even at the low frequency end, the position of maxima and minima of the amplitude of the frequency response were found to be identical to those given in the literature. The disagreement towards the low frequency end, however, does not prevent the use of this approximate solution as input data for the proposed inverse scattering model of Chapter Four. This is because the proposed inverse scattering model is expected to be good at the relatively high frequency region only. In order to give a better insight into the behaviour of the impulse scattering model proposed in (5.17), values of Γ, T_c and α' for polarization angle of $\alpha = 30°$ and $-60°$ (i.e., $\alpha - \pi/2$) are compiled in the Table I.

The cross-polarized frequency response obtained from the approximate solution was compared with another published approximate result [28] (which, to the best of the author's knowledge, is the only such result available in literature) and a good agreement for the basic nature and

TABLE I

PARAMETER VALUES FOR IMPULSE RESPONSE WAVEFORM

(i) POLARIZATION ANGLE $\alpha = 30°$, $\theta = 90°$

ϕ (deg.)	2Γ	T_c	α'
0	4.0000	4.9648	3.2366
10	3.9546	4.9094	3.2697
20	3.8206	4.7670	3.2971
30	3.6060	4.5751	3.2154
40	3.3236	4.3570	3.0091
50	2.9938	4.1300	2.7271
60	2.6468	3.9160	2.4273
70	2.3256	3.7419	2.1578
80	2.0892	3.6321	1.9635
90	2.0000	3.5958	1.8906

(ii) POLARIZATION ANGLE $\alpha = -60°$, $\theta = 90°$

ϕ (deg.)	2Γ	T_c	α'
0	4.0000	4.9648	3.2366
10	3.9546	4.9463	3.1479
20	3.8206	4.8987	2.8936
30	3.6060	4.8347	2.5351
40	3.3236	4.7619	2.1602
50	2.9938	4.6861	1.8282
60	2.6468	4.6147	1.5614
70	2.3256	4.5565	1.3641
80	2.0892	4.5199	1.2392
90	2.0000	4.5077	1.1953

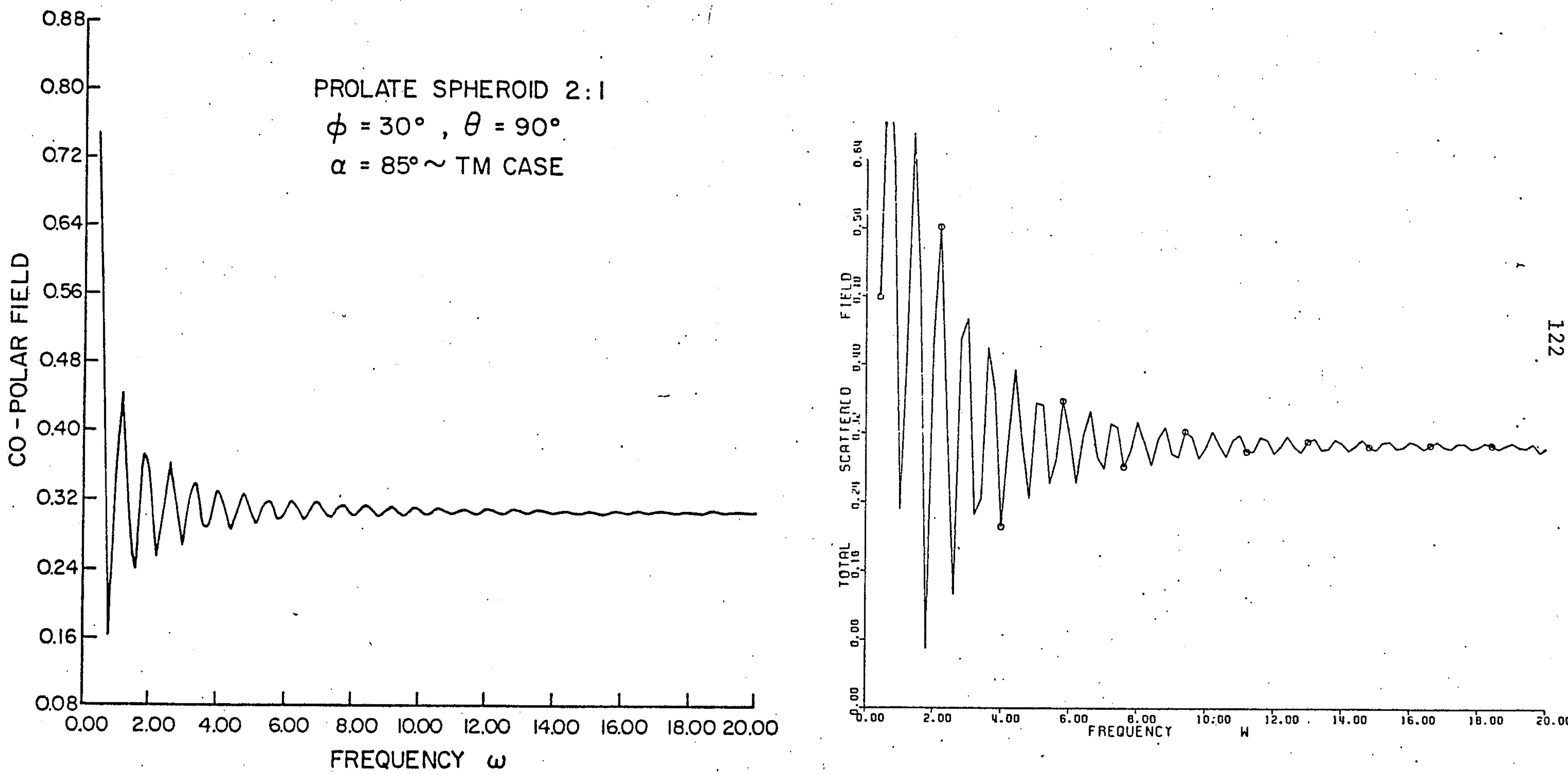

Fig. 5.7a Frequency Domain Backscattered Co-Polarized Field Obtained From The Approximate Impulse Response Model (θ=90°, ϕ=30°,$\alpha \sim$TM) And Total Scattered Field Obtained From [12] (θ=90°, ϕ=30°, TM Case)

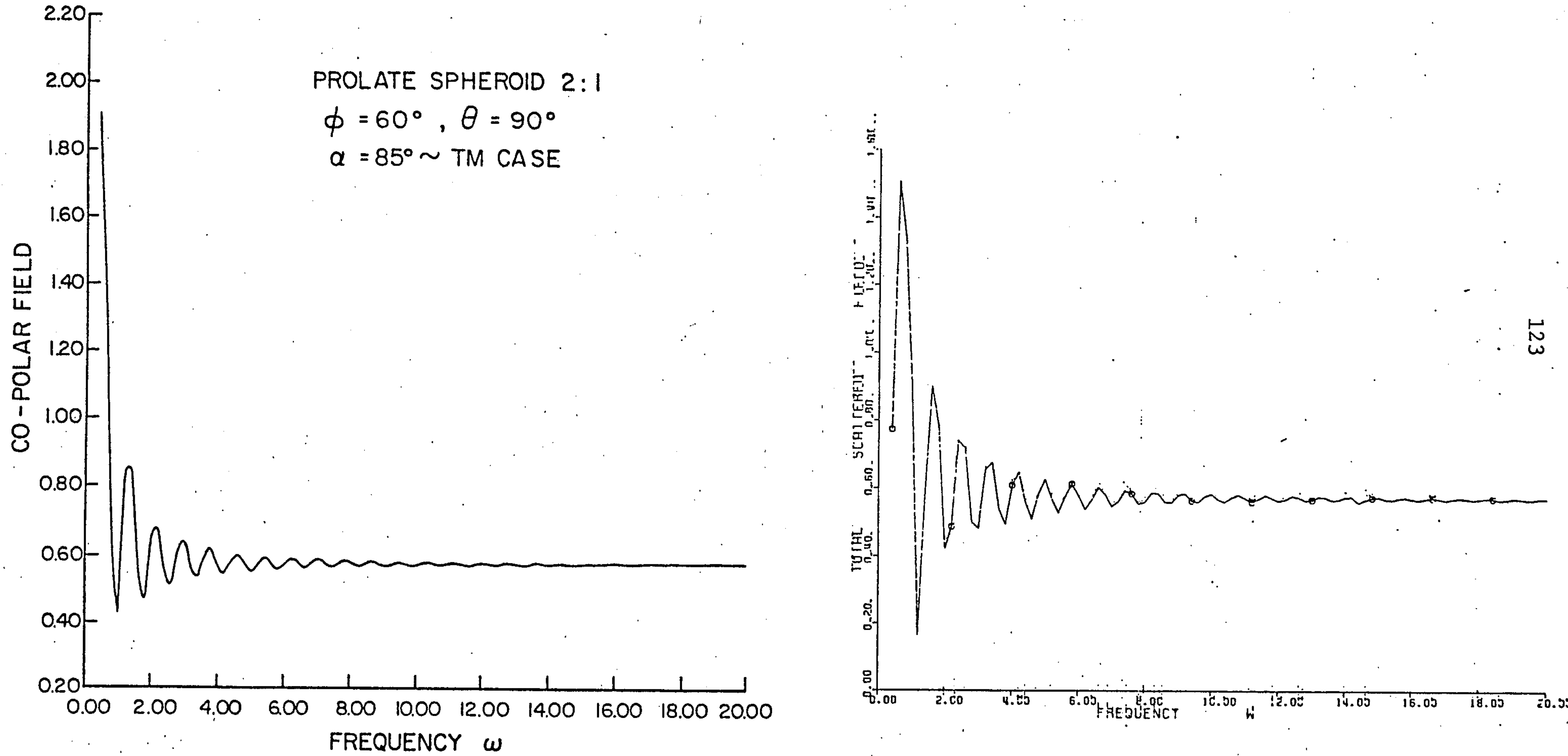

Fig. 5.7b Frequency Domain Backscattered Co-Polarized Field Obtained From The Approximate Impulse Response Model (θ=90°, ϕ=60°, $\alpha \sim$TM) And Total Scattered Field Obtained From [12] (θ=90°, ϕ=60°, TM Case)

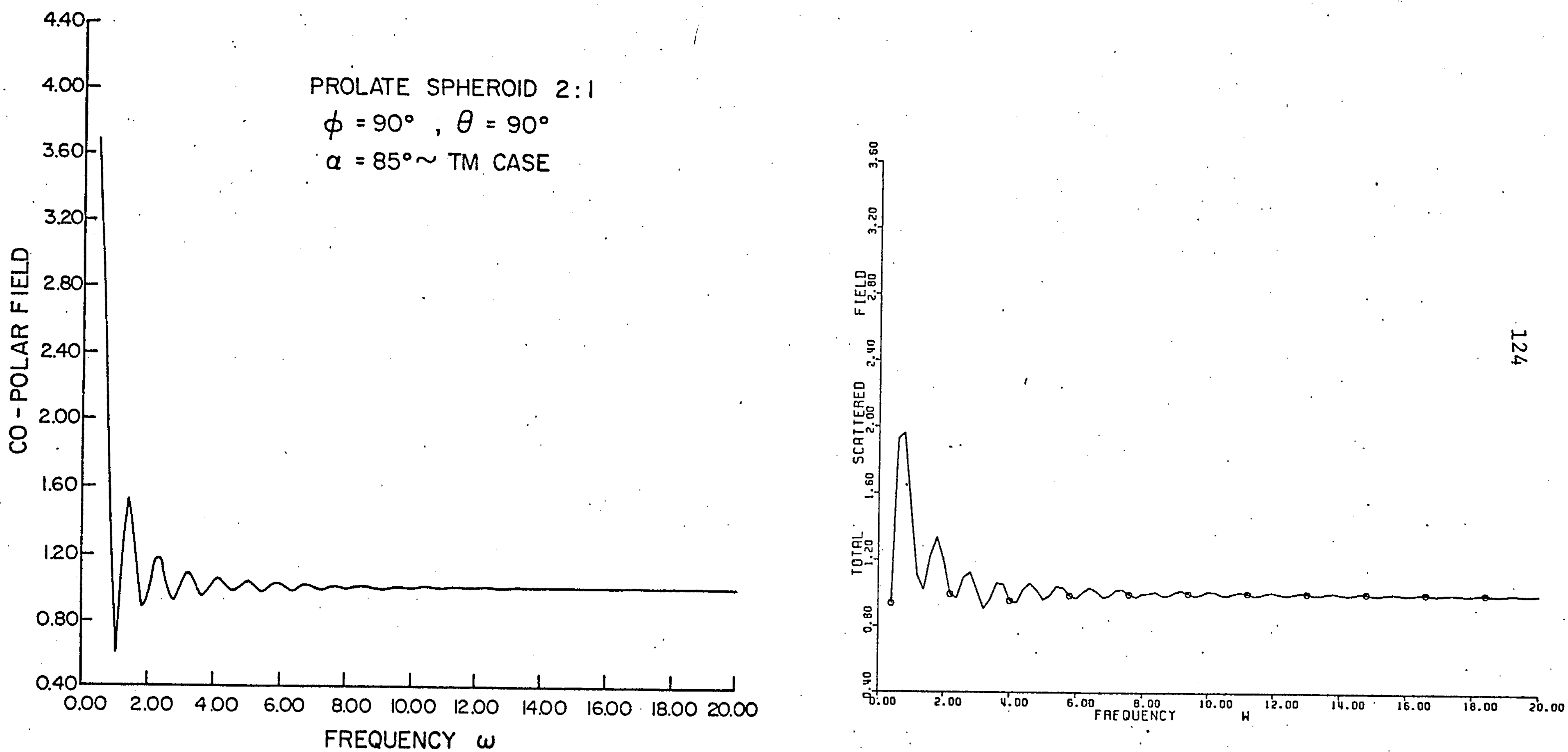

Fig. 5.7c Frequency Domain Backscattered Co-Polarized Field Obtained From The Approximate Impulse Response Model (θ=90°, ϕ=90°, $\alpha \sim$ TM) And Total Scattered Field Obtained From [12] (θ=90°, ϕ=90°, TM Case)

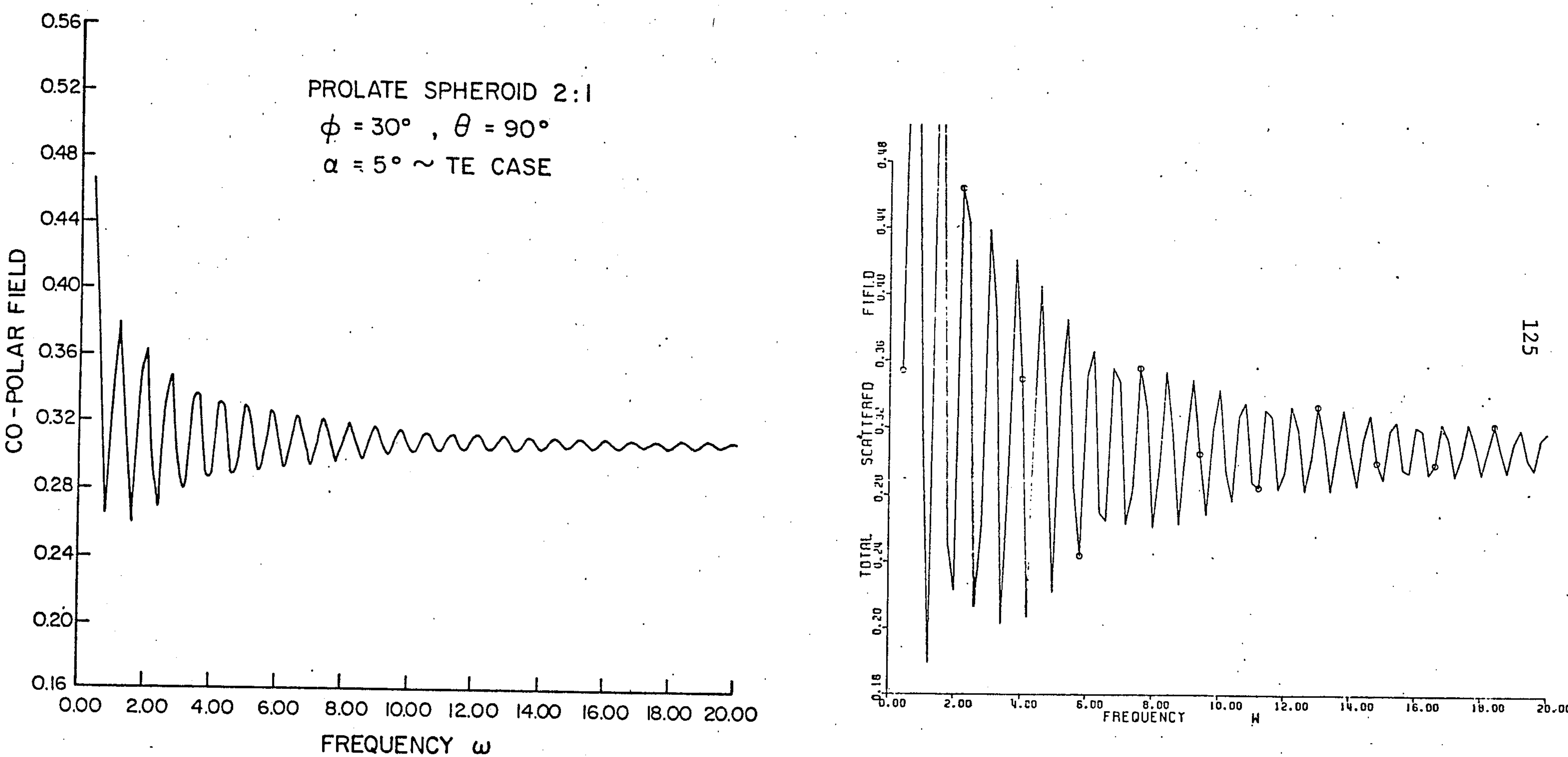

Fig. 5.7d Frequency Domain Backscattered Co-Polarized Field Obtained From The Approximate Impulse Response Model (θ=90°, ϕ=30°, α∿TE) And Total Scattered Field Obtained From [12] (θ=90°, ϕ=30°, TE Case)

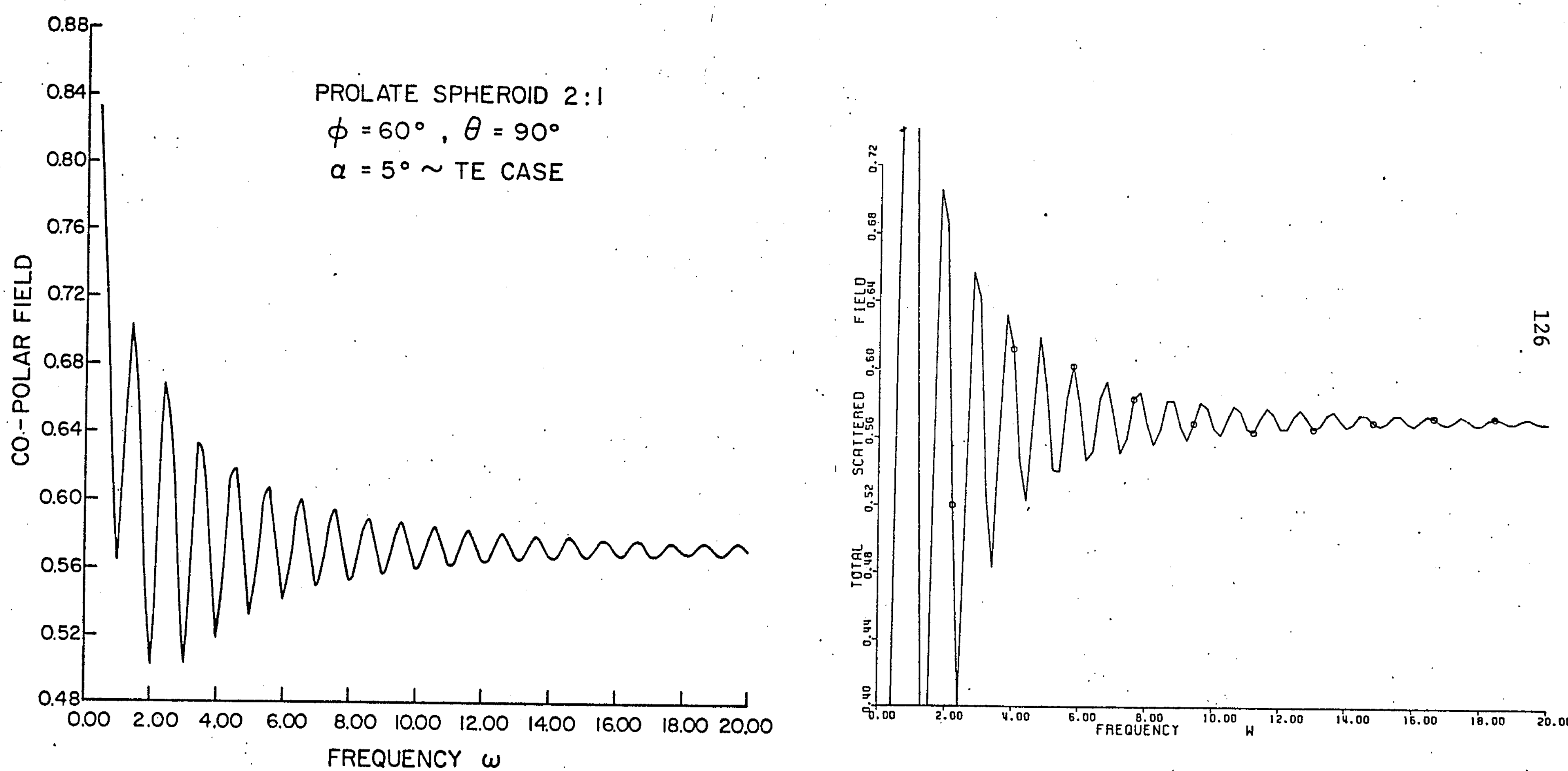

Fig. 5.7e Frequency Domain Backscattered Co-Polarized Field Obtained From The Approximate Impulse Response Model ($\theta=90°$, $\phi=60°$, $\alpha \sim$ TE) And Total Scattered Field Obtained From [12] ($\theta=90°$, $\phi=60°$, TE Case)

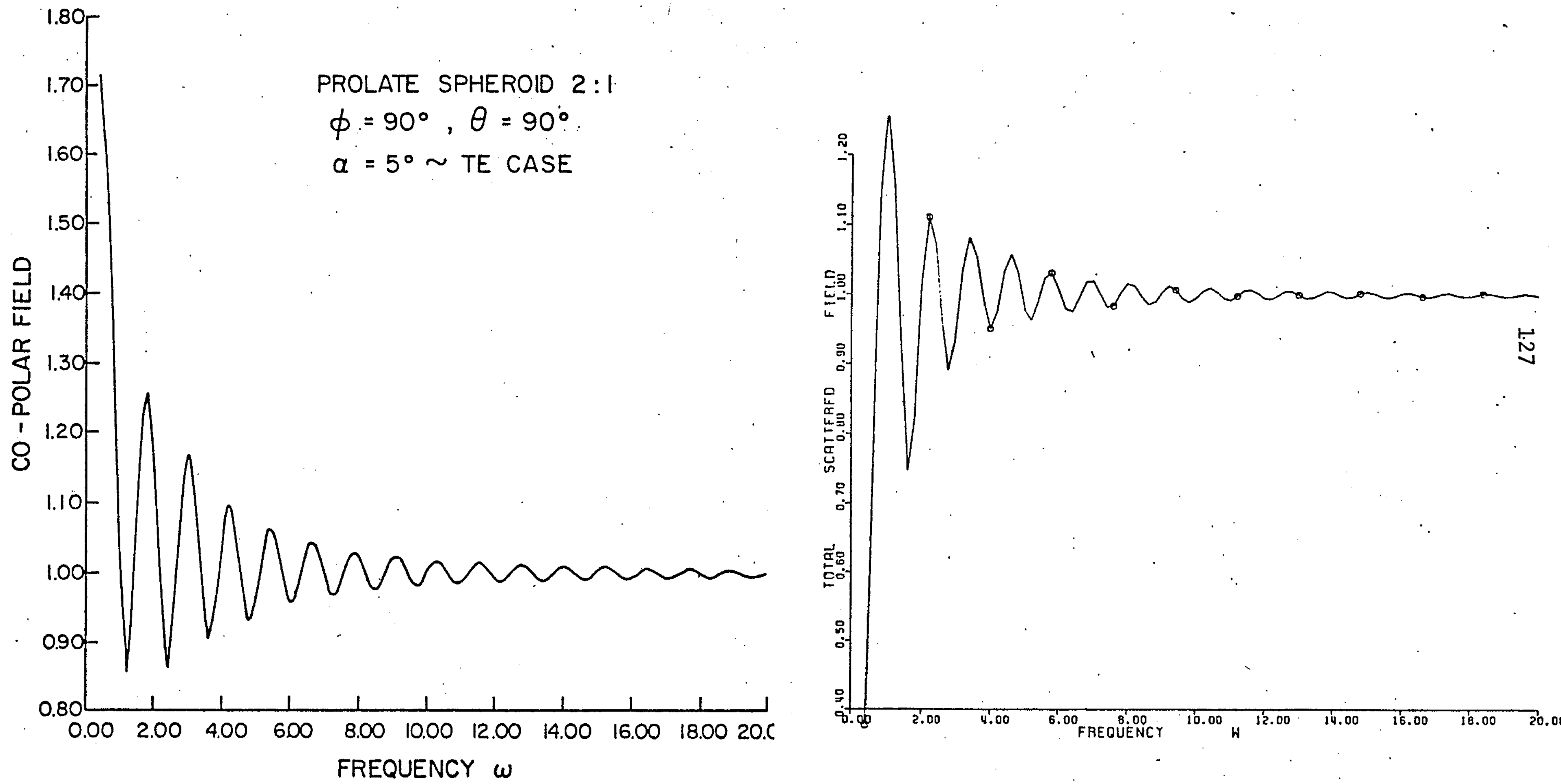

Fig. 5.7f Frequency Domain Backscattered Co-Polarized Field Obtained From The Approximate Impulse Response Model (θ=90°, ϕ=90°, $\alpha \sim$ TE) And Total Scattered Field Obtained From [12] (θ=90°, ϕ=90°, TE Case)

shape of the curves was obtained (see Figs 5.8a–5.8c). Absolute values could not be compared because of different normalization used in [28]. Furthermore, sufficiently accurate numerical values could not be obtained from the plots given in [28]. In [28,p.27] it has been clearly pointed out that the results presented therein are accurate as far as the shape is concerned and the absolute values could be about three times too low.

To sum up, although the solutions (5.17) and (5.18), obtained for the backscattered fields, were based on certain liberal engineering approximations, it is evident that they are reliable enough to be used as input data in (4.28) and (4.29) for $\omega > 5.0$. In the next chapter, (4.28), (4.29) and (4.30) have been used to express a, b, c as functions of a, b, c as well as of the input data (i.e., the backscattered far-field) and thus an iteration scheme for computation is made possible.

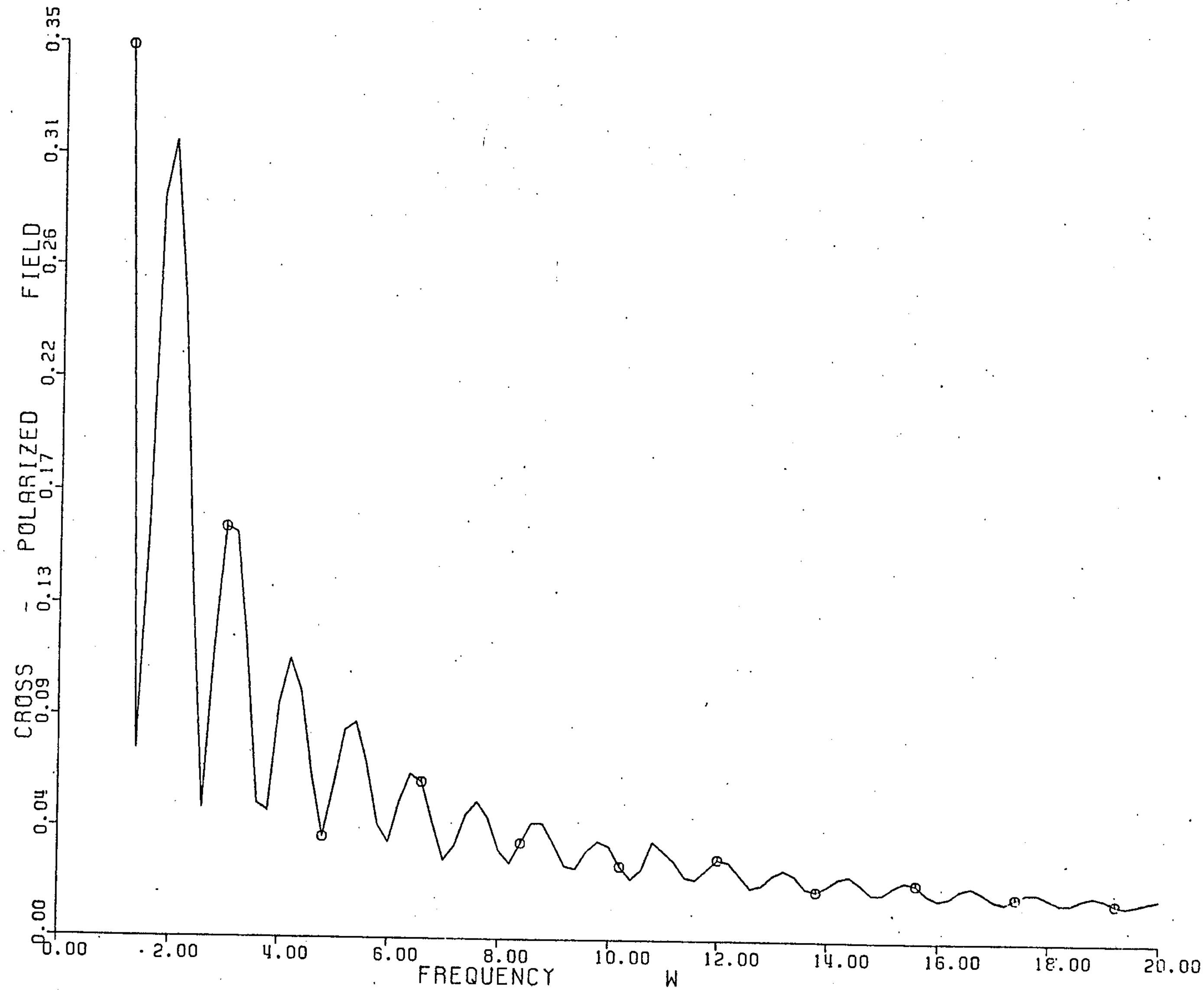

Fig. 5.8a Frequency Domain Backscattered Cross-Polarized Field Of A 2:1 Prolate Spheroid, Obtained From The Approximate Impulse Response Model, For Broad-Side Plane Wave Incidence With Polarization Angle $\alpha = 30°$

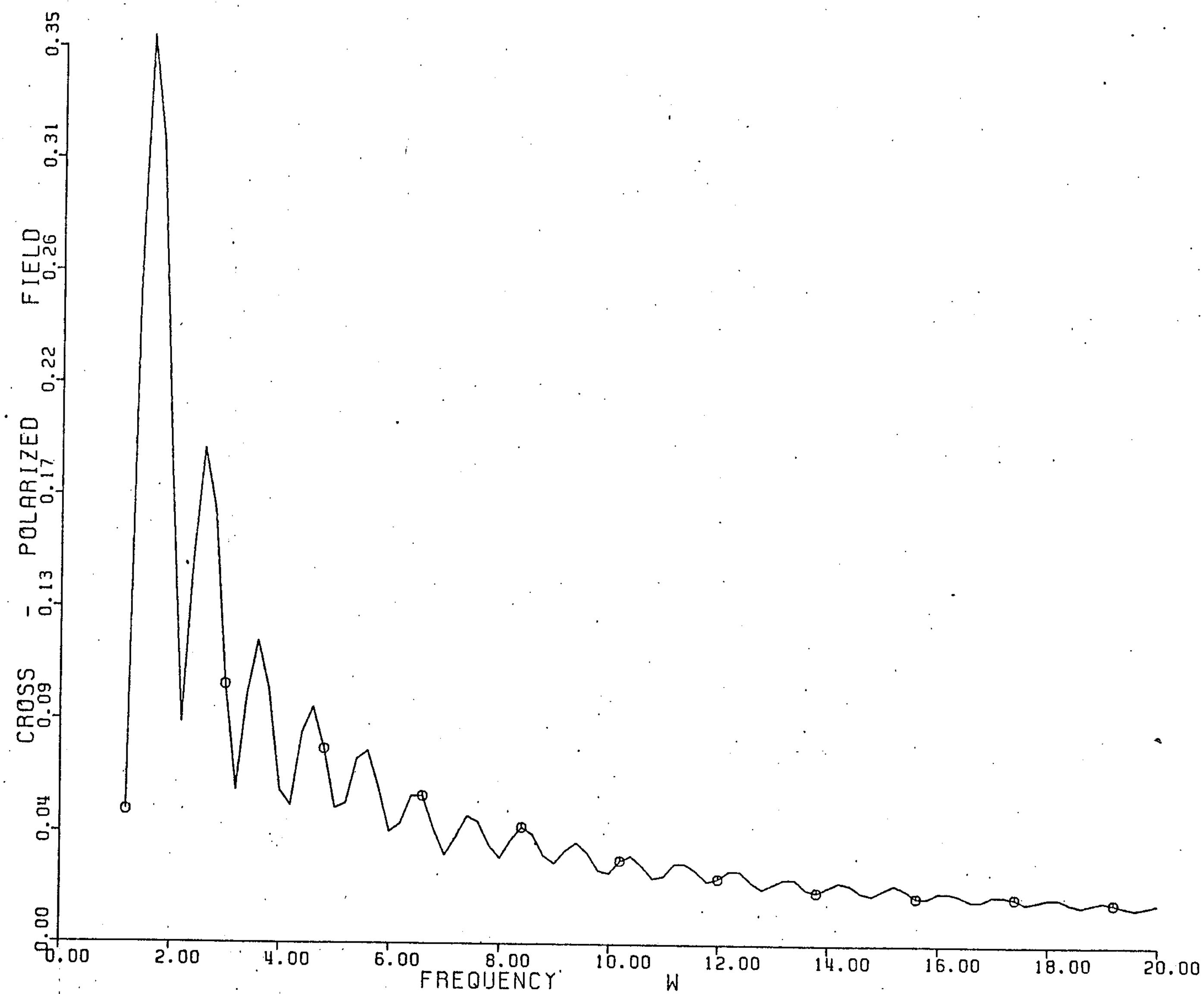

Fig. 5.8b Frequency Domain Backscattered Cross-Polarized Field Of A 2:1 Prolate Spheroid, Obtained From The Approximate Impulse Response Model, For Broad-Side Plane Wave Incidence With Polarization Angle $\alpha = -60°$

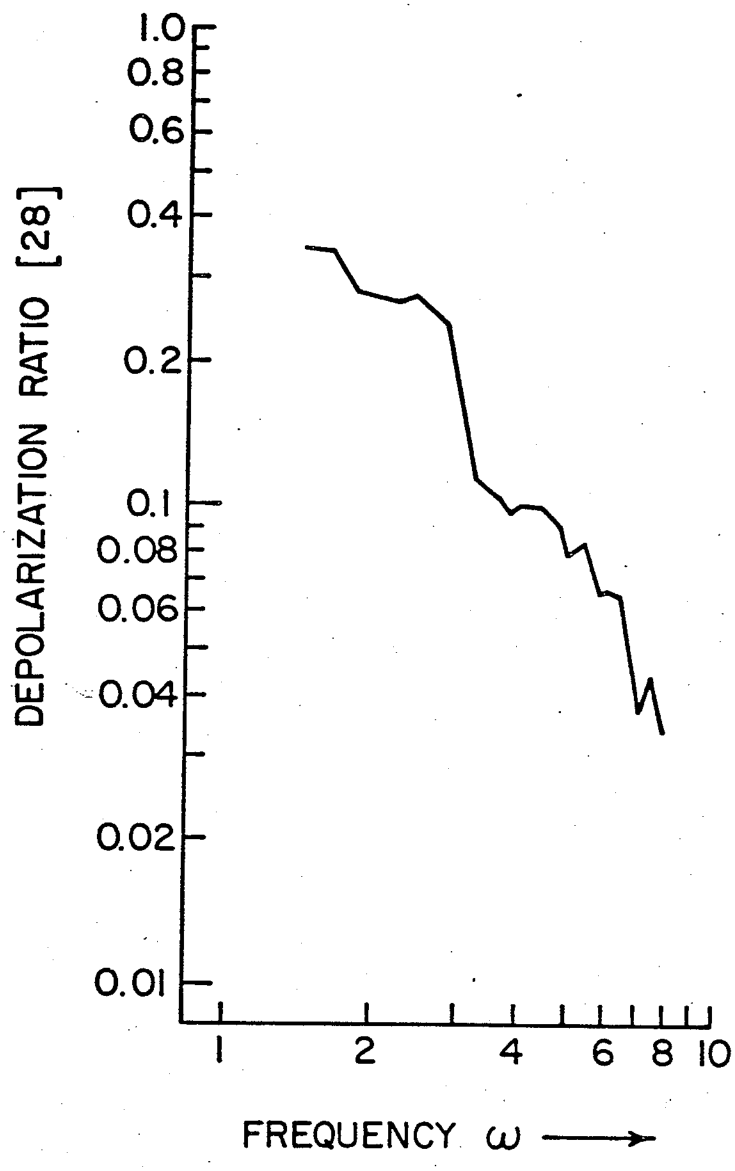

Fig. 5.8c Frequency Domain Depolarization Ratio For The Backscattered Field Of A 2:1 Prolate Spheroid, Obtained From [28], With Broad-Side Plane Wave Incidence

chapter six

APPLICATION OF THE PROPOSED INVERSE SCATTERING MODEL IN PROFILE INVERSION OF A PERFECTLY CONDUCTING PROLATE SPHEROID

6.1 INTRODUCTION

Once the formal solution to the problem has been set in Chapter Four, the next obvious step is to check its validity numerically. The system of equations proposed in Chapter Four for the recovery of the surface profile utilizes certain physical as well as geometrical optics approximations. Therefore, the solution is expected to be good in the high-frequency region only. The frequency range over which this system yields best results needs to be investigated. Furthermore (3.14) and (3.24), used in a major way to develop the formal solution, have been derived by liberal application of engineering approximations. Their validity and accuracy under various different situations needs to be checked.

Application of the inverse scattering model, developed in Chapter Four, to the test case of a perfectly conducting prolate spheroid has been undertaken in this chapter. The major difficulty in this direction is that the kind of input data needed is not readily available for most of the scatterer shapes. It is to be noted that although a complete set of the required data is available for the sphere, the sphere cannot be a test case. This is because the two principal radii of curvature are the same at all points on the sphere causing (3.24) to break down. To circumvent this difficulty an approximate solution of the backscattering by a perfectly conducting prolate spheroid has been developed in

Chapter Five and this solution has been used to generate all the input data required in the present chapter.

In Section 6.2, the iteration scheme for the actual computational recovery of the surface of a perfectly conducting prolate spheroid is developed. Various numerical results showing frequency dependence and the limitations of the proposed inverse scattering model are presented in Section 6.3. A possible modification of the iteration scheme has been considered in Section 6.4. Furthermore, comparison of the results obtained from the modified iteration scheme with those obtained from the original iteration scheme are also presented in this section. Finally, in Section 6.5, shortcomings of the inverse scattering model, as verified by numerical calculations are discussed.

6.2 ITERATION SCHEME

Eqs. (4.30), (4.31) and (4.32) have been used to express implicitly a, b, c as functions of a, b, c as well as of the input data (i.e., backscattered far-field) and thus an iteration scheme for computation was made possible. The expression for $(K_1 - K_2)$, the difference between two principal curvatures at the specular point, where the normal direction of incidence is given by (ξ,η,ζ), was obtained in terms of the semi-axes of the corresponding equivalent ellipsoid (a,b,c) in (I-9) of Appendix I. Substitution of this expression for $(K_1 - K_2)$ into (4.31) yields an expression for 'a' as

$$a = f(a,b,c) = \left[\frac{-b^2c^2(\eta^2+\zeta^2) \pm \dfrac{|H_{1c}|/\cos(\alpha)\sin(\alpha)}{K_{12}\,|(G/\omega^2)^2+(2\Gamma G/\omega)^2|^{1/2}}}{c^2(\xi^2-\zeta^2) - b^2(1-\zeta^2)} \right] \tag{6.1}$$

where

$$K_{12} = \frac{(a^2\xi^2 + b^2\eta^2 + c^2\zeta^2)^{1/2}}{(a\ b\ c)^2} \quad .$$

The sign before the second term on the right-hand-side of (6.1) is taken to be either positive or negative depending on whether

$$|a^2c^2(\xi^2-\zeta^2) - a^2b^2(1-\zeta^2) + b^2c^2(\eta^2+\zeta^2)| \gtrless 0 \quad ,$$

respectively. This criterion arises because of the fact that the absolute value of (K_1-K_2) is to be considered in (4.31).

From (4.32), an expression for 'b' as a function of a, b, c and the scattered field data was obtained as

$$b = g(a,b,c) = b\left[\frac{\{|H_{1p}|^2+|H_{2p}|^2+2|H_{1p}|\cdot|H_{2p}|\cos(\phi_{1p}-\phi_{2p})\}^{1/2}}{2\{(2\Gamma G)^2 + (G/\omega)^2\}^{1/2}} \right] \tag{6.2}$$

Similarly from (4.30), an expression for 'c' is obtained as

$$c = h(a,b,c) = [(a\xi)^2 + (b\eta)^2 + (c\zeta)^2][\frac{4\sigma}{a^2b^2}]^{1/2} \quad . \tag{6.3}$$

The development of these expressions for a, b and c was mainly guided by the requirement that the resulting set of equations, i.e., (6.1), (6.2) and (6.3), for the iteration scheme should not become ill-conditioned. The particular set of functions f(a,b,c), g(a,b,c) and h(a,b,c) were arrived at by performing trials on various other sets of functions. To elaborate on this point note that if (6.1), (6.2) and (6.3) are chosen in such a manner that the numerical values of the right-hand-sides of these equations are comparable during the iteration cycles, then the hyperplanes corresponding to these equations will intersect at nearly 90°. In such a system, the intersection point (or solution) is relatively insensitive to a slight movement of these hyperplanes and to round-off errors. Such a system of equations is called a well-conditioned system. On the other hand, if the hyperplanes intersect at small angles, the round-off errors and slight movement of the hyperplanes cause appreciable motion of the intersection point with a low degree of accuracy of the resulting solution. Such systems are termed ill-conditioned.

In the above set of equations, i.e., (6.1) to (6.3), it appears for the iteration scheme that the process could be simplified by using (4.30) to solve for one of the variables (say c) and then to just iterate over the remaining two variables (i.e., a and b). However, the fact remains that this simplification cannot be incorporated into the iteration scheme. This is because (4.30) gives a fourth-order equation for any of the variables a, b or c, and it is not possible to discriminate the proper value of the variable from the four roots of this equation since very frequently two of the four roots are positive real numbers. This multivalued nature of the analytical roots prevents the convergence of the iteration scheme and therefore this modification of the iteration scheme is not possible.

The flow chart for the numerical solution process on the computer is shown in Fig. 6.1. In this scheme the backscattered radar cross-section

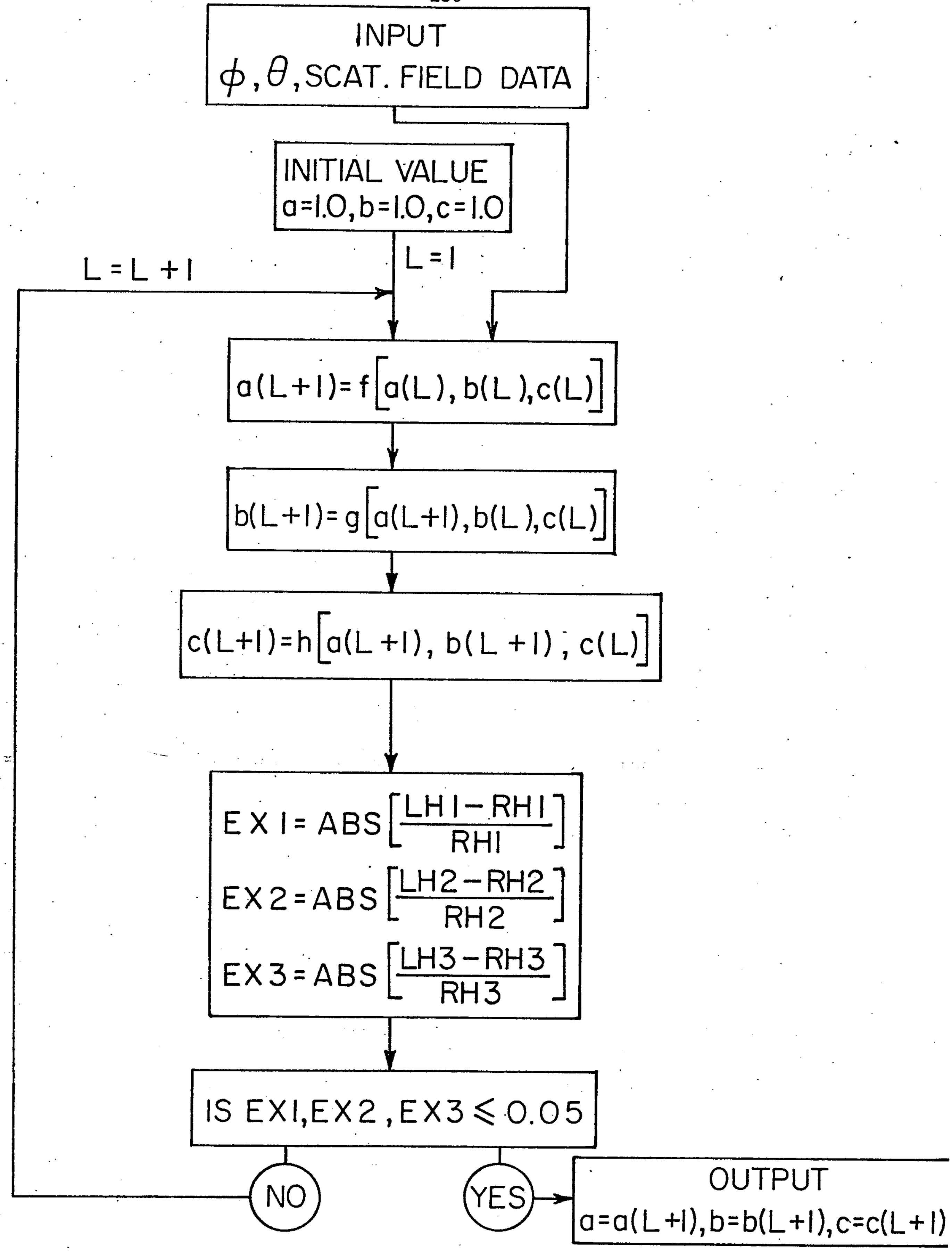

Fig. 6.1 Flow chart for iteration scheme.

at a sufficiently high frequency $(\omega = ka \gtrsim 10)$ and the two co-polarized backscattered fields $|H_{1p}|, |H_{2p}|$ along with their phase difference $(\phi_{1p} - \phi_{2p})$ and also the magnitude of the cross-polarized component $|H_{1c}|$ have been used as the input data. In addition, the direction of the incident wave (θ,ϕ) with respect to an arbitrary pre-fixed coordinate system (with origin in the interior of the scattering object) must be specified with the input data. In order to start the iterations, the initial values of a, b, c are assumed to be unity, i.e., it is assumed that the specular point corresponding to the backscattered direction (θ,ϕ) is situated on a unit sphere. Once the required input data and the initial values are known, a modified value of 'a' is obtained from (6.1). This new value of 'a' along with old values of 'b' and of 'c' are substituted into the right-hand-side of (6.2) to obtain a modified value of 'b'. Similarly, the new values of 'a' and of 'b' are substituted along with the old value of 'c' into the right-hand-side of (6.3) to give a modified value of 'c'. Once a new set of values for a, b, c is obtained, this set is substituted in the left-hand-side of (4.30), (4.31) and (4.32) to yield the exit parameters EX1, EX2 and EX3, respectively. These exit parameters, as shown in Fig. 6.1, are the absolute values of the fractional difference between the left-hand-side and the right-hand-side of these equations. Next, an exit criterion was set out by restricting EX1, EX2 and EX3 to 0.05, i.e., the left-hand-side of each equation is within 5% of the right-hand-side. Note that these exit criteria are flexible and can be changed according to need. If the modified values of a, b, c satisfied the exit criteria, then those values of a, b, c were accepted as the solution for that particular direction (θ,ϕ) of the incident wave, otherwise the iterative process was continued in order to achieve further modified values of a, b, c as shown in Fig. 6.1.

Once the values of a, b and c are recovered from the iteration scheme, the coordinate (x,y,z) of the corresponding specular point is known from (4.33a), (4.33b) and (4.33c).

6.3 COMPUTATIONAL RESULTS

The iteration scheme shown in Fig. 6.1 has been applied to the test case of a perfectly conducting prolate spheroid. The required input data for the present computation have already been discussed in Chapter Five. In order to study the frequency dependence of the inverse scattering model, the points on the spheroid corresponding to $\theta = 90°$ and $\phi = 0°$ to $180°$ in steps of $10°$, were recovered for various frequencies ranging from $\omega = 5.0$ to $\omega = 15.0$. Results of these computations for $\omega = 5$, 7.4, 10, 12.6 and 15 are shown in Figs. 6.2a to 6.2e. From these results it appears that the rate of change of curvature as well as the difference in principal curvature, i.e., (K_1-K_2), will play an important role in the recovery. Towards the pointed end of the prolate spheroid, where the rate of change of the curvature is quite rapid compared to the broad side, the inverse scattering model yields unsatisfactory results as expected (see Section 3.4). Finally, for the case of nose-on incidence ($\phi = 0°$ and $180°$), the inverse scattering model fails to recover the specular point as at those points the difference between the principal curvatures, i.e., (K_1-K_2) goes to zero causing (3.24) to break down.

The inverse scattering model does not yield satisfactory results for frequencies below 5.0 mainly because of two reasons. First, as has already been mentioned in Chapter Five, the input data used in the computation are not reliable enough for $\omega < 5.0$, secondly, the inverse scattering model itself is based on high frequency assumptions. It was expected that as the frequency is increased higher and higher, the model will yield better results. However, this is not the case as can be seen in Figs. 6.2a to 6.2e. The deterioration of the results for $\omega > 10.0$ is explained by the fact that as the frequency increases the magnitude of the cross-polarized backscattered field becomes smaller [8] (see Fig. 5.8) and finally it falls 40 dbs compared to the co-polarized component. This fact causes the iteration scheme to become ill-conditioned and extremely sensitive as is evident from (4.31) and (4.32) and discussed in Section 6.2. Thus because of the difficulties at the lower and higher end of the frequency domain, an optimum range over which the inverse scattering model yields satisfactory results is between $\omega = 5.0$ and $\omega = 10.0$. It is to be noted that at some points the recovered shape is inside the actual shape and at other points it is outside the actual shape (see Fig. 6.2b). This is explained by the fact that the exit criteria were fixed as "within 5%", which could be "plus" or "minus" 5% (see Fig. 6.1).

In order to study the effect of the rate of change of curvature on the results yielded by the inverse scattering model, the lines on a prolate spheroid corresponding to $\theta = 30°$, $60°$, $90°$ and $\phi = 0°$ to $90°$ (in steps of 10°) were recovered and the results are shown in Fig. 6.3. The best recovery is obtained for the line $\theta = 30°$, where the curvature

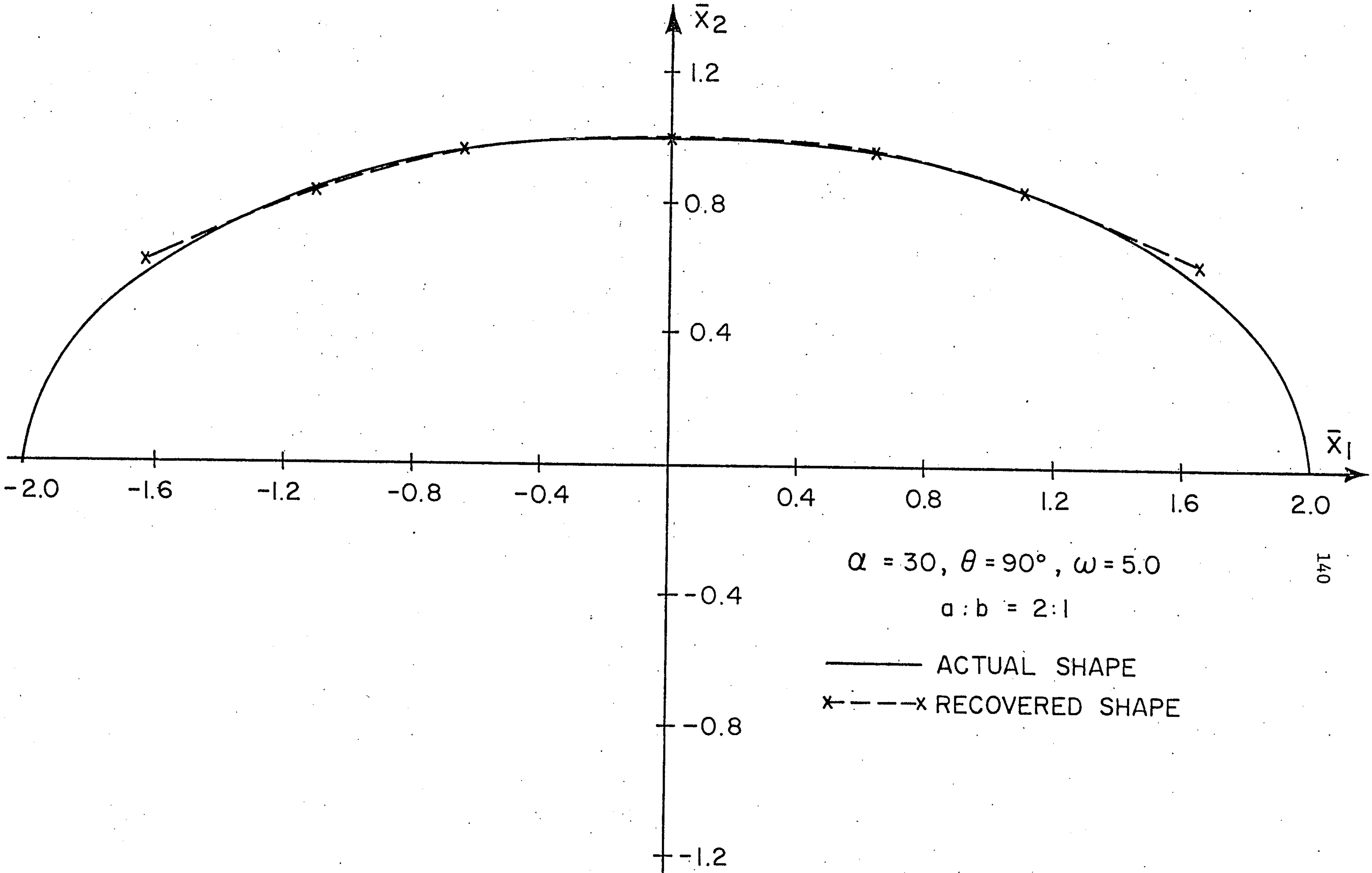

Fig. 6.2a Results Of Computational Recovery Of The Profile Of 2:1 Prolate Spheroid (θ=90°, ϕ=0° to 180°) At The Frequency ω = 5.0

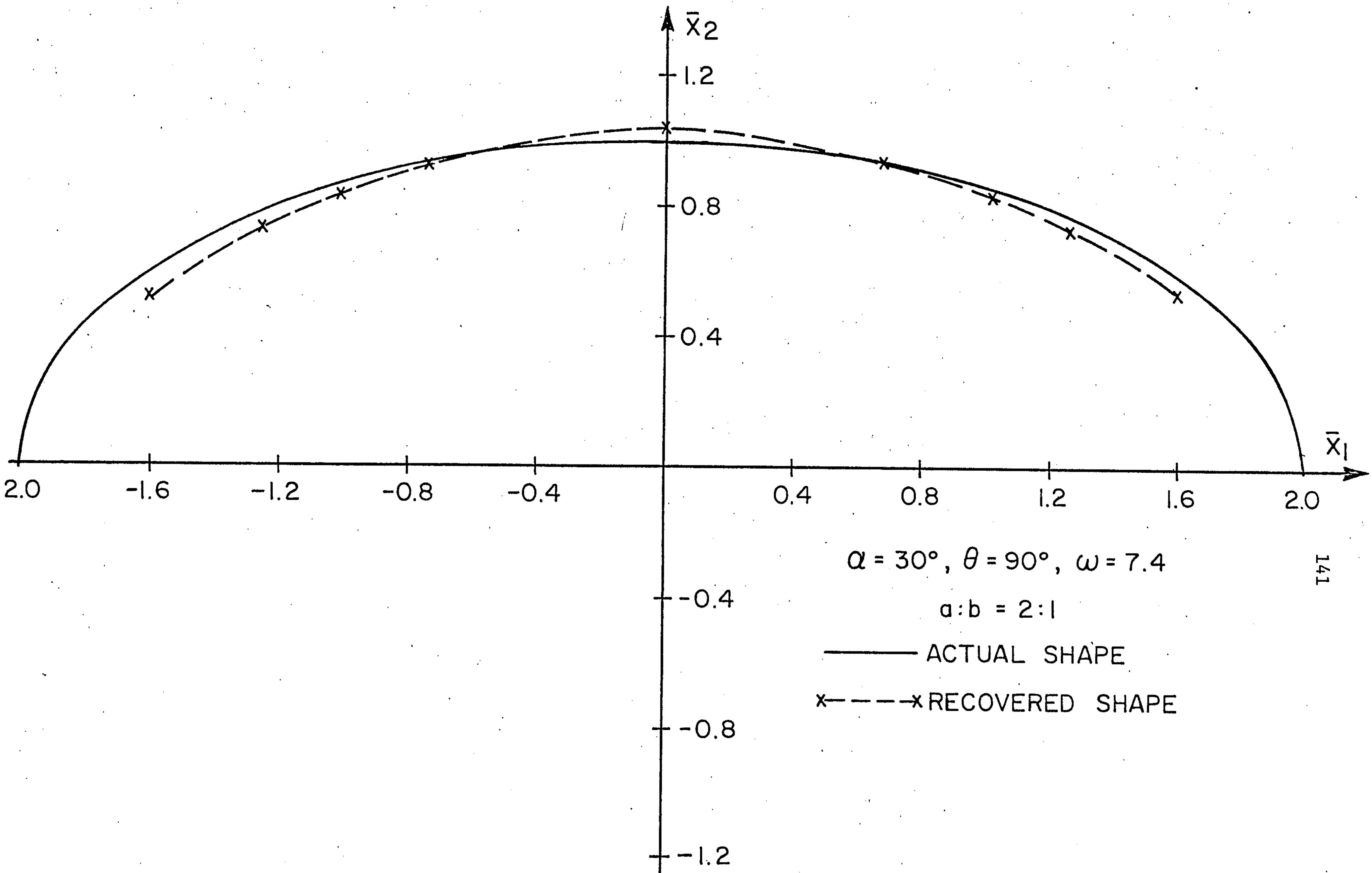

Fig. 6.2b Results Of Computational Recovery Of The Profile Of 2:1 Prolate Spheroid (θ=90°, ϕ=0° to 180°) At The Frequency ω = 7.4

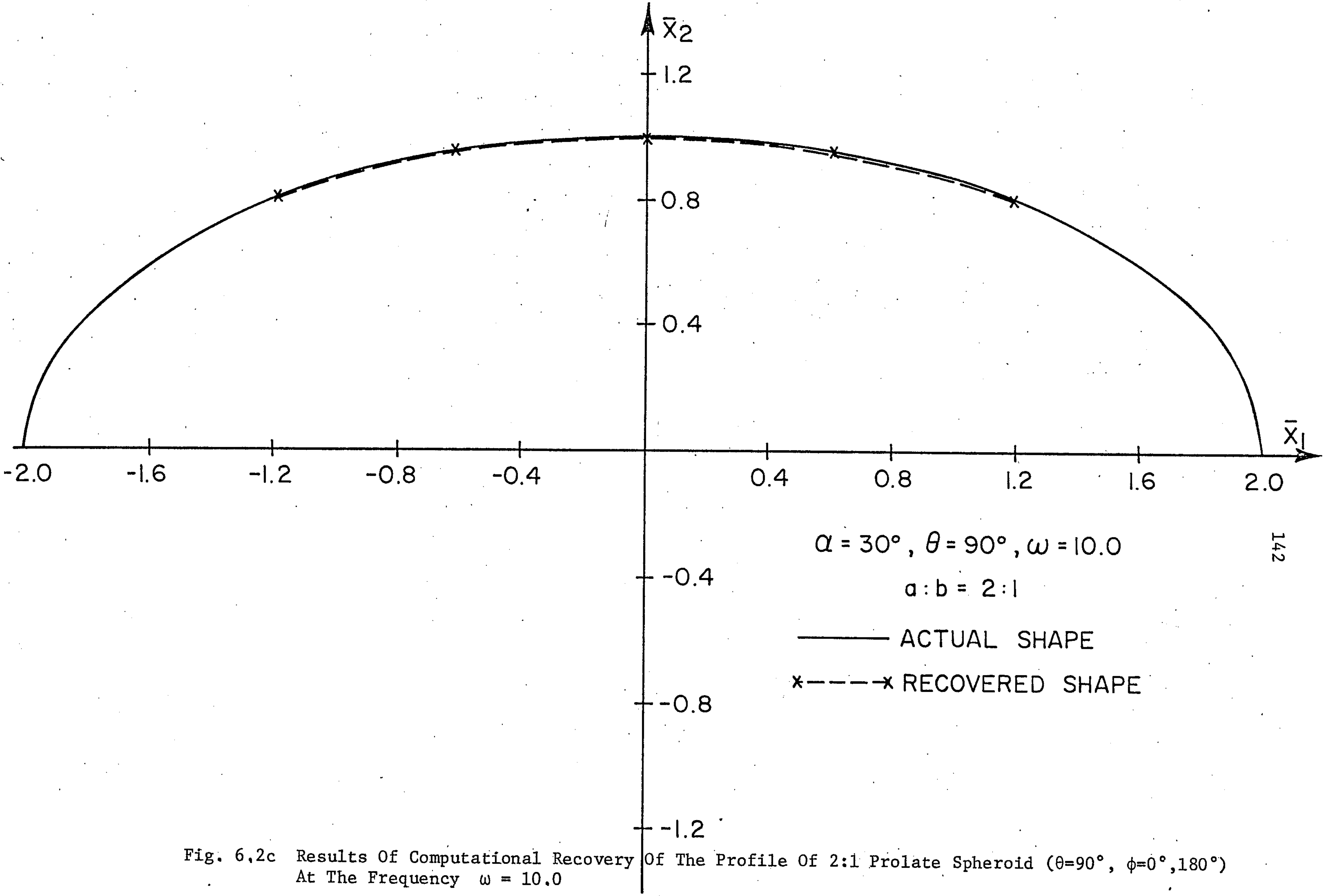

Fig. 6.2c Results Of Computational Recovery Of The Profile Of 2:1 Prolate Spheroid (θ=90°, ϕ=0°,180°) At The Frequency ω = 10.0

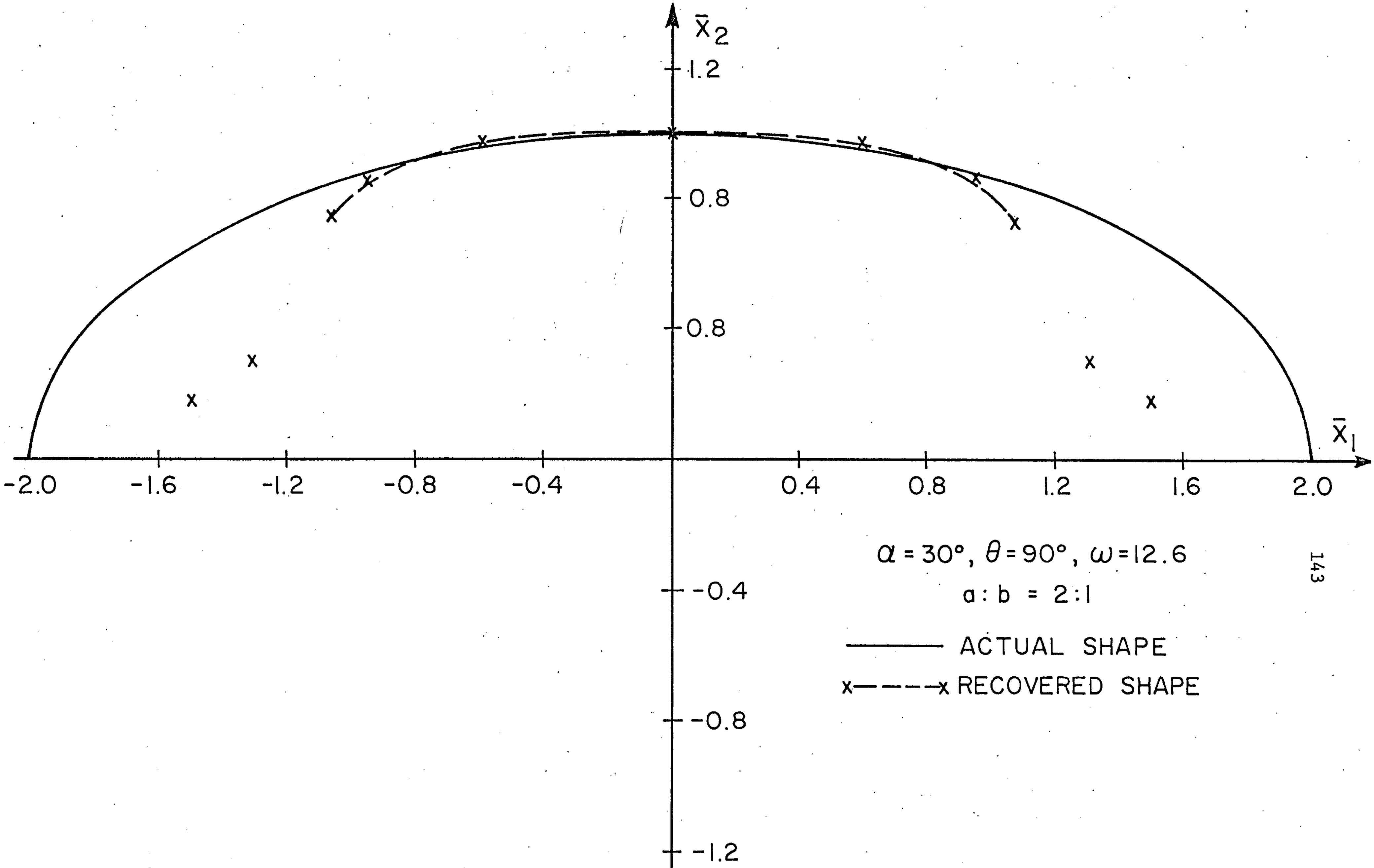

Fig. 6.2d Results Of Computational Recovery Of The Profile Of 2:1 Prolate Spheroid (θ=90°, ϕ=0° to 180°) At The Frequency ω = 12.6

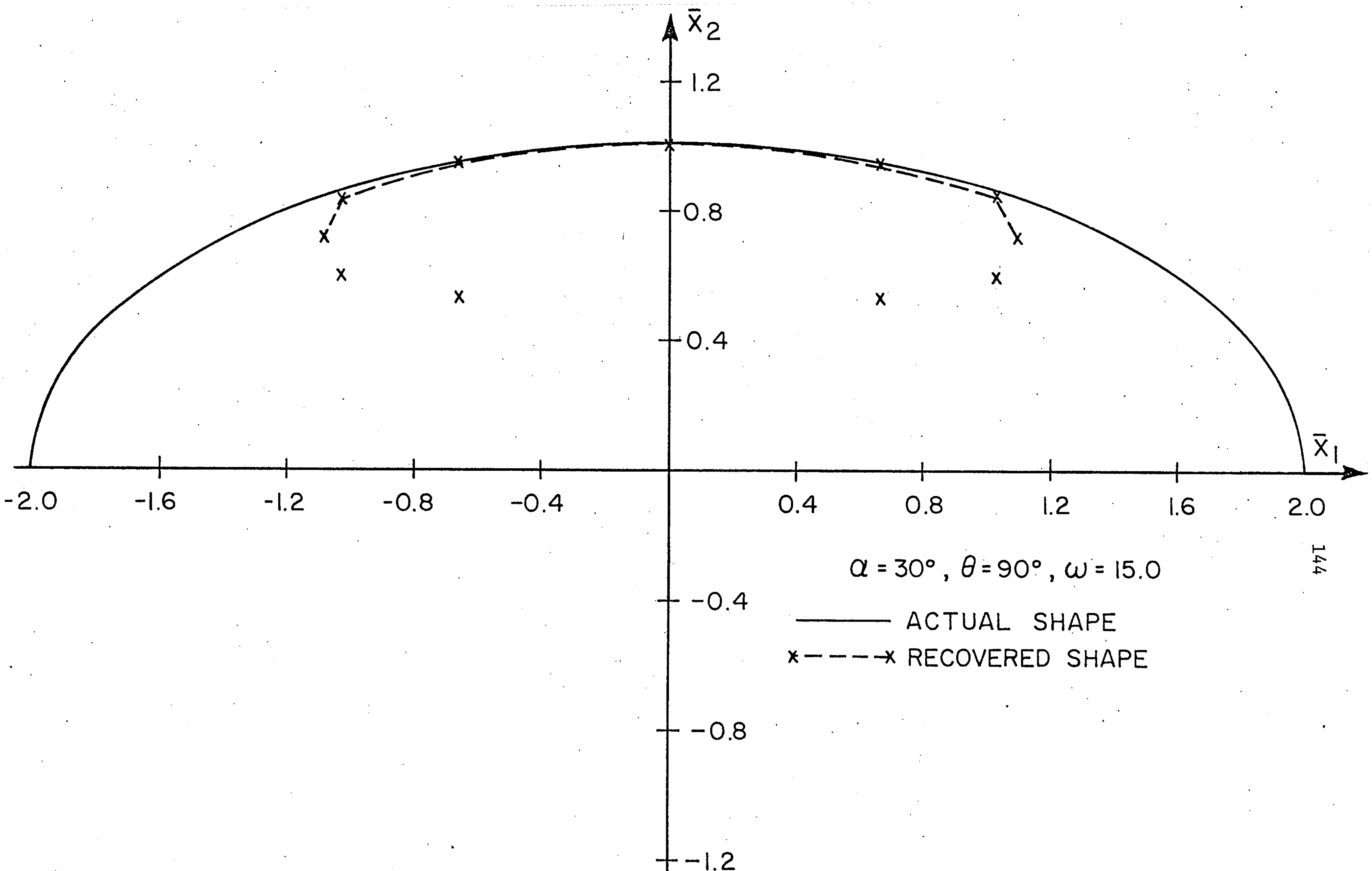

Fig. 6.2e Results Of Computational Recovery Of The Profile Of 2:1 Prolate Spheroid (θ=90°, ϕ=0° to 180°) At The Frequency ω = 15.0

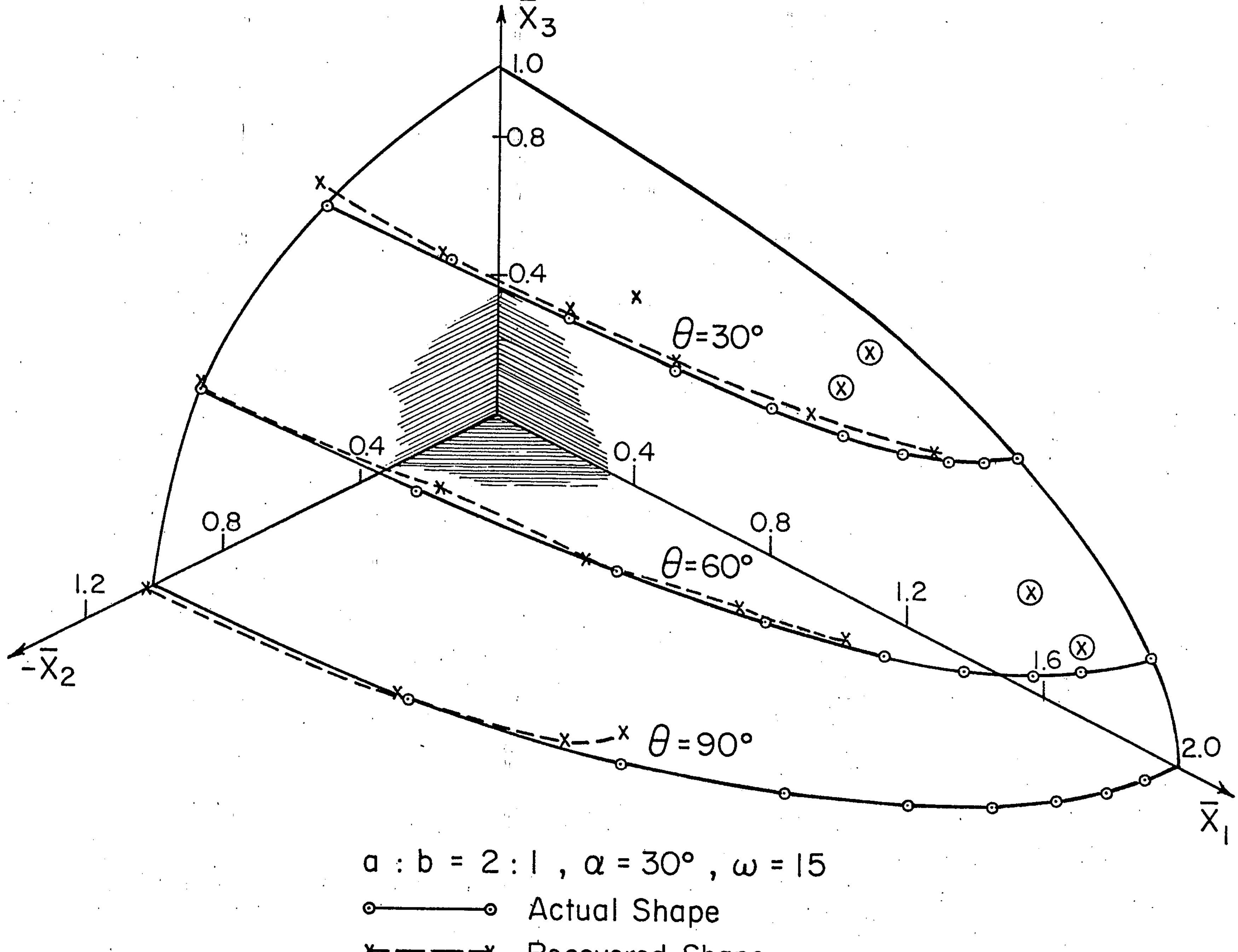

Fig. 6.3 Results Of Computational Recovery Of The Profile Of 2:1 Prolate Spheroid For ϕ=0° to 90° and θ=30°, 60°.90°

changes most slowly out of all the three curves. The most unsatisfactory recovery was for $\theta = 90°$, where the curvature changes quite rapidly. The results of another computation undertaken to study the effect of the rate of change of the curvature on the inverse scattering model is presented in Figs.6.4a to 6.4c, where the profiles of the prolate spheroids of axial ratio 5 : 4 (i.e., 1.25 : 1), 2 : 1 and 3 : 1 are recovered, respectively. As expected from the results of the earlier computations, the best recovery was for the case of a 5 : 4 spheroid because in this case the curvature changes most gently. However, also in this case, the end points could not be recovered as the difference in the principal curvatures at the end points goes to zero. The recovery for the case of the 3 : 1 prolate spheroid is poor because in this case the curvature changes very rapidly around the end zone.

6.4 MODIFIED ITERATION SCHEME

From the results of the application of the proposed inverse scattering model in Section 6.3, it was inferred that the rate of change of curvature as well as the difference in principal curvature, i.e., (K_1-K_2) will play an important role in the recovery. It has been suggested [14] that the difficulty arising due to the difference in curvatures becoming very small could be obviated by first solving the inverse problem assuming that the curvatures are the same (i.e., considering the simple physical optics approximation), and then by refining the results by use of the first order correction to the physical optics approximation (i.e., use of the depolarization information). In order to incorporate this modification in the iteration scheme, the expression for the difference

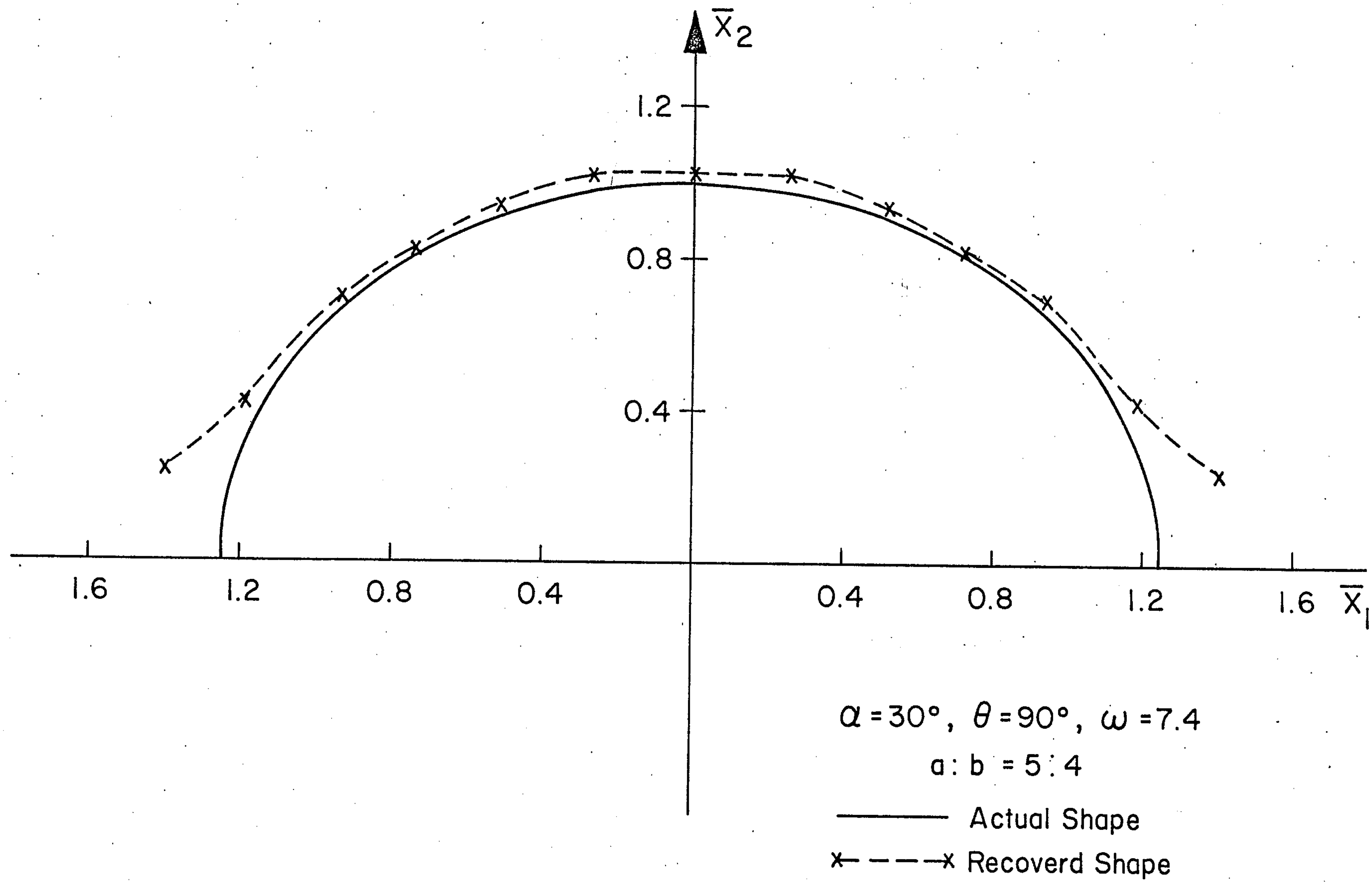

Fig. 6.4a Results Of Computational Recovery Of The Profile Of A 5:4 (i.e., 1.25:1) Prolate Spheroid

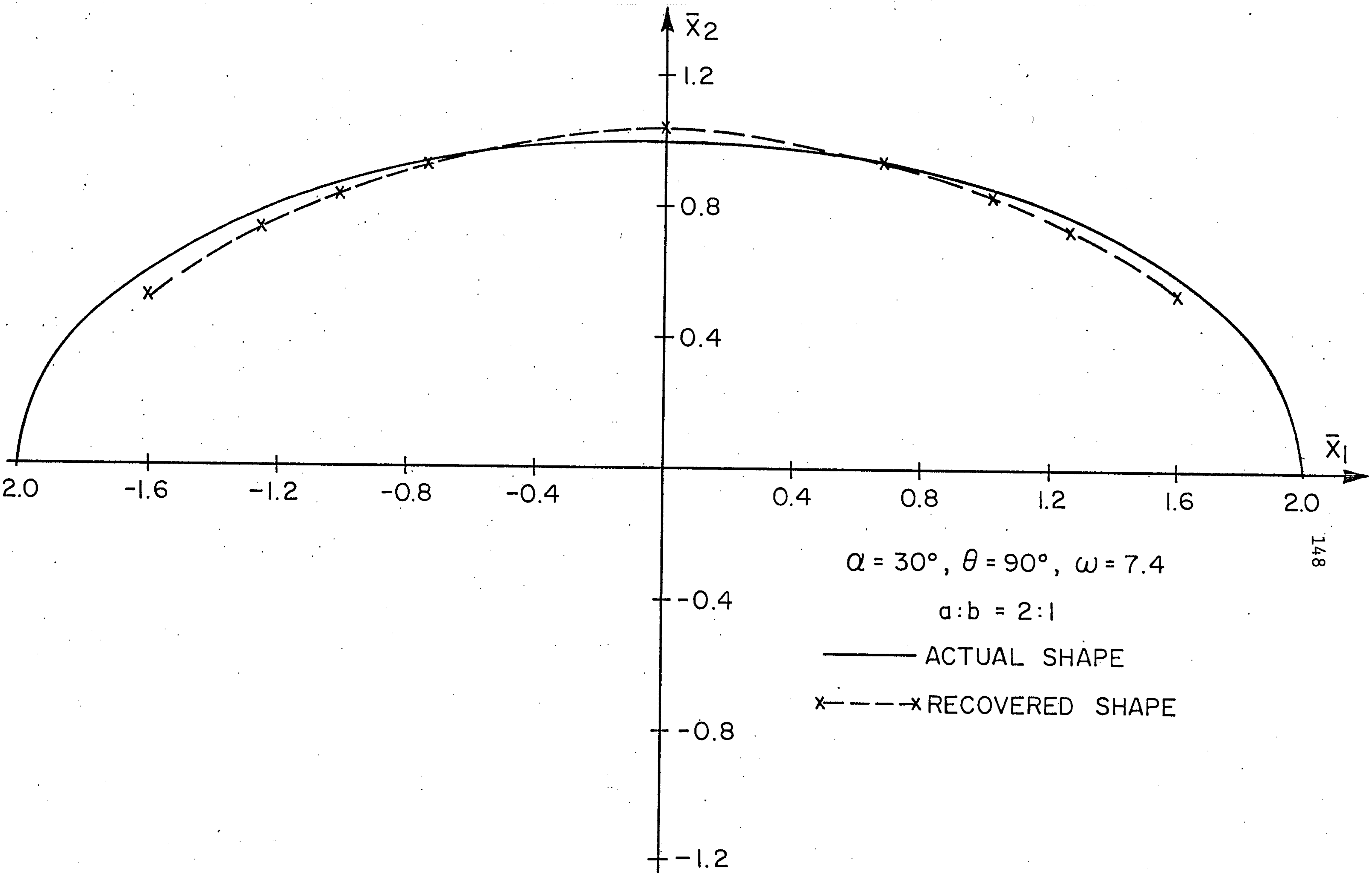

Fig. 6.4b Results Of Computational Recovery Of The Profile Of A 2:1 Prolate Spheroid

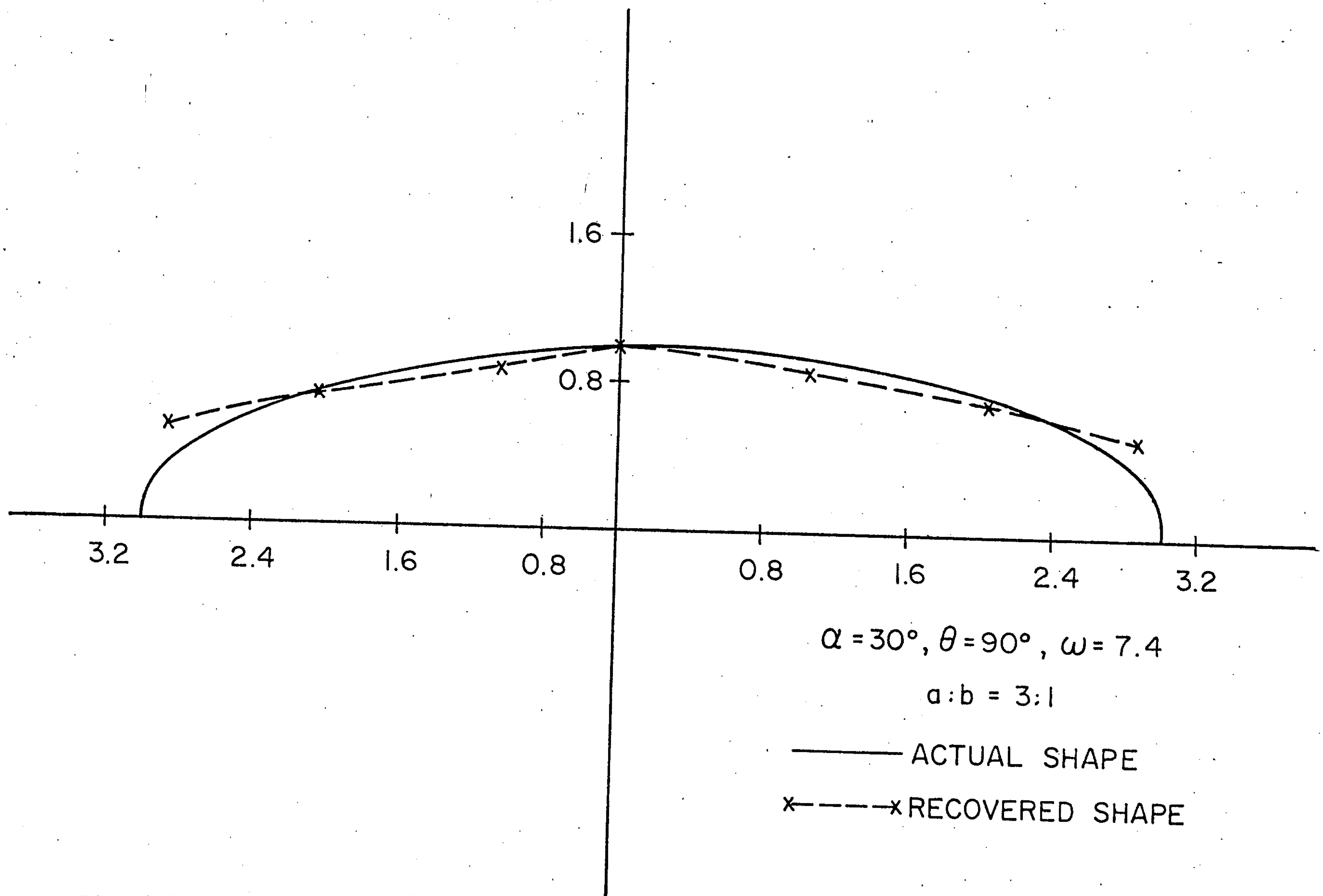

Fig. 6.4c Results Of Computational Recovery Of The Profile Of A 3:1 Prolate Spheroid

in the principal curvatures, i.e., (K_1-K_2), needs to be looked into.

The expression for (K_1-K_2), the difference between the two principal curvatures at the specular point with the normal direction given by (ξ,η,ζ), has been obtained in Appendix I in terms of the semi-axes of the corresponding equivalent ellipsoid [i.e., (a,b,c)] as

$$K_1-K_2 = -[a^2\xi^2(b^2-c^2)+b^2\eta^2(a^2-c^2)+c^2\zeta^2(a^2-b^2)] \cdot \frac{(a^2\xi^2+b^2\eta^2+c^2\zeta^2)^{1/2}}{(a\ b\ c\ )^2} \tag{6.4}$$

If it is assumed that the two principal curvatures are identical then from (6.4) for real values of a, b and c (which is the case here), we find

$$a^2\xi^2(b^2-c^2) + b^2\eta^2(a^2-c^2) + c^2\zeta^2(a^2-b^2) = 0 \quad . \tag{6.5}$$

This yields an expression for 'a' as

$$a = f_a(b,c) = [\frac{b^2c^2(\eta^2+\zeta^2)}{b^2(1-\zeta^2) - c^2(\xi^2-\zeta^2)}]^{1/2} \quad , \tag{6.6}$$

which is identical to (4.31), when $|H_{1c}| = 0$. Now the inverse problem for identical curvatures can be solved by iterating (6.2) and (6.3) for the values of 'b' and 'c' with a value of 'a' supplied by (6.6). The solution of this iteration scheme is then used as the initial value of a, b, c for the iteration scheme described in Fig. 6.1, which will refine the results according to the available depolarization information (i.e., H_{1c}). The complete modified iteration scheme for the cases where (K_1-K_2) is very small, is described in Fig. 6.5. It is to be noted that in this iteration scheme only the initial values of 'b' and 'c' need to

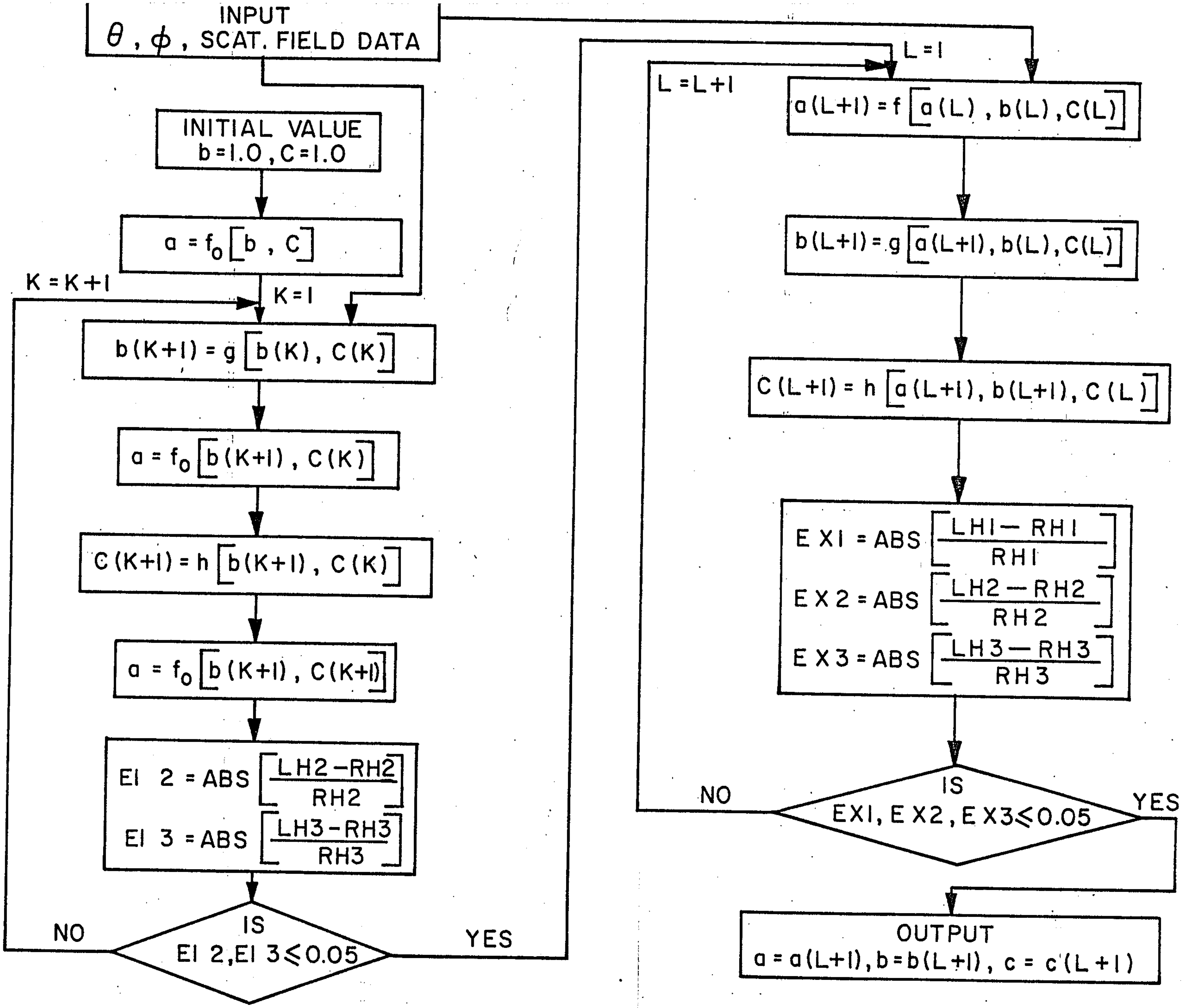

Fig. 6.5 Flow Chart For The Modified Iteration Scheme

be specified, and the initial value of 'a' is found by using the function f_a described in (6.6). Once the initial conditions are set, a modified new value of 'b' is obtained from (6.2). In the next step, this new value of 'b' along with the old value of 'c' is used to update the corresponding value of 'a'. In the next sequence the new value of 'b' and the old value of 'c' are substituted along with the updated value of 'a' into the right-hand-side of (6.3) to give a modified value of 'c'. Once again with the modified value of 'b' and the modified value of 'c', the value of 'a' is updated. The new set of values for a, b, c thus obtained, is substituted in the left-hand-side of (4.30) and (4.32) to yield the exit parameters EI2 and EI3, respectively. Note, this time, only two exit parameters are required because evaluation of 'a' through (6.6) guaranteed that (4.31) is satisfied as long as $|H_{1c}| = 0$. Again the exit-criterion was set by restricting EI1 and EI2 to 0.05. If the values of a, b, c satisfied this criterion, then those values of a, b, c were transferred to the second iteration loop (see Fig. 6.5) as the initial values, otherwise the first iteration loop was continued in order to achieve further refinement of the values of a, b, c as shown in Fig. 6.5. The second iteration loop which achieves refinement of the solution through depolarization information (i.e., $|H_{1c}|$) is identical to the one described in Fig. 6.1.

In order to study the effectiveness of the modified iteration scheme in overcoming the difficulty encountered in recovery around the region where (K_1-K_2) is very small, the lines on a prolate spheroid corresponding to $\theta = 30°$, $60°$ and $\phi = 0°$ to $90°$ (in steps of 10°) were recovered by using the iteration scheme of Fig. 6.1 as well as that of Fig. 6.5.

Results of these two iteration schemes are compared in Fig. 6.6. The best recovery is obtained for the line $\theta = 30°$, where the curvature changes most slowly out of the two curves. Improvement obtained by using the modified iteration scheme can be seen within the region $\phi = 0°$ to $30°$ ($\theta = 30°$ curve), where the difference in the principal curvatures is very small. An interesting observation to be made on the line corresponding to $\theta = 60°$ is that, although the modified iteration scheme achieves improvement in recovery in the region $\phi = 50°$ to $\phi = 30°$, it fails to recover the profile for $\phi < 30°$ (with $\theta = 60°$). This is because there are two distinct causes for this complication, i.e., the rapid rate of change of curvature and the difference in the principal curvature becoming very small. The modified iteration scheme of Fig. 6.5 is capable of overcoming the latter difficulty, however when the rapid rate of change of the curvature is the dominant cause (which is the case for $\theta = 60°$, $\phi < 30°$) this modified scheme is of little help.

In another calculation the modified iteration scheme of Fig. 6.5 was applied to recover the points on the spheroid corresponding to $\theta = 90°$ and $\phi = 0°$ to $180°$ in steps of $10°$, for the values of $\omega = 5, 7.4, 10, 12.6$ and 15. In all the above cases, the modified iteration scheme (Fig. 6.5) produced identical results to those shown in Figs. 6.2a to 6.2e, i.e., it did not give any improvement over the results produced by the iteration scheme shown in Fig. 6.1 [for $\theta = 90°$, $\phi = 0, 180°$ (in steps of $10°$)]. It is thought that this is due to the fact that in all of the above cases (i.e., Figs.6.2a to 6.2e) θ was held at $90°$ (i.e., $\zeta = 0$) throughout, which reduced the flexibility and the information content of (6.6) and thus making the modification not so effective.

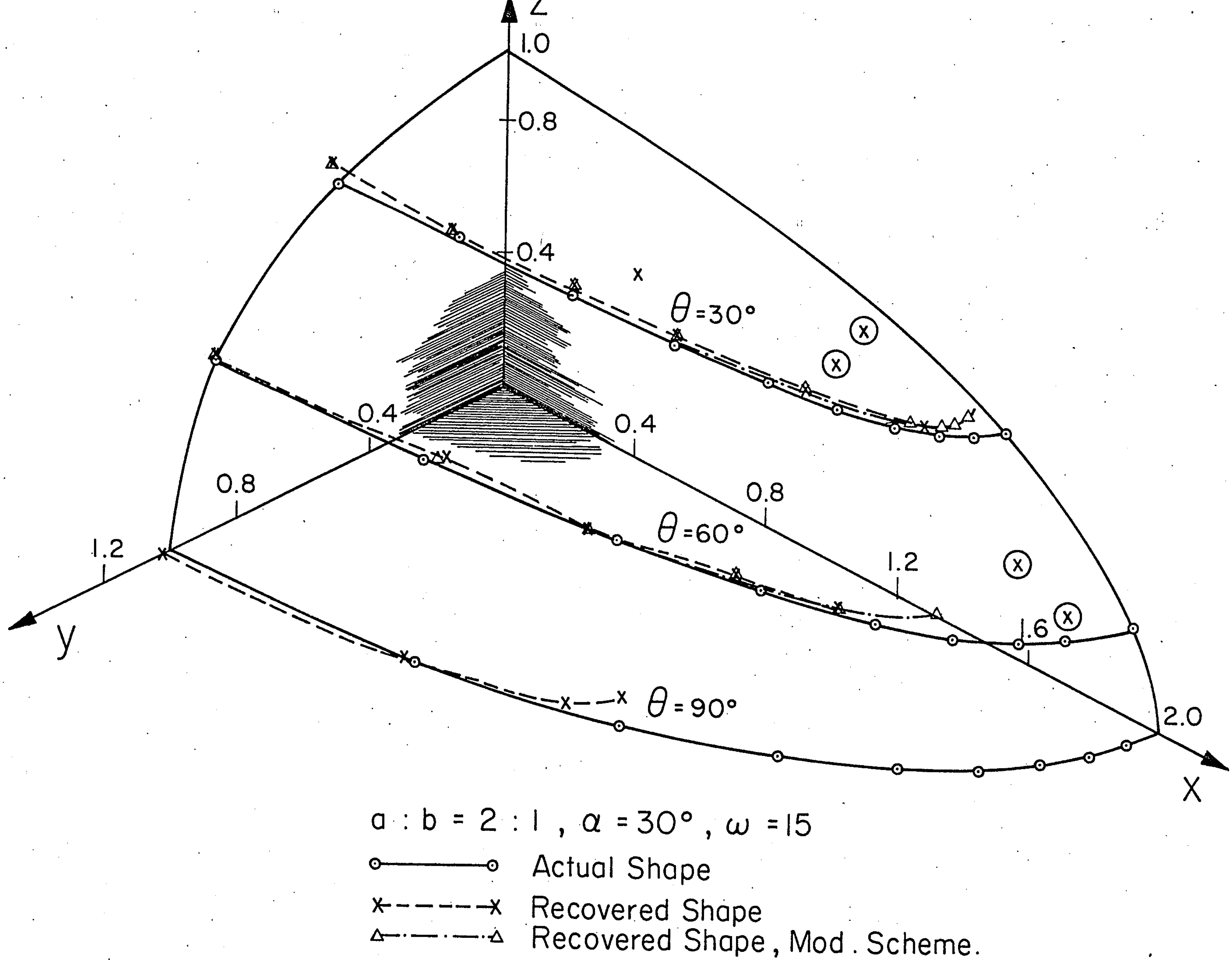

Fig. 6.6 Comparison Of The Computational Results Obtained From The Iteration Schemes Of Figs. 6.1 and 6.5

6.5 ERRORS AND LIMITATIONS OF THE INVERSE SCATTERING MODEL

The performance of the proposed monostatic inverse scattering model was studied with the test case of a perfectly conducting prolate spheroid. The computational results in Section 6.3 indicate that an optimum frequency range over which the inverse scattering model yields satisfactory results is between $\omega = 5$ and $\omega = 10$. However, when the difference between the two principal curvatures at the specular point goes to zero, the recovery of that particular specular point is not possible as indicated by the computational results of Section 6.3 and of Section 6.4.

In a region where the difference in curvature is very small, the system of equations in iteration scheme of Fig. 6.1 becomes ill-conditioned and thus the convergence is not achieved. This is evident from the data compiled in Table II and Table III. In Table II, the values of a, b, c at the end of each iteration cycle (L) is shown (see Fig. 6.1), for the direction (of incidence) $\theta = 90°$ and $\phi = 40°$. Under normal circumstances (i.e., when $K_1 - K_2$ is not very small), the values of a, b, c oscillate about a central value as is clear from the data compiled in Table III, and finally, the iteration loop converges on the solution point (in Table III, it is $a = 1.92$, $b = 1.01$, $c = 1.04$ for $\theta = 90°$, $\phi = 80°$ and $a = 2.02$, $b = 0.99$, $c = 0.97$ for $\theta = 90°$, $\phi = 90°$). On the other hand, for the ill-conditioned case, presented in Table II, no such oscillation about a central point exists, rather the values of a, b, c keep on growing monotonically with the number of iteration cycles (L) and go right past the expected solutions (see Table II, values of a, b, c for $L = 14, 15, 16$).

TABLE II

OUTPUT OF THE ITERATION LOOP (Ill conditioned Case)

$\theta = 90°$ $\phi = 40°$ $|H_{1p}| = 0.372960$ $|H_{2p}| = 0.349844$

$|H_{1c}| = 0.011203$ $\alpha = 22.05$

L = 10	Γ = 1.3215570	AA = 1.54	BB = 0.93	CC = 0.88
L = 11	Γ = 1.3826530	AA = 1.62	BB = 0.94	CC = 0.90
L = 12	Γ = 1.4519950	AA = 1.72	BB = 0.96	CC = 0.93
L = 13	Γ = 1.5316660	AA = 1.82	BB = 0.98	CC = 0.95
L = 14	Γ = 1.6242650	AA = 1.95	BB = 1.00	CC = 0.98
L = 15	Γ = 1.7330820	AA = 2.09	BB = 1.02	CC = 1.02
L = 16	Γ = 1.8623560	AA = 2.27	BB = 1.05	CC = 1.06
L = 17	Γ = 2.0175730	AA = 2.47	BB = 1.08	CC = 1.10
L = 18	Γ = 2.2059360	AA = 2.72	BB = 1.12	CC = 1.15
L = 19	Γ = 2.4369770	AA = 3.03	BB = 1.17	CC = 1.22
L = 20	Γ = 2.7233950	AA = 3.40	BB = 1.23	CC = 1.29
L = 21	Γ = 2.0822520	AA = 3.87	BB = 1.29	CC = 1.37
L = 22	Γ = 3.5366370	AA = 4.47	BB = 1.38	CC = 1.47
L = 23	Γ = 4.1179850	AA = 5.23	BB = 1.47	CC = 1.59
L = 24	Γ = 4.8694970	AA = 6.21	BB = 1.59	CC = 1.74
L = 25	Γ = 5.8508540	AA = 7.50	BB = 1.73	CC = 1.91
L = 26	Γ = 7.1449770	AA = 9.19	BB = 1.91	CC = 2.11
L = 27	Γ = 8.8681190	AA =11.44	BB = 2.11	CC = 2.36
L = 28	Γ = 11.1845400	AA =14.47	BB = 2.36	CC = 2.65
L = 29	Γ = 14.3277000	AA =18.57	BB = 2.66	CC = 3.01
L = 30	Γ = 18.632880	AA =24.19	BB = 3.03	CC = 3.44

TABLE III

OUTPUT OF THE ITERATION LOOP (Converging Case)

$\theta = 90.00 \quad \phi = 80.00 \quad |H_{1p}| = 0.907525$

$|H_{2p}| = 0.927038 \qquad |H_{1c}| = 0.026764$

$\alpha = 55.01$

L = 1	Γ =	1.1459780	AA = 1.47	BB = 1.13	CC = 1.44
L = 2	Γ =	1.0195230	AA = 2.16	BB = 0.96	CC = 0.92
L = 3	Γ =	1.0611880	AA = 1.81	BB = 1.03	CC = 1.11
L = 4	Γ =	1.0448660	AA = 1.92	BB = 1.01	CC = 1.04

EX1 = 0.00 EX2 = 0.00 EX3 = 0.03 A = 1.92 B = 1.01 C = 1.04

$\theta = 90.00 \quad \phi = 90.00 \quad |H_{1p}| = 0.990605$

$|H_{2p}| = 1.006794 \qquad |H_{1c}| = 0.036732$

$\alpha = 51.21$

L = 1	Γ =	1.1229170	AA = 1.58	BB = 1.12	CC = 1.42
L = 2	Γ =	0.9258109	AA = 2.32	BB = 0.93	CC = 0.80
L = 3	Γ =	1.0360730	AA = 1.85	BB = 1.04	CC = 1.12
L = 4	Γ =	0.9730850	AA = 2.09	BB = 0.97	CC = 0.93
L = 5	Γ =	1.0069570	AA = 1.95	BB = 1.01	CC = 1.03
L = 6	Γ =	0.9863715	AA = 2.02	BB = 0.99	CC = 0.97

EX1 = 0.00 EX2 = 0.00 EX3 = 0.04 A = 2.02 B = 0.99 C = 0.97

This complication due to ill-conditioning of the iteration scheme was circumvented (at least partially) by a modified iteration scheme where the inverse problem is first solved by assuming that the curvatures are the same, and then the results are refined by use of polarization information. Another limitation of the inverse scattering model is that when the rate of change of the curvature is large around the specular point, the recovery becomes very difficult and the results are rather poor. It is thought that this limitation arises because of two reasons. One, because of the restrictions imposed on the derivation of the polarizational correction term, i.e., (3.24), which was used in a major way to develop the inverse scattering model. In the derivation of the polarizational correction term it was assumed that the difference in principal curvatures remains the same in the vicinity of the specular point, which means that the rate of change of the curvature of the surface must be very gentle. Thus, it is expected that by improving the polarizational correction term this limitation of the model can be at least partially rectified. Another reason for the limitation is felt to be that the input data used in the computation were generated from an approximate model. Thus, it is necessary to develop more accurate input data.

The results in this chapter indicate the potentiality of this inverse scattering model in recovering target shape parameters with a relatively smaller amount of data than required by other available target identification techniques such as Bojarski's inverse identity, the concept of inverse boundary conditions, etc. Moreover, this method is quite successful in providing partial recovery of the target profiles, as in this method each specular point is recovered separately from data at one point.

chapter seven

CONCLUSIONS

7.1 SUMMARY OF THE CONTRIBUTIONS

This dissertation has clearly demonstrated that polarization information can indeed be utilized in the profile inversion of scattering objects, which was the main objective of the present investigation. One of the most complicated and neglected problems connected with electromagnetic theory is the question of what happens to the original polarization of the incident wave after the wave has been scattered. This is a problem which, even in the case of simple scatterers, has not yet been solved completely (perhaps not even seriously attacked). In the light of the above facts, it can hardly be expected that a complete general and rigorous solution of the inverse electromagnetic problem may be found in the near future which is based on depolarization characteristics of the scattered field. Nevertheless, in the opinion of the author, the work represented in this dissertation constitutes an important fundamental step towards achieving the above objective.

Besides polarization-depolarization characteristics, differential geometry as related to the surface profile inversion has been given very little importance in inverse scattering investigations in the past. It is to be noted that for the vector treatment of scattering at the surface of a convex three-dimensional object, as is the case here, differential geometry provides additional insight to the physical phenomenon that governs the interaction between the object and the electromagnetic fields.

Although many investigators [42,92,93] have pointed out the similarity between the Minkowski problem of differential geometry and the profile inversion problem of electromagnetic theory, no serious attempt (according to the literature available to the author) at integrating the well established concepts of the Minkowski problem into the profile inversion problem of electromagnetic theory has been reported. Therefore, to the best of the author's knowledge, in the present investigation the concepts of the Minkowski problem have been utilized successfully for the first time in solving the problem of recovery of the surface profile of the scatterer from the far-field scattered data.

It is well established that at sufficiently high frequencies the scattered field's magnitude about the monostatic direction contains information on the curvature of the scatterer at the specular point. On the basis of this approximation it was assumed that for any three-dimensional, smooth, slowly and uniformly varying convex shaped scatterer, an "equivalent ellipsoid" centered at the origin and of identical curvatures about the monostatic direction gives rise to an identical backscattered field magnitude. Representation of each point of the scatterer by such an equivalent model made it possible to combine the mathematical concepts of the Minkowski problem with the polarization-depolarization aspects of the electromagnetic scattering concepts and yielded a system of equations for the recovery of the surface of the scatterer.

The performance of the proposed monostatic inverse scattering model was studied with the test case of a perfectly conducting prolate spheroid. However, to the best of the author's knowledge the input data required for this purpose are not readily available for most of the scatterer shapes. To circumvent this difficulty, an approximate solution for the backscattered fields given off by a prolate spheroid was developed in the course of the present investigation. Starting with the space-time vector integro-differential equation for the induced current on the surface of the scatterer, and by applying the physical optics approximations, the time domain representation for the co- and cross-polarized backscattered far-field were obtained. The simplicity of the various approximations used in constructing the different segments of the time domain response and the reliability of the resulting scattered field data have definitely brought into light the relative advantages of the time domain approach over the frequency domain approach to the electromagnetic scattering problems for more complicated structures.

The computational results obtained from the application of the proposed inverse scattering model to the test case of a perfectly conducting prolate spheroid indicate that an optimum frequency range over which the inverse scattering model yields satisfactory results is between $\omega = 5$ and $\omega = 10$. From these computational results it was also inferred that the rate of change of curvature as well as the difference in principal curvature, i.e., $(K_1 - K_2)$, will play an important role in the recovery. In a region where the rate of change of the curvature is large around the specular point, the recovery becomes very difficult and the results are rather inaccurate. It is felt that this limitation arises because of two reasons. One is due to the restrictions imposed on the derivation of the first-order correction to the physical optics approximation, which was used in a major way to develop the inverse scattering model.

In the derivation of the first-order correction term, it was assumed that the difference in principal curvatures remains the same in the vicinity of the specular point, which means that the rate of change of the curvature of the surface must be very gentle. The other reason for the limitation is felt to be due to the input data used in the computation, which were generated from an approximate model.

In a region where the difference in curvature is very small, the computational results indicate that the system of equations in the iteration scheme becomes ill conditioned and thus the convergence is not achieved. Thus, the difficulty arising in a region where $(K_1 - K_2)$ is very small is not due to a limitation of the inverse scattering model itself; rather it is due to the limitation of the computing scheme. In fact the inverse scattering model holds true even when $(K_1 - K_2)$ vanishes.

The computational results presented in this work clearly indicate the capability of this inverse scattering model in recovering target shape parameters with a relatively smaller amount of data than required by other available target identification techniques such as Bojarski's inverse identity, application of inverse boundary conditions, etc. Moreover as indicated by the test case of the prolate spheroid, the proposed inverse scattering method is quite successful in providing partial recovery of the target profiles, because in this method each specular point is recovered separately from data at one point. Thus, there is no minimum limit on the required input data, like in some other inverse scattering schemes [24,91-94].

To sum up, in this work the mechanism (at least to a first approximation) responsible for the depolarization of the incident wave at a scatterer's surface has been used to develop a set of conditions (which may be viewed as a set of inverse boundary conditions). These conditions must be satisfied by the profile parameters of an object in order to have a certain given pattern of co- and cross-polarized backscattered far-field components. Thus, the scheme proposed here is in no way a pattern recognition technique [57,63,83,88], where the far-field features of the unknown scatterers are compared with a catalogue or dictionary entry which is available to the observer *a priori*.

7.2 SUGGESTION FOR FUTURE STUDIES

A very useful topic for future investigation would be an extension of the work presented here to the low frequency region, i.e., to incorporate some low frequency characteristics (such as the moment conditions) of the response wave form into the inverse scattering model. It is felt that in order to achieve this objective, the polarization dependence and the information content of the Rayleigh coefficient K_r must be studied thoroughly. It should be possible to relate the surface parameters of the scattering object to the radar measurables via the second moment condition and the Rayleigh coefficient, and thus, additional conditions on the inverse scattering model could be imposed. With the addition of this feature the inverse scattering model would be ready to extract information from all the segments (i.e., leading edge as well as trailing edge) of the impulse response waveform.

Another interesting related problem for future studies is to investigate the possibility of improving the first order correction to the physical optics approximation provided by Bennett and co-workers [12]. A good starting point would be the expression for ρ_0 (the radius of the circular patch about the specular point) given in (3.23). There instead of neglecting the square term one could retain it and observe the resulting modification of the expression for $\vec{H}_{p01}$ in (3.24) via the relation (3.22). It should be possible to obtain some other modification to (3.23) [and therefore to (3.24)], which would take into account the fact that the radius of curvature around the specular point is not necessarily constant. It is the opinion of the author, that not only the cross-polarized component of the scattered field but the rate of change (with respect to the configuration space) of the cross-polarized component also contains information regarding the scatterer and this factor should somehow appear in the picture while considering the "correction" to the physical optics approximation.

Before the proposed inverse scattering model could be considered from the practical point of view, its performance under noisy input data conditions should be checked computationally. To start with, this could be studied only when a very reliable and accurate set of input data is available. Therefore a more rigorous (than the one presented in Chapter Five) analysis of the direct problem of depolarization of electromagnetic waves from smooth, closed convex objects must be undertaken.

To sum up, this dissertation establishes the potentials of detection and identification systems based on polarization phenomena. Aside from applicational viewpoints, it is hoped that the thoughts, concepts and ideas brought forth in this work will provide the reader with better insight into the mechanism responsible for the depolarization phenomena in electromagnetic reflectors and thus help to improve the understanding of the underlying principles.

REFERENCES

General:

[1] "Radar reflectivity", Special Issue, Proceedings IEEE, Vol. 53, No.8, 1965.

[2] "Modern radar technology and applications", Special Issue, Proceedings IEEE, Vol.62, No.6, June 1974.

[3] "National Conference on Electromagnetic Scattering", Proceedings, University of Illinois at Chicago Circle, June 1976 (Conference Organized With Support From Air Force Office Of Scientific Research, Air Force System Command, U.S. Air Force Grant AFOSR-76-2888).

Specific:

[4] Abramowitz, M , Stegun, I.A., "Handbook of mathematical functions with formulas, graphs, and mathematical tables", Dover Publications Inc., N.Y., 1954.

[5] Andreasen, M.G., "Scattering from bodies of revolution", IEEE Trans. on Ant. and Prop., Vol.AP-13, March 1965, pp.303-310.

[6] Baum, C.E., "On the singularity expansion method for the solution of electromagnetic interaction problems", Interaction Note 88, Air Force Weapons Laboratory, Kirtland Air Force Base, New Mexico, December 1971 (and private collection of papers by C.E. Baum).

[7] Beckmann, P., Spizzichino, A., "The scattering of electromagnetic waves from rough surfaces", Pergamon Press, N.Y., 1963.

[8] Beckmann, P., "The depolarization of electromagnetic waves", Golem Series in Electromagnetics, Vol.1, The Golem Press, Boulder, Colorado, 1968.

[9] Bennett, C.L., "A technique for computing approximate electromagnetic impulse response of conducting bodies", Ph.D. dissertation, Purdue University, Lafayette, Indiana, August 1968.

[10] Bennett, C.L., Weeks, W.L., "A technique for computing approximate electromagnetic impulse responses of conducting bodies", Purdue University Report TR-EE-68-11, 1968.

[11] Bennett, C.L., DeLorenzo, J.D., Auckenthaler, A.M., "Integral equation approach to wideband inverse scattering", Sperry Rand Research Center, Sudbury, Mass., Final Report on Contract No. F30602-69-C-0332, June 1970.

[12] Bennett, C.L., Auckenthaler, A.M., Smith, R.S., DeLorenzo, J.D., "Space-time integral equation approach to the large body scattering problem", Sperry Rand Research Center, Sudbury, Mass., Final Report on Contract No. F30602-71-C-0162, AD763794, May 1973.

[13] Bennett, C.L., Menger, K.S., Hieronymus, R., DeLorenzo, J., Patterson, D., Maloy, C., "Space-time integral equation approach for targets with edges", Sperry Rand Research Center, Sudbury, Mass., Final Report on Contract No. F30602-73-C-0124, February 1974.

[14] Bennett, C.L., Private communications, January 1976.

[15] Bickel, S.H., "Some invariant properties of the polarization scattering matrix", MITRE Corp., Bedford, Mass., Contract No. AF19(628)-2390, 1965.

[16] Boerner, W.M., Vandenberghe, F.H., Hamid,M.A.K., "Determination of the electrical radius ka of a circular cylindrical scatterer from the scattered field", Canadian Journal of Physics, 49 (7), 1971, pp.804-819.

[17] Boerner, W.M., Vandenberghe, F.H., "Determination of the electrical radius ka of a spherical scatterer from the scattered field", Canadian Journal of Physics, 49 (9), 1971, pp.253-259.

[18] Boerner, W.M., Ahluwalia, H.P.S., "On a continuous wave electromagnetic inverse boundary condition", Canadian Journal of Physics, 50 (23), 1972, pp.3023-3061.

[19] Boerner, W.M., "Identification of stationary and moving scatterers in clutter", Annual Report, Defence Research Board of Canada, Grant No. 3880-08(UG), October 1974.

[20] Boerner, W.M., Aboul-Atta, O.A., "Vectorial impedance identity for the natural dependence of harmonic fields on closed boundaries", Canadian Journal Of Physics, 53, 1975, pp.1404-1407.

[21] Bojarski, N.N., "Signal processing studies and analysis; a study of electromagnetic inverse scattering", Contract No. AF 30(602)-3961, Syracuse University Research Corp., N.Y., September 1966.

[22] Bojarski, N.N., "Three-dimensional electromagnetic short pulse inverse scattering", Syracuse University Research Corp., Syracuse, N.Y., February 1967.

[23] Bojarski, N.N., "The generalized polarization scattering matrix", Syracuse University Research Corp., N.Y., Special Project Lab., Report No. SPL-TR-65-71, 1968.

[24] Bojarski, N.N., "K-space formulation of the electromagnetic scattering problem", Air Force Avionics Lab., Wright Patterson Air Force Base, Ohio, Technical Report No. AFAL-TR-71-75, AD882040, March 1971.

[25] Bojarski, N.N., "Inverse Scattering", Final Report, Contract No. N00019-72-C-0462, Naval Air System Command, 1973.

[26] Born, M., Wolf, E., "Principles of optics, electromagnetic theory of propagation, interference and diffraction of light", Second (Revised) edition, Pergamon Press, N.Y., 1964.

[27] Bowman, J.J., Senior, T.B.A., Uslenghi, P.L.E. (eds), "Electromagnetic and acoustic scattering by simple shapes", North Holland Publishing, Amsterdam, 1969.

[28] Chytil, B., "The depolarization of electromagnetic wave backscattered from certain bodies", Prâcé Ústavu Radiotech. Elektroniky (Czechoslovakia), No.17, 1961, 38 pages.

[29] Chytil, B., "Polarization-dependent scattering cross-section", Prâcé Ústavu Radiotech. Elektroniky (Czechoslovakia), No.21, 1961, 13 pages.

[30] Colin, L. (ed), "Mathematics of profile inversion", NASA Technical Memo., TMX-62, 150, August 1972.

[31] Darboux, G., "Théorie des surfaces", Vol.3, Paris, 1894.

[32] Erteza, A., Doran, J.A., "A bistatic radar method for the determination of ε and μ for a smooth spherical target", Radio Science, Vol.1, August 1966, pp.995-1001.

[33] Erteza, A., Doran, J.A., "Bistatic determination of ε and μ for a smooth convex target", Proceedings IEEE, Vol.54, October 1966, pp.1473-1474.

[34] Freeny, C.C., "Experimental and analytical investigation of target scattering matrices", General Dynamics/Fort Worth, Texas, Report No. FZE-473, 1965.

[35] Friedman, M.B., Shaw, R., "Diffraction of pulse by cylindrical obstacles of arbitrary cross-section", Transactions ASME, Series E, 1962, pp.40-47.

[36] Garbacz, R.J., "A generalized expansion for radiated and scattered fields", Ph.D. dissertation, Ohio State University, Columbus, Ohio, 1968.

[37] Goggins, W.B., "Identification of radar targets by pattern recognition", Ph.D. dissertation, Faculty of the School of Engineering, Air Force Institute of Technology, Air University, June 1973.

[38] Hilbert, D., "Grundzüge einer allgemeinen Theorie der linearen Integral-gleichungen", Leipzig und Berlin, 1912, Chapter 18,19.

[39] Huynen, J.R., "Phenomenological theory of radar targets", Ph.D. dissertation, Technical University, Delft, The Netherlands, 1970.

[40] Kanareykin, D.B., "Radar polarization effects", Moscow 1966, (C.C.M. Information Corporation, a subsidary of Carwell, Collier and Macmillan Inc., 900 Third Avenue, N.Y., 10022 translation from Russian).

[41] Keller, J.B., Lewis, R.M., "Asymptotic solutions of some diffraction problems", Comm. Pure and Appl. Math., 9, 1956, pp.207-265.

[42] Keller, J.B., "The inverse scattering problem in geometrical optics and the design of reflectors", IRE Trans. on Ant. and Prop., Vol.AP-7, No.2, April 1959, pp.146-149.

[43] Keller, J.B., "Geometrical theory of diffraction", Journal of Opt. Soc. Am., Vol. 52, 1962, pp.116-130.

[44] Kennaugh, E.M., Cosgriff, R.L., "The use of impulse response in electromagnetic scattering problem", IRE National Convention Record, Part I, 1958, pp.72-77.

[45] Kennaugh, E.M., Moffatt, D.L., "Transient and impulse response approximations", Proceedings IEEE, Vol.53, August 1965, pp.893-901.

[46] Kline, M., Kay, I., "Electromagnetic theory and geometrical optics", New York, Interscience, 1965.

[47] Kouyoumjian, R.G., "Asymptotic high-frequency methods", Proceedings IEEE, Vol.53, August 1965, pp.864-875.

[48] Laurentier, M.M., "Some improperly posed problems of mathematical physics", Springer Verlag, N.Y., 1967.

[49] Leontovich, M.A., "Investigations of propagation of radio waves", Part II (Moscow, USSR), 1948.

[50] Lewis, R.M., "Short pulse inverse diffraction theory", MITRE Corp., Bedford, Mass., Supplement 1, January 1967.

[51] Lewis, R.M., "Physical optics inverse diffraction", IEEE Trans. on Ant. and Prop., Vol. AP-17, No.3, 1969, pp.308-314.

[52] Lewy, H., "On differential geometry in the large, I (Minkowski's Problem)", Transaction Am. Math. Soc., Vol.43, No.2, 1938, pp. 258-270.

[53] Lipschutz, M.M., "Theory and problem of differential geometry", McGraw-Hill Book Co. Inc., N.Y., 1969.

[54] Luneberg, R.K., "Mathematical theory of optics", Brown University Notes, Providence, R.I., 1944.

[55] Mains, R.K., Moffatt, D.L., "Complex natural resonance of an object in detection and discrimination", Report 3424-1, Ohio State University Electroscience Lab., Department of Electrical Engg., prepared under Contract F 19628-72-C-0203 for Air Force System Command, June 1974.

[56] Manz, J.E., "A Ladar cloud/target polarization discrimination technique", Air Force Weapons Lab., Kirtland Air Force Base, New Mexico, Technical Report No. AFWL-TR-70-76, October 1970.

[57] Miller, E.K., Deadrick, F.J., Hudson, H.G., Poggio, A.J., Landt, J.A., "Radar target classification using temporal-mode analysis", Lawrence Livermore, Lab., University of California, Livermore, California, UCRL-51825, May 1975.

[58] Minkowski, H., "Volumen und Oberfläche", Mathematische Annalen, Vol. 57, 1903, pp.447-495.

[59] Moffatt, D.L., Kennaugh, E.M., "The axial echo area of the prolate spheroid", Proceedings IEEE, Vol.52, October 1964, pp.1252-1253.

[60] Moffatt, D.L., Kennaugh, E.M., "The axial echo area of a perfectly conducting prolate spheroid", IEEE Trans. Ant. and Prop., Vol.AP-13, May 1965, pp.401-409.

[61] Moffatt, D.L., "Interpretation and application of transient and impulse response approximations in electromagnetic scattering problems", Electroscience Lab. of Electrical Engg., Ohio State University, Colombus, Report No.2415-1, Contract No. F19628-67-C-239, U.S. Air Force Cambridge Research Lab., March 1968.

[62] Moffatt, D.L., "The echo area of a perfectly conducting prolate spheroid", IEEE Trans. on Ant. and Prop., Vol.AP-17,No.3, May 1969, pp.299-307.

[63] Moffatt, D.L., Mains, R.K., "Detection and discrimination of radar targets", IEEE Trans. on Ant. and Prop., Vol.AP-23, No.3, May 1975, pp.358-367.

[64] Nirenberg, L., "The Weyl and Minkowski problems in differential geometry in the large", Comm. on Pure and Appl. Math., Vol.VI, 1953, pp.337-394.

[65] Oshiro, F.K., "A source distribution technique for the solution of general electromagnetic scattering problem", Northrop Corp., Norair Div., Phase I Report No. NOR-65-271, Contract No. AF33(615)-3166, U.S. Air Force, Avionics Lab., Wright Patterson AFB, Ohio, October 1965.

[66] Perry, W.L., "On the Bojarski-Lewis inverse scattering method", IEEE Trans. on Ant. and Prop., Vol.AP-22, No.6, 1974, pp.826-829.

[67] Poggio, A.J., Miller, E.K., "Solution to three-dimensional scattering problems", Chapter 4, Computational techniques for electromagnetics (ed. R. Mittra), International series of monographs in electrical engineering, Vol.7, Pergamon Press, 1973.

[68] Pogorelov, A.V., "Intrinsic estimates for the derivatives of the radius vector of a point on a regular convex surface", Doklady, Akademia nank, S.S.S.R., (N.S.) 66, 1949, pp.805-808.

[69] Repjar, A.G., "The linear separability of multiple-frequency radar returns with applications to target classification", Electroscience Laboratory, Ohio State University, Report No. 2768-5, Grant AFOSR-69-1710A, November 1970. (Also see Ksienski et.al., Proc. IEEE, Vol.63, No.12, 1975, pp.1651-1660).

[70] Rumsey, V.H., "Reaction concept in electromagnetic theory", Physical Review, Vol.94, No.6, June 1954, pp.1483-1491.

[71] Sayre, E.P., Harrington, R.F., "Transient response of straight wire scatterers and antennas", Proceedings International Antenna and Propagation Symposium, Boston, Mass., 1968, p.160.

[72] Senior, T.B.A., "Impedance boundary conditions for statistically rough surfaces", Appl. Science Res., Vol.8B, 1960, pp.437-462.

[73] Senior, T.B.A., "A note on impedance boundary conditions", Canadian Journal of Physics, Vol. 40, 1962, pp.663-665.

[74] Shupyatskii, A.G., Morgunor, S.P., "The application of polarization methods to radar studies of clouds and precipitation", Air Force Cambridge Research Lab., L.G. Hanscom Field, Mass., Report No. AFCRL-68-0483, AFCRL-Trans-21 (translation from Russian), September 1968.

[75] Silver, S., "Microwave antenna theory and design", McGraw-Hill Book Co. Inc., N.Y., 1947.

[76] Soules, G.W., Mitzner, K.M., "Pulses in linear acoustics", Northrop Nortronics Report, ARD66-60R, 1967.

[77] Steinbach, K.H., "Non-conventional aspects of radar target classification by polarization properties", U.S. Army Mobility Equipment Research and Development Center, Fort Belvoir, Virginia, Report No. 2065, 1973.

[78] Stoker, J.J., "On the uniqueness theorems for the embedding of convex surfaces in three-dimensional space", Comm. on Pure and Appl. Math., Vol.III, No.3, 1950, pp.231-257.

[79] Stratton, J.A., "Electromagnetic theory", McGraw-Hill Book Co. Inc., N.Y., 1941.

[80] Struik, D.J., "Lectures on classical differential geometry", Addison Wesley Publishing Company Inc., Reading, Mass., U.S.A. and London, England, 1961.

[81] Tabbara, W., "On an inverse scattering method", IEEE Trans. on Ant. and Prop., Vol.AP-21, No.2, 1973, pp.245-247.

[82] Tesche, F.M., "On the analysis of scattering and antenna problems using the singularity expansion technique", IEEE Trans. on Ant. and Prop., Vol.AP-21, No.1, 1973, pp.53-62.

[83] Van Blaricum, M.L., Mittra, R., "An efficient scheme for radar target recognition based on the complex natural resonances of the target", IEEE AP-S/URSI International Symposium, University of Illinois, Urbana, Illinois, June 1975.

[84] Van Blaricum, M.L., Mittra, R., "A technique for extracting the poles and residues of a system directly from its transient response", IEEE Trans. on Ant. and Prop., Vol.AP-23, No.6, November 1975, pp.777-781.

[85] Vandenberghe, F.H., "Aspects of inverse scattering from rotationally symmetric bodies", Ph.D. Dissertation, Faculty of Graduate Studies, University of Manitoba, Winnipeg, Canada, 1971.

[86] Vandenberghe, F.H., Boerner, W.M., "On the inverse problem of electromagnetic scattering by a perfectly conducting elliptic cylinder", Canadian Journal of Physics, 50 (17), 1972, pp.1987-1992.

[87] Vandenberghe, F.H., Boerner, W.M., "On the inverse problem of scattering from perfectly conducting prolate spheroid", Canadian Journal of Physics, 50 (8), 1972, pp.754-759.

[88] Vandenberghe, F.H., Boerner, W.M., "A system synthesis approach to the inverse problem of electromagnetic scattering for the high-frequency case", Radio Science, 7(12), 1972, pp.1163-1171.

[89] Vandenberghe, F.H., Boerner, W.M., "Optimization of Vandermonde determinants", Utilitas Mathematica, Vol.7, 1975, pp.105-120.

[90] Waterman, P.C., "Electromagnetic scattering by conducting spheroids", MITRE Corp. ARPA order 596, Contract No. AF19(628)-5165, Advanced Research Projects Agency, February 1967.

[91] Weiss, M.R., "Inverse scattering in the geometric-optics limit", Journal Opt. Soc. Am., Vol.58, No.11, November 1965, pp.1524-1528.

[92] Weston, V.H., Bowman, J.J., Er, A., "Inverse scattering investigations", Final report, University of Michigan, Ann Arbor, Mich., Contract AF-19(628)-4884, 1966.

[93] Weston, V.H., Boerner, W.M., "Inverse scattering investigations", Report No. 8579-1F (ESD-TR-67,517), Radiation Lab., University of Michigan, Ann Arbor, 1968.

[94] Weston, V.H., Boerner, W.M., "An inverse scattering technique for electromagnetic bistatic scattering", Canadian Journal of Physics, 47 (11), 1969, pp.1177-1183.

[95] Young, J.D., "Target imaging from multiple frequency radar returns", Ohio State University, ESL Rep. 2786-6, June 1971.

[96] Young, J.D., "Radar imaging from ramp response signature", IEEE Trans. on Ant. and Prop., Vol.AP-24, No.3, May 1976, pp.276-282.

List of Publications Resulting From This Thesis

[1] Chaudhuri, S.K., Boerner, W.M., "Application of Polarization Aspects of the Space-time Integral Equation to Electromagnetic Inverse Scattering", IEEE AP-S/URSI International Symposium, University of Illinois, Urbana, Illinois, June 1975, Proceedings, pp.138-141.

[2] Chaudhuri, S.K., Boerner, W.M., "Utilization of Polarization-Depolarization Characteristics in Profile Inversion of a Perfectly Conducting Prolate Spheroid", URSI/USWC Annual Meeting, University of Colorado, Boulder, Colorado, October 1975, p.183.

[3] Chaudhuri, S.K., Boerner, W.M., "A Monostatic Inverse Scattering Model Based on Polarization Utilization", Applied Physics, Vol. 11, No. 4, 1976, pp.337-350.

[4] Chaudhuri, S.K., Boerner, W.M., "Polarization Utilization in Profile Inversion of a Perfectly Conducting Prolate Spheroid", IEEE Trans. on AP,1977 (to appear in July issue).

[5] Chaudhuri, S.K., Boerner, W.M., "Approximate Co- and Cross-Polarized Backscattered Fields of a Conducting Prolate Spheroid", Triennial URSI Symposium on Electromagnetic Wave Theory, Stanford University, June 1977.

APPENDIX I

The functional representation of an ellipsoid with semi-axes a, b, c is given as

$$f(x,y,z) = \frac{x^2}{a^2} + \frac{y^2}{b^2} + \frac{z^2}{c^2} - 1 = 0 \qquad \text{(I-1)}$$

Thus the unit normal $\hat{n}$ at a point (x,y,z) on the surface of the ellipsoid is

$$\hat{n} = \nabla f(x,y,z)/|\nabla f(x,y,z)|$$

$$= \frac{(2x/a^2)\hat{a}_x+(2y/b^2)\hat{a}_y+(2z/c^2)\hat{a}_z}{2[(x/a^2)^2+(y/b^2)^2+(z/c^2)^2]^{1/2}} \qquad \text{(I-2)}$$

where $\hat{a}_x$, $\hat{a}_y$ and $\hat{a}_z$ are the unit vectors in x, y and z directions respectively. From (I-2), the direction cosines ξ,η,ζ of the unit normal $\hat{n}$ are obtained as

$$\xi = \frac{x}{a^2Q} \quad , \quad \eta = \frac{y}{b^2Q} \quad , \quad \zeta = \frac{z}{c^2Q} \quad , \qquad \text{(I-3)}$$

where

$$Q = [(x/a^2)^2 + (y/b^2)^2 + (z/c^2)^2]^{1/2} \quad .$$

From (I-3) it can be shown directly that

$$x = \frac{\xi a^2}{\zeta c^2} z \quad , \quad y = \frac{\eta b^2}{\zeta c^2} z \quad .$$

Substituting these values of x and y in (I-1), yields

$$z = \pm \frac{\zeta c^2}{p} \quad , \quad \text{and therefore} \qquad \text{(I-4a)}$$

$$y = \pm \frac{\eta b^2}{p} \qquad \text{(I-4b)}$$

$$x = \pm \frac{\xi a^2}{p} \qquad \text{(I-4c)}$$

where $\quad p = [(a\xi)^2 + (b\eta)^2 + (c\zeta)^2]^{1/2}$

Minkowski's support function $M(\xi,\eta,\zeta)$ of the equivalent ellipsoid, as shown in Fig. 4.1, is given by

$$M(\xi,\eta,\zeta) = \vec{r} \cdot \hat{n} = (x\xi+y\eta+z\zeta) \quad .$$

Substituting values of x, y, z from (I-4)

$$M(\xi,\eta,\zeta) = [(a\xi)^2 + (b\eta)^2 + (c\zeta)^2]^{1/2} \tag{I-5}$$

using this expression for $M(\xi,\eta,\zeta)$, one obtains

$$M_\xi = \frac{\partial M}{\partial \xi} = a^2\xi[(a\xi)^2 + (b\eta)^2 + (c\zeta)^2] \quad ,$$

$$M_\eta = \frac{\partial M}{\partial \eta} = b^2\eta[(a\xi)^2 + (b\eta)^2 + (c\zeta)^2] \quad ,$$

$$M_\zeta = \frac{\partial M}{\partial \zeta} = c^2\zeta[(a\xi)^2 + (b\eta)^2 + (c\zeta)^2] \quad ,$$

$$M_{\xi\xi} = \frac{\partial^2 M}{\partial \xi^2} = a^2[(a\xi)^2 + (b\eta)^2 + (c\zeta)^2]^{-1/2} - (a^2\xi)^2[(a\xi)^2 + (b\eta)^2 + (c\zeta)^2]^{-3/2} \quad ,$$

$$M_{\eta\eta} = \frac{\partial^2 M}{\partial \eta^2} = b^2[(a\xi)^2 + (b\eta)^2 + (c\zeta)^2]^{-1/2} - (b^2\eta)^2[(a\xi)^2 + (b\eta)^2 + (c\zeta)^2]^{-3/2} \quad ,$$

$$M_{\zeta\zeta} = \frac{\partial^2 M}{\partial \zeta^2} = c^2[(a\xi)^2 + (b\eta)^2 + (c\zeta)^2]^{-1/2} - (c^2\zeta)^2[(a\xi)^2 + (b\eta)^2 + (c\zeta)^2]^{-3/2} \quad ,$$

$$M_{\xi\eta} = \frac{\partial^2 M}{\partial \xi \partial \eta} = -a^2b^2\xi\eta(a\xi)^2 + (b\eta)^2 + (c\zeta)^2]^{-3/2} \quad ,$$

$$M_{\xi\zeta} = \frac{\partial^2 M}{\partial \xi \partial \zeta} = -a^2c^2\xi\zeta(a\xi)^2 + (b\eta)^2 + (c\zeta)^2]^{-3/2} \quad ,$$

$$M_{\eta\zeta} = \frac{\partial^2 M}{\partial \eta \partial \zeta} = -b^2c^2\eta\zeta(a\xi)^2 + (b\eta)^2 + (c\zeta)^2]^{-3/2} \quad .$$

Thus

$$M_{\xi\xi}M_{\eta\eta} - M^2_{\xi\eta} = \frac{(abc\zeta)^2}{p^4}$$

$$M_{\xi\xi}M_{\zeta\zeta} - M^2_{\xi\zeta} = \frac{(abc\eta)^2}{p^4}$$

$$M_{\eta\eta}M_{\zeta\zeta} - M^2_{\eta\zeta} = \frac{(abc\xi)^2}{p^4} \quad .$$

Now (2.10) yields

$$\frac{a^2b^2c^2}{p^4}(\xi^2 + \eta^2 + \zeta^2) = D_1D_2 = 1/K \quad .$$

Since $(\xi^2 + \eta^2 + \zeta^2) = 1$;

$$\left(\frac{abc}{p^2}\right)^2 = D_1D_2 = 1/K \quad . \qquad \text{(I-6)}$$

By substituting the expression for M from (I-5) into (2.9) one obtains

$$[a^2\xi^2(b^2+c^2) + b^2\eta^2(a^2+c^2) + c^2\zeta^2(a^2+b^2)]/p^3 = -(D_1+D_2) \quad . \qquad \text{(I-7)}$$

Furthermore,

$$(D_1-D_2)^2 = [(D_1+D_2)^2 - 4D_1D_2] \quad ,$$

therefore from (I-6) and (I-7)

$$[a^2\xi^2(b^2-c^2) + b^2\eta^2(c^2-a^2) + c^2\zeta^2(a^2-b^2)]/p^3 = (D_1-D_2) \quad .$$

The difference between two principal curvatures at the specular point is

$$(K_1-K_2) = \frac{1}{D_1} - \frac{1}{D_2} = -\frac{D_1-D_2}{D_1D_2} \quad ,$$

which, when values of D_1D_2 and D_1-D_2 are substituted from (I-6) and (I-8), yields

$$(K_1-K_2) = -[a^2\xi^2(b^2-c^2) + b^2\eta^2(c^2-a^2) + c^2\zeta^2(a^2-b^2)] \cdot \frac{p}{(abc)^2} \quad . \qquad \text{(I-9)}$$

APPENDIX II

For obtaining the expression for the projected area function $A(t)$ the coordinate system, as shown in Fig. A.II.1, is rotated around the z and y axes such that in the new coordinate system the x-axis is along the direction of the incident wave. The transformed equation of the surface of the equivalent ellipsoid is then used to obtain the expression for the projected area as function of a, b, c, (ξ,η,ζ) and time t.

In the cartesian coordinate system the equation of the equivalent ellipsoid is

$$\frac{x^2}{a^2} + \frac{y^2}{b^2} + \frac{z^2}{c^2} = 1 \qquad \text{(II-1)}$$

In the first transformation the coordinate system is rotated about the z axis by ϕ as shown in Fig. A.II.1. Thus

$$x = -y'\sin\phi + x'\cos\phi$$

$$y = y'\cos\phi + x'\sin\phi$$

Substituting x and y in (II-1), the transformed equation of the ellipsoid becomes

$$\frac{(f_1 x' + y')^2}{(g_1 + h_1 x'^2)} + \frac{g_1 z^2}{c^2(g_1 + h_1 x'^2)} = 1 \qquad \text{(II-2)}$$

where

$$f_1 = \frac{C_1(\phi)}{B_1(\phi)} \quad , \quad g_1 = \frac{a^2 b^2}{B_1(\phi)} \quad , \text{ and } \quad h_1 = \left[\frac{C_1^2(\phi)}{B_1^2(\phi)} - \frac{E_1(\phi)}{B_1(\phi)}\right]$$

with

$$B_1(\phi) = b^2\sin^2\phi + a^2\cos^2\phi$$

$$C_1(\phi) = (a^2 - b^2)\sin\phi\cos\phi$$

$$E_1(\phi) = a^2\sin^2\phi + b^2\cos^2\phi$$

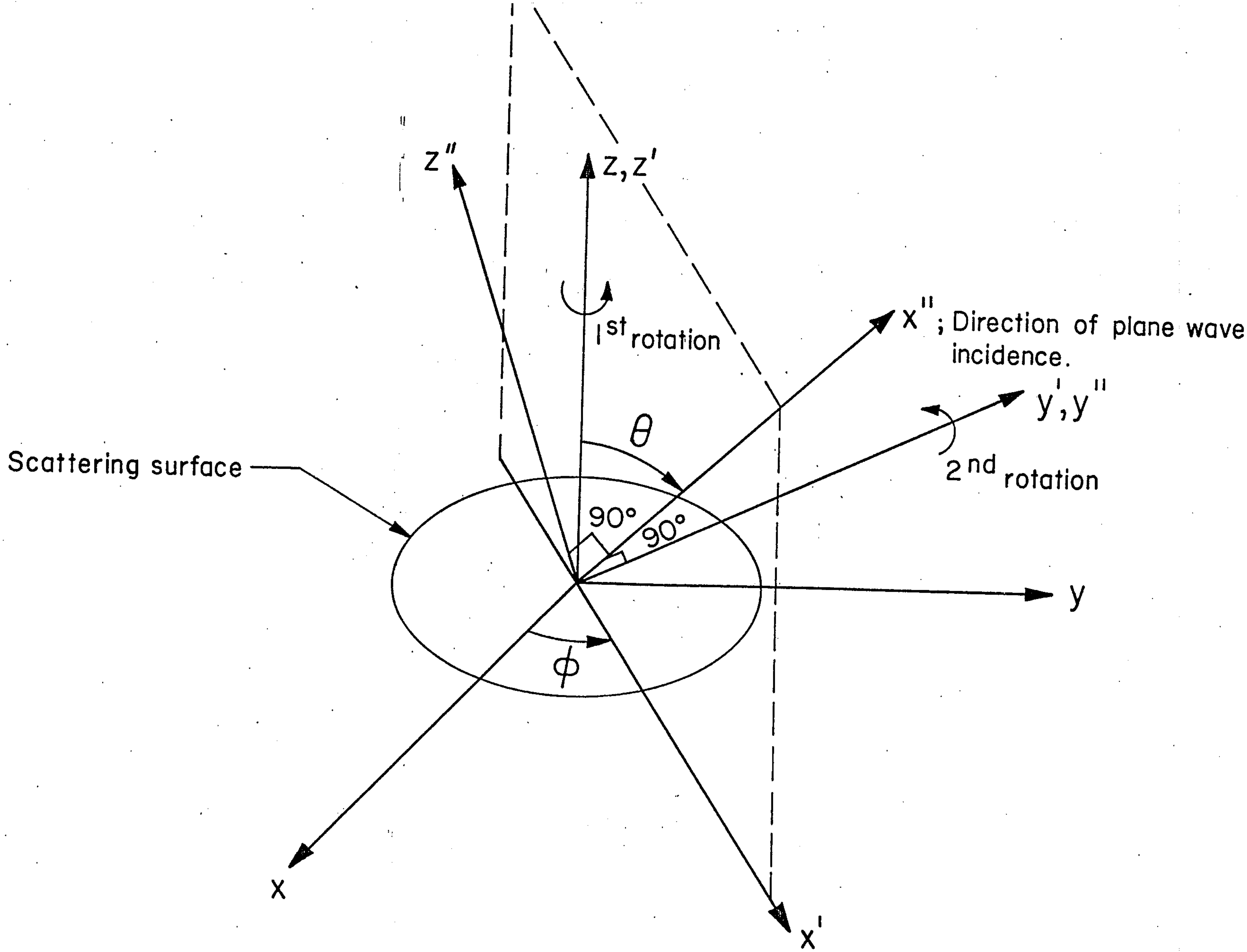

Fig. A.II.1 Eulerian Transformation Of The Target Coordinates

In the second transformation the coordinate system is rotated about the y' axis by θ as shown in Fig. A.II.1.

$$x' = -z''\cos\theta + x''\sin\theta \quad ,$$

$$z = z''\sin\theta + x''\cos\theta \quad .$$

Substitution of these expressions for x' and z into (II-2) yields the final transformed equations of the ellipsoid, i.e.,

$$y''^2 - 2(f_1\cos\theta z'' - t_1 x'')y'' + [f_2(z''+t_2x'')^2 - (f_2p_2 - t_1^2x''^2)] = 0 \qquad \text{(II-3)}$$

where $\quad t_1 = f_1\sin\theta \quad , \quad f_2 = \dfrac{g_1\sin^2\theta}{c^2} + (f_1^2 - h_1)\cos^2\theta$

$$t_2 = g_2/f_2 \quad , \quad p_2 = g_1/f_2 + \frac{(f_2h_2+g_2^2)}{f_2^2}x''^2$$

with $\quad g_2 = [\dfrac{g_1}{c^2} + (h_1 - f_1^2)]\sin\theta\cos\theta \quad ,$

$$h_2 = h_1\sin^2\theta - \frac{g_1\cos^2\theta}{c^2} \quad .$$

If x'' = constant, then (II-3) represents the equation of the curve enclosing the cross-section of the ellipsoid delineated by the plane x'' = constant. Using this fact along with the indefinite integral [4] expression

$$\int (A^2-x^2)^{1/2}dx = \frac{1}{2}[x(A^2-x^2) + A^2\sin^{-1}\frac{x}{|A|}] \quad ,$$

the cross-sectional area of the equivalent ellipsoid as delineated by a plane wave moving along the x'' axis is obtained as a function of a, b, c, (ϕ,θ) and x'' as

$$A(x'') = \pi \cdot \frac{g_1[\frac{g_1}{c^2}\sin^2\theta - h_1(\cos^2\theta - \frac{x''^2}{c^2})]}{(\frac{g_1}{c^2}\sin^2\theta - h_1\cos^2\theta)^{3/2}} \qquad \text{(II-4)}$$

Since x'' is the direction of plane wave incidence, the distance along this axis may directly be related to the time t (by scaling with respect to the half free-space velocity of light) as

$$x'' = -t/2 \quad [\text{scaling factor } c_0 \text{ understood}]$$

which, on substitution into (II-4), yields the expression

$$\frac{1}{2\pi} A(t) = \frac{g_1 c}{8h_1^{1/2}\Gamma^3(\theta,\phi)} [4\Gamma^2(\theta,\phi)-t^2]u[t+2\Gamma(\theta,\phi)] \tag{II-5}$$

where

$$\Gamma(\theta,\phi) = [\frac{a^2b^2B_1(\phi)\sin^2\theta}{C_1^2(\phi) - B_1(\phi)E_1(\phi)} - c^2\cos^2\theta] \quad .$$

Expression (II-5) has been multiplied by the unit step function in order to take care of the fact that the projected area function $A(t)$ is zero until the incident plane wave reaches the specular point. It is to be noted that in case of backscattering the direction cosines ξ, η, ζ of the unit normal to the surface of the ellipsoid at the specular point are related to the direction (θ,ϕ) of the incident wave as

$$\xi = \cos\phi\sin\theta \quad , \quad \eta = \sin\phi\sin\theta \quad , \quad \zeta = \cos\theta \quad .$$

Taking the first derivative of $A(t)$ with respect to time t gives

$$\frac{\partial A(t)}{\partial t} = -2\pi t G u(t+2\Gamma) \tag{II-6}$$

where the factor $(g_1 c/4h_1^{1/2}\Gamma^3)$ has been replaced by G.

Differentiating (II-6) again, yields

$$\frac{\partial^2 A(t)}{\partial t^2} = 2\Gamma G\delta(t+2\Gamma) - Gu(t+2\Gamma) \tag{II-7}$$

Converting the expression in (II-6) and (II-7) from the time domain t to the frequency domain ω by appropriate Fourier transformation (see Section 3.2) yields

$$F\left[\frac{\partial A(t)}{\partial t} \right] = -2\pi G \left(\frac{1}{\omega^2} - j \frac{2\Gamma}{\omega} \right) e^{2j\omega\Gamma} \qquad \text{(II-8)}$$

and

$$F\left[\frac{\partial^2 A(t)}{\partial t^2} \right] = 2\pi G (2\Gamma - j/\omega) \; e^{2j\omega\Gamma} \qquad \text{(II-9)}$$

where F represents the Fourier transform.

APPENDIX III

It is of interest to document the relationships between the time domain response and the frequency domain response described in Chapter Five.

Using the normalized variables t and $\omega = kb$, one obtains the frequency domain phasor response as

$$r_0 H_S(j\omega) = G(j\omega) \cdot bH_i(j\omega)$$

and the time domain response as

$$r_0 H_S(t) = bF_I(t) * H_i(t)$$

where b denotes the characteristic dimension of the scatterer (i.e., semi axis, diameter, length etc.). When the incident magnetic field is impulsive, i.e.

$$bH_i(t) = \delta(t) \quad \text{and}$$

$$bH_i(j\omega) = 1.$$

Thus $G(j\omega)$ vs ω and $F_I(t)$ vs t yields a mapping between the time domain and the frequency domain governed by the Fourier transformation pair

$$G(j\omega) = \mathcal{F}\{F_I(t)\} = \int_{-\infty}^{+\infty} F_I(t)e^{-j\omega t}dt \qquad \text{(A.III.1)}$$

$$F_I(t) = \mathcal{F}^{-1}\{G(j\omega)\} = \frac{1}{2\pi}\int_{-\infty}^{+\infty} G(j\omega)e^{j\omega t}d\omega \quad . \qquad \text{(A.III.2)}$$

Now using the initial value theorem of the Fourier transform theory i.e.,

$$\lim_{t\to 0} F_I(t) = \lim_{\omega\to\infty} j\omega G(j\omega)$$

it is evident that the leading edge of the response in time domain contributes most to the final values (i.e. large values of ω) of the response in the frequency domain. Hence the segment (1) of the time domain response in Fig.5.5 corresponds to the steady state value in Fig. 5.7.

Next, by making use of the final value theorem of Fourier transform theory i.e.,

$$\lim_{j\omega \to 0} j\omega G(j\omega) = \lim_{t \to \infty} F_I(t)$$

it is seen that the trailing edge of the response in the time domain contributes most to the initial values (i.e., small values of ω) of the response in frequency domain. Thus the segment (4) of the time domain response in Fig. 5.5 corresponds to the initial values in Fig. 5.7. Finally, the values of the frequency response for intermediate values of ω in Fig. 5.7 receive contributions mostly from segments (2) and (3) in Fig. 5.5.

VITA

Sujeet Kumar Chaudhuri was born on August 25, 1949 at Calcutta, India. His secondary schooling was taken at Birla multipurpose higher secondary school, Pilani, India. In July, 1965 he began attending Birla Institute of Technology and Science and in April, 1970 received the B.E. (Hons) degree in Electronics Engineering from that institute. In July, 1970 he joined the Indian Institute of Technology/New Delhi and received the M. Tech degree in Electronics and Communications in October, 1971.

In October of 1971 Mr. Chaudhuri came to Canada as a Landed Immigrant and started his graduate studies at the University of Manitoba. After completing the degree of M.Sc. in Electrical Engineering, In February, 1973 he began a course of study in Electromagnetic Theory for the Ph.D. degree in Electrical Engineering. During his studies at the University of Manitoba he was employed as a research and teaching student in the Department of Electrical Engineering.